Progress in Nuclear Magnetic Resonance Spectroscopy 124–125 (2021) 99–128

Contents lists available at ScienceDirect

Progress in Nuclear Magnetic Resonance Spectroscopy

journal homepage: www.elsevier.com/locate/pnmrs

Swelling layered minerals applications: A solid state NMR overview

Esperanza Pavón [a,b,*], María D. Alba [a]

[a] Instituto Ciencia de los Materiales de Sevilla (CSIC-US), Avda. Américo Vespucio, 49, 41092 Sevilla, Spain
[b] Departamento de Física de la Materia Condensada, Universidad de Sevilla, Avda. Reina Mercedes, s/n, 41012 Sevilla, Spain

ARTICLE INFO

Article history:
Received 21 October 2020
Accepted 12 April 2021
Available online 21 May 2021

Keywords:
Swelling clay minerals
Solid State NMR
Clay applications
Structure
Dynamics

ABSTRACT

Swelling layered clay minerals form an important sub-group of the phyllosilicate family. They are characterized by their ability to expand or contract in the presence or absence of water. This property makes them useful for a variety of applications, ranging from environmental technologies to heterogeneous catalysis, and including pharmaceutical and industrial applications. Solid State Nuclear Magnetic Resonance (SS-NMR) has been extensively applied in the characterization of these materials, providing useful information on their dynamics and structure that is inaccessible using other characterization methods such as X-ray diffraction. In this review, we present the key contributions of SS-NMR to the understanding of the mechanisms that govern some of the main applications associated to swelling clay minerals. The article is divided in two parts. The first part presents SS-NMR conventional applications to layered clay minerals, while the second part comprises an in-depth review of the information that SS-NMR can provide about the different properties of swelling layered clay minerals.

Contents

* Corresponding author at: Instituto Ciencia de los Materiales de Sevilla (CSIC-US), Avda. Américo Vespucio, 49, 41092 Sevilla, Spain.
E-mail address: epavon@us.es (E. Pavón).

https://doi.org/10.1016/j.pnmrs.2021.04.001
0079-6565/

1. Introduction

1.1. Swelling clay minerals: Definition and classification

Clay minerals are layered silicates that are usually formed as products of chemical weathering of other silicate minerals at the earth's surface. Moreover, they represent some of the most important, if not the most important, industrial minerals.

They form an important group of the phyllosilicate or layered silicate family, which are distinguished by layered structures composed by two types of sheets linked through oxygen: one formed by tetrahedra and another one formed by octahedra with thicknesses of 3 Å and 4 Å, respectively [1]. The center of each tetrahedron is commonly occupied by Si^{4+}, frequently substituted by Al^{3+} and sporadically by Fe^{3+}. The center of each octahedron is occupied by Al^{3+}, Mg^{2+}, and Fe^{2+} and, sometimes, by Fe^{3+} and Li^{+}, among others [2].

Based on the number and arrangement of tetrahedral (silica) and octahedral (alumina-magnesia) sheets, phyllosilicates can be classified into three different groups (Fig. 1)

(a) 1:1 phyllosilicate
(b) 2:1 phyllosilicate
(c) 2:1:1 (or) 2:2 phyllosilicate

The subgroups are sometimes defined based on the number of certain positions occupied by cations. When two-thirds of the octahedral positions are occupied, the mineral is named dioctahedral; when all three octahedral positions are occupied, it is named trioctahedral.

2:1 phyllosilicates can be classified as a function of their layer charge. Except for talc and pyrophyllite, whose layers are neutral, the rest of the 2:1 phyllosilicates exhibit some amount of layer charge. Its origin lies in the isomorphic substitutions of either Si^{+4} for Al^{+3} occurring in the tetrahedral sheet or cation substitutions in the octahedral one. To achieve clay mineral neutrality, layer charge created is balanced by the presence of cations in the interlayer space, that in some cases are surrounding by water molecules. A useful clay mineral classification outlining the nomenclature and differences between clay minerals is shown in Fig. 2 [3].

Swelling clays comprise only a small group in the clay mineral classification (shown in red in Fig. 2). They correspond to those clays that are able to expand or contract in the presence or absence of water.

This phenomenon is associated with the hydration of clay; however, not all clays swell when hydrated [4]. The Kaolinite group, for example, exhibits little (halloysite) or no (kaolinite) swelling capacity, whereas smectites and vermiculites characteristically swell in water to many times their dry volume. The hydrous micas, or so-

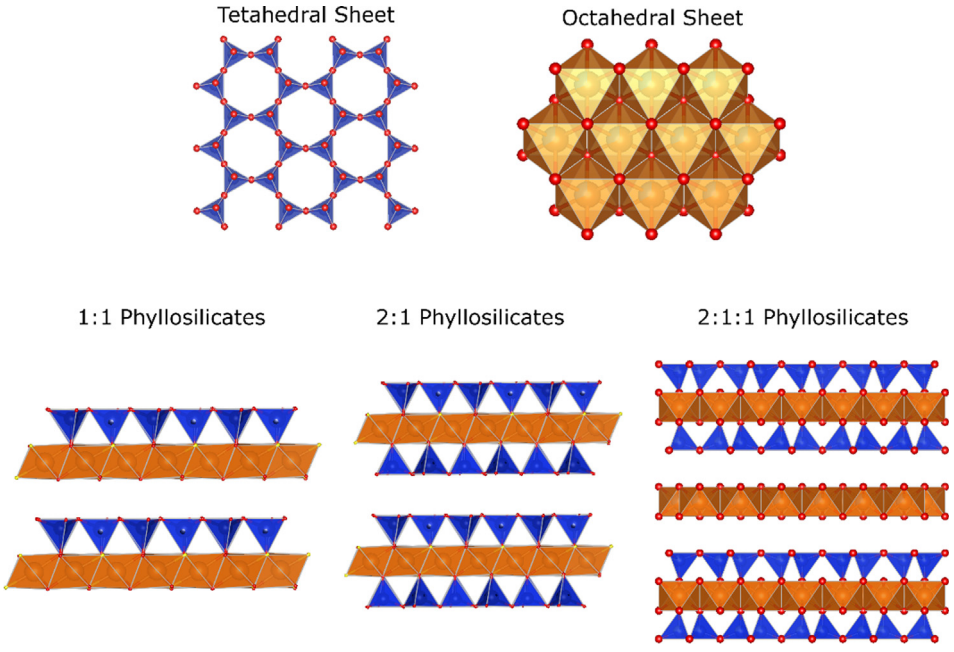

Fig. 1. Graphical representation of the tetrahedral and octahedral sheets in phyllosilicates (up) and phyllosilicates classification in function of the number of tetrahedral and octahedral sheets (down).

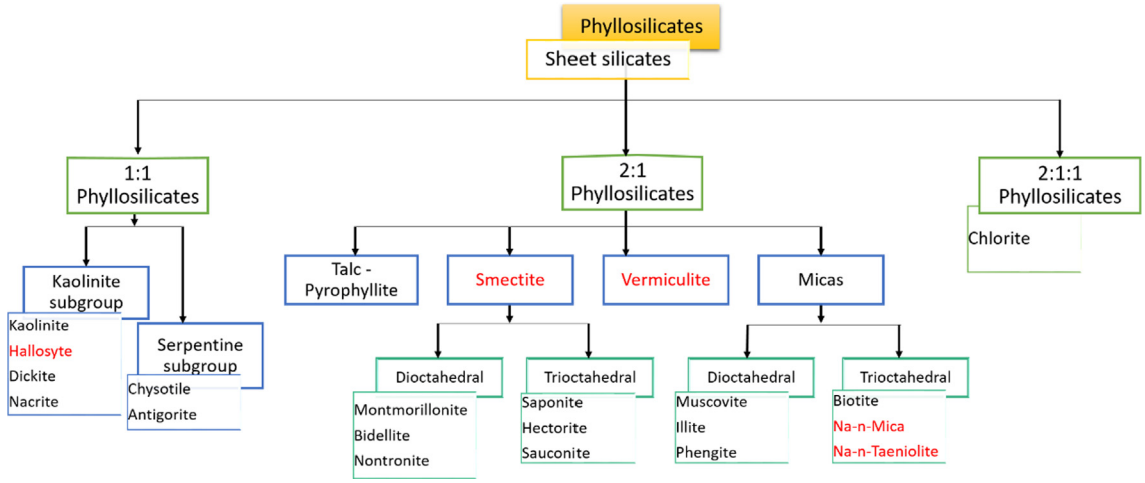

Fig. 2. Clay minerals classification. Swelling clay minerals are marked in red.

called illites, and attapulgite fall between these two extremes in their swelling properties, but are, in general, much closer to kaolinite than to sodium montmorillonite in their increase in volume on hydration. Recently, a new family of synthetic swelling micas with tuned layer charge between 2.0 and 4.0 per unit cell, Na-n-Mica and Na-n-Taeniolite, has been synthesized that are able to swell [5,6]. These differences in the swelling characteristics of different clays are related to their chemical composition, to the kind and degree of isomorphous replacements in their structure, and to the amount and nature of their associated exchangeable cations [4,7].

1.2. Properties of swelling clay minerals

Both layer charge and interlayer cations are the responsible for the properties that make clay minerals so useful for many applications: swelling capacity, cation exchange capacity and plasticity. A short description of them follows below; several books and reviews can be consulted for a deeper understanding [8-13].

(a) Swelling capacity

Swelling is the spontaneous increase of the interlayer distance of clay mineral particles, due to the adsorption of molecules in the interlayer space. Layer charge, the type of interlayer cation and the type of adsorbing molecule or ion govern this process. [8,10]

(b) Cation Exchange capacity (CEC)

Cation exchange capacity is defined as the ability of clay minerals to absorb cations in such a form that they can be easily exchanged for other cations present in an aqueous solution [9]. This parameter defines the number of cations capable of exchange, and it is usually expressed in miliequivalent per 100 g of clay [10].

(c) Plasticity

It can be defined as the ability of a clay material to be molded into a certain shape without rupturing when stress is applied, and for this shape to be retained after the stress is removed.

1.3. Conventional application of SS-NMR to clay minerals

Clay minerals have traditionally been studied with X-ray diffraction methods allowing phase identification and quantification [14]. However, the application of Solid State Nuclear Magnetic Resonance (SS-NMR) spectroscopy over the last three decades has provided valuable structural information that remained inaccessible to XRD methods [15,16].

The main factor underlying this successful application arises from the properties of the heteroatoms involved in the clay mineral structure: Si, Al, Mg and Na, among others. While these elements exhibit only small changes in scattering factor values (*f*), leading to limited selectivity in X-ray diffraction, their gyromagnetic ratios (γ) are substantially different (Fig. 3) allowing SS-NMR to selectively observe the different types of atoms and characterize their chemical shifts.

Since the 1980s, SS-NMR spectroscopy has been widely utilized in clay mineral systems, as first described in the comprehensive text by Engelhardt and Michel published in 1987 [17]. Since then, several reviews and books have summarized the main contributions of SS-NMR in the structure elucidation of clay minerals [15,16,18,19], including applications of conventional SS-NMR spectroscopy to investigation of the structural (crystallographic sites, cation coordination, silicate network distortion, and cation distributions) and dynamic aspects of clay minerals. Moreover, in some cases, the analysis of ^{23}Na, ^{27}Al, and ^{29}Si MAS-NMR spectra has allowed the investigation of interlayer, octahedral, and tetrahedral sheets of mixed-layer clay minerals [20,21].

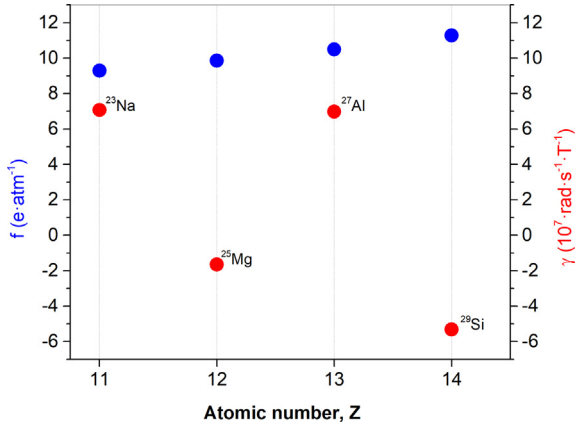

Fig. 3. Comparison of the scattering factor values (f, blue) and gyromagnetic radio (γ, red) vs atomic number (Z).

^{29}Si (I = 1/2, 4.7% abundance) is the most widely used nucleus when structural characterization of a clay mineral is required. Its chemical shifts depend on the degree of tetrahedral polymerization and the number of substitutions in the nearby tetrahedra. In 2:1 clay minerals, ^{29}Si chemical shifts are usually found between −75 and −95 ppm, corresponding to Q^3 environments. The exact position depends on the number of substitutions of Al^{3+} for Si^{4+} in neighboring tetrahedra, which cause the ^{29}Si lines to shift to lower fields; this allows the resolution of Si atoms surrounded by 3Si, 2Si1Al, 1Si2Al, or 3Al, denoted as Q^3(mAl) where m = 0,1,2 and 3 [19] (Fig. 4). In addition, ^{29}Si chemical shifts are sensitive to layer distortions arising from the matching of tetrahedral and octahedral sheets, making Si chemical shifts change according to the twisting angle between contiguous tetrahedra [22,23].

The quantitative analysis of the ^{29}Si MAS-NMR spectra of clay minerals enables the tetrahedral composition of samples with Si > Al to be estimated, and the Si/Al(IV) ratio can be derived from the expression [19]:

$$\frac{Si}{Al} = \frac{\sum I_n}{1/3 \sum n I_n}$$

where I_n stands for the relative intensity of Si NMR components associated with nAl and (3-n)Si.

In clay minerals, ^{27}Al (I = 5/2, 100% abundance) can be either present in octahedral alumina sheets or contained within tetrahedral sheets as seen above. The distribution of Al in tetrahedral and octahedral sheets is related to the distribution of the negative charge and is often used to explain the physicochemical properties of different clay minerals. ^{27}Al MAS-NMR spectroscopy can provide direct information on Al coordination, as the signals corresponding to octahedral and tetrahedral aluminum are well separated (Al(VI) ca. 0 ppm and Al(IV) at ca. 70 ppm, Fig. 4). If quantitative excitation conditions are applied for the central (−1/2 ↔ +1/2) transition – which is the transition typically observed in routine characterization experiments – then the fractions of each of the two species can be determined.

Sodium (^{23}Na, I = 3/2 and 100% abundance) is an interesting nucleus for clay mineral characterization, as it is often present in the interlayer space of many clay minerals. It is easy to obtain a ^{23}Na MAS-NMR spectrum despite its quadrupolar nature. Three types of ^{23}Na can be resolved, corresponding to non-exchangeable (ca. 40 ppm) and exchangeable (between −2.3 and −20 ppm) species [18,24] (Fig. 4). The peak at ca. −2.3 ppm was assigned to hydrated Na^+ trapped in the interlayer space, while that at −20 ppm was assigned to non-hydrated species. Usually, these two last contributions are not well resolved and ^{23}Na spectra reflect only the average environment.

2. Applications of swelling clay minerals: What information can NMR provide?

Solid State-NMR (SS-NMR) has been extensively applied in the structure elucidation of clay minerals, as seen in section 1.3, and can provide useful information about dynamics aspects of these materials. One of the main advantages of using this technique is that the local information obtained using SS-NMR is more accurate than the one obtained with other characterization tehcniques that demand a long-range crystal order. On the one hand, specific information about structural networks, crystallographic sites and cation distributions can be obtained using high-resolution magic angle spinning (MAS-NMR). On the other, conventional NMR techniques are useful for investigating the orientation and anisotropic mobility of adsorbed molecules in oriented aggregates. Several books and papers review the use of SS-NMR to tackle these basic scientific questions [15,16,18,25,26]. In this section, however, we will concentrate on the key contribution of SS-NMR in understanding the inherent mechanisms that govern some of the main applications associated to clay minerals.

2.1. Environmental technologies

The main properties of clays (layer charge and swelling capacity) make them especially useful in adsorbing and immobilizing extraneous species. Consequently, they have been extensively applied in many environmental applications, from pesticides carriers to barriers in nuclear waste management, heavy metal removal or, more recently, in hydraulic fracking and CO_2 capture systems. In this section, the main contributions of SS-NMR techniques in solving some of the problems associated with the use of clay minerals in such applications is summarized.

2.1.1. Agricultural applications: Pesticide carriers and slow-release fertilizers

Clay minerals are natural and relatively cheap components of soils that play a significant role in agricultural applications; especially important is their contribution as pesticide carriers and for the release of fertilizers, as will be discussed in the following section.

As pesticides carriers, clays control the leaching, photodegradation, sorption and volatilization of pesticides. SS-NMR is a suitable analysis technique that allows studying the physico-chemical interactions and transformation of pesticides when in contact with soils and clay minerals. It is especially useful, for example, in examining the interactions of phosphorus-containing pesticides, as ^{31}P has a 100% natural abundance and its chemical shifts have large sensitivity to structural variation.

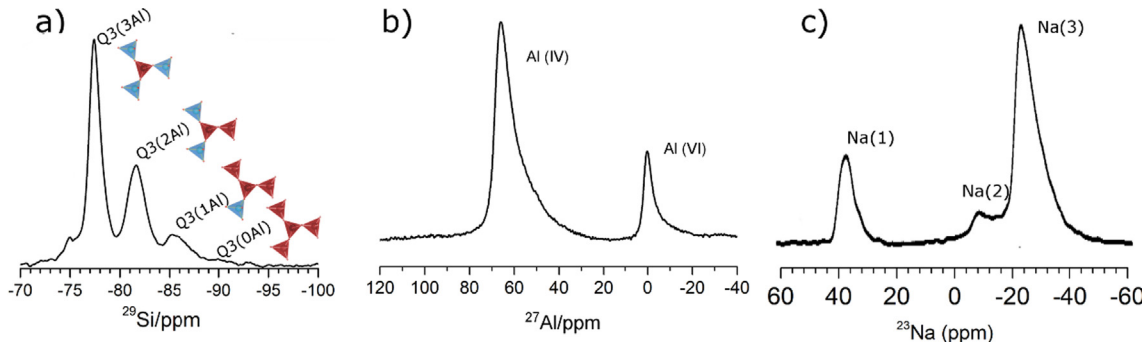

Fig. 4. a) ^{29}Si MAS NMR of a clay mineral exhibiting well resolved Q^3(mAl) sites; b) ^{27}Al MAS NMR spectrum where the Al(VI) and Al(IV) are displayed; and c)^{23}Na MAS NMR with the three distinguishable structural sites observables. Spectra recorded by the authors on Na-n-Mica (a and b) whereas c) is . adapted from [24]

An important issue concerning pesticides is to determine if their decomposition over time produces chemical compounds with severe toxicity. In this sense, several studies carried out by Seger and Maciel [27-29] have dealt with the decomposition of organothiophosphate pesticides. Specifically, they have used ^{31}P NMR (CP-MAS and DP-MAS) to study the non-photochemical/non-biological behavior of two representative pesticides from this family: chlorpyrifus and methyl parathion, when sorbed on soil components and, particularly, on montmorillonite and kaolinite.

Initially, chlorpyrifus and methyl parathion are physisorbed on both clay minerals, (δ(^{31}P) ~ 61 and 67 ppm, respectively) showing an almost liquid like ^{31}P spectrum, revealing that it exhibits significant motion at the molecular level, as evidenced by the strong ^{31}P DP-MAS and the lack of ^{31}P CP-MAS signal [27-29]. The time-evolution of ^{31}P signals (ranging from hours to years) revealed that unreacted pesticide peaks diminish and new peaks resulting from different decomposition modes (hydrolysis, isomerization, mineralization and oxidation reactions) appear. ^{31}P MAS spectra showed that the predominant modes of decomposition of chlorpyrifus and methyl parathion on partially hydrated kaolinite and montmorillonite are quite different [28,29]. For kaolinite, the predominant decomposition mode are oxidation for chlorpyrifus and isomerization for methyl parathion [27,29]. In montmorillonite, the outcome depends on the interlayer cation [27,28], as shown in Table 1.

Kinetics of the decomposition was also observable by ^{31}P CP-MAS and ^{31}P DP-MAS showing that Zn-, Cu(II)- and Al-montmorillonites cause faster decomposition of the pesticides, than do Ca-montmorillonite or kaolinite. The new decomposition compounds are much more tightly bound to the clay than the physisorbed chlorpyrifus molecules, as seen by ^{31}P CP-MAS [28,29].

The mobility of pesticides at a molecular level is a significant question that should be resolved before applying them into soils and agricultural crops. In general, mobility of pesticides is conditioned by their interaction with soils, and especially with clay minerals. Two kinds of interaction can be found: weak and covalent bonds. In the first case, pesticides are more bioavailable for microbes and plants, and consequently, more mobile, whereas in the second, they are no longer extractable.

To study these interactions SS-NMR can be very effective as shown by Chamignon et al. [30–32] Before this, several approaches were developed to study covalent and non-covalent bonds between several pesticides and soils [32,33]. Most of these studies were taking benefit of labeled ^{15}N or ^{13}C compounds to overcome the relatively low sensitivity of NMR techniques.

In the case of weak or non-covalent interactions, which imply a higher degree of mobility, there are several strategies that have been proposed using NMR:

- Indirect approach: in this case, SS-NMR only plays a role in determining the structural groups of Organic Matter (OM), establishing correlations between organic carbon and normalized sorption coefficients (K_{oc} values) of pollutants with soil matrices and structural elements of the OM [34–38]. The technique most often used is ^{13}C CP-MAS NMR in this case.
- ^{2}H MAS NMR spectra can be used as fingerprints of orientation and movement of ^{2}H-labelled pesticides, taking advantage of NMR properties connected to the orientation or movement of the molecules [39]. The main drawback is that this technique requires labelled compounds.
- T_1 relaxation time. Decreases in T_1 reflect a stronger interaction between the pollutant and the matrix [40].
- Studies of the molecular species at the liquid/solid interface: highly mobile molecules give narrow signals, similar to liquid NMR spectra. In contrast, when the strength of the interaction increases, the signals become progressively broader as shown by Kohl et al. [41] or Seger et al. [28] using ^{19}F, ^{31}P and ^{1}H MAS-NMR.
- ^{1}H HR-MAS: the development of this technique allowed the characterization of inhomogeneous compounds with liquid-like dynamics and has already been applied to study the interaction of pesticides with clays [32,42].

As discussed before, clay minerals play a key role on the release of fertilizers. In fact, after mechanochemical activation with a soluble phosphate [43-46], they produce amorphous phases that can slowly release K, N and P, acting as slow-release fertilizers. This procedure reduces the pollution caused by using an excess of nutrients in agriculture [47] at the same time enhancing the production of food [48].

Mechanochemical activation increases the reactivity of clay minerals, allows reactions in the solid state and decreases the decomposition temperature, causing structural defects and structural transformations, formation of metastable amorphous or hybrid materials, etc. [49-62]. The effectiveness of this procedure depends mainly on the stoichiometric proportions of the materials, time and energy of milling. SS-NMR spectroscopy is a useful technique to elucidate the chemical composition of the new materials formed after milling [46].

Wypych et al. [46,63-65] have worked extensively on the production of slow-release fertilizer using clay minerals and different phosphate species. In their studies, they have used SS-NMR techniques to elucidate the mechanisms of mechanochemical activation of clay minerals and the composition of the obtained materials. They showed that this reaction produces amorphous materials formed by combining the elements originally present in the clay mineral and the phosphates, as shown by ^{29}Si, ^{31}P and ^{27}Al MAS-NMR, and the production of slow release fertilizers on demand is inferred [46]. In fact, the NMR spectra indicate a greater number of sites with amorphous Si species and changes in the chemical environment of Al sites after milling. Some of these Si sites resemble amorphous SiO_2, which might improve the reactivity of the ground clay minerals [63].

2.1.2. Recent energy applications

Hydraulic fracturing or fracking is considered extremely environmental controversial, due to the chemicals added to the water to produce the deep-rock cracking, the heavy metals and other contaminants in flowback water, the intense use of water and the physical damage to the rock formation that can affect the sub-

Table 1
Summary of organothiophosphate pesticides decomposition mode when in contact with kaolinite and montmorillonite homionized with different interlayer cations.

Partially hydrated clay	Methyl parathion decomposition mode		Chlorpyrifos decomposition mode	
	Predominant	δ ^{31}P, ppm	Predominant	δ ^{31}P, ppm
kaolinite	isomerization	27	oxidation	−6 to −9
Ca-montmorillonite	isomerization	33	isomerization	30, 20
Zn-montmorillonite	all	27, 51, 3, −5	hydrolysis	45
Al-montmorillonite	isomerization	30	mineralization	5
Cu(II)-montmorillonite	oxidation	−11	oxidation	−6

surface hydrology [66]. Therefore, there is a need for alternatives to conventional fracking fluids, and the use of supercritical CO_2 ($scCO_2$) is a promising technology that will become, as well, a potential carbon storage facility.

However, its efficient implementation requires a precise understanding of the dynamics and reactivity of this gas in shales. In this sense, clay minerals have received a great deal of attention, as they are important components of the deep sedimentary formations that are potential reservoirs for gas production and, even, for CO_2 geological sequestration [67-82].

The competitive interactions between CO_2, H_2O and CH_4 (methane is the most common gas in natural gas) with clays are, consequently, critical to understanding fluid behavior in these situations. The combination of NMR and computational studies has been particularly effective in shedding light on these problems. Moreover, recent developments in NMR allow investigation of fluid behavior in confined geometries at pressure up to 138 bar and 427 K [83,84].

Experimental studies have shown that CO_2 can be intercalated into smectites interlayers [85,86]. Kirkpatrick et al. [87] made an extensive review of the use of NMR and molecular dynamics (MD) in the study of the structural and dynamical behavior of cations, anions, H_2O and CO_2 in the interlayer galleries of clay minerals, while Bowers' group has made important contributions in this area using in situ high pressure and high temperature NMR experiments. In hectorite, Bowers et al. [88] demonstrated the importance of the interlayer cation in understanding the intercalation of CO_2 and the dynamics of interlayer CO_2 molecules through the use of ^{13}C MAS-NMR at variable humidity. Their results were later confirmed by computational molecular modeling [89-95].

Intercalation of dry CO_2 (solid $scCO_2$) in smectite interlayers has been less extensively studied but it may have significant application when dry CO_2 is injected into the subsurface. Dry CO_2 can dehydrate the smectite interlayers, cause swelling or shrinking of the clay, and thus can generate mechanical stresses and alter the overall pore structure of shale caprocks. Using in situ NMR at 90 bar and 323 K Loganathan et al. [89] examined the structure, dynamics and energetic intercalation of dry CO_2 in hectorite, containing divalent interlayer cations (Ca^{+2}, Cs^{+2}) with different ranges of hydration and solvation properties. Their experimental results, combined with Grand Canonical Molecular Dynamics (GCMD) simulations, showed that the intercalated CO_2 molecules are oriented on average with their O-C-O axes parallel to the basal hectorite surfaces.

Using the same NMR equipment that allows high pressure and high temperature measurements, Schaef et al. [96] analyzed the interaction between $scCO_2$ and a montmorillonite clay with different interlayer cations: Na^+, Cs^+ and NH_4^+ (Fig. 5). Their NMR results, combined with GCMD, revealed that $scCO_2$ does not strongly solvate the interlayer cations, and the tendency to swell is controlled by the strength of the interlayer cation interaction with the aluminosilicate framework; Cs^+ and NH_4^+ are the interlayer cations that preferentially favor the incorporation of $scCO_2$ [96].

The efficient selection of a new alternative for hydraulic fracturing requires a detailed understanding of CH_4 binding and dynamics in shales and specifically in clays. This remains challenging under reservoir pressure and temperature conditions [97], where H_2O is likely to have a significant effect on CH_4 adsorption and dynamics. Much of what is known about the interactions between CH_4 and smectites comes from GCMC methods, since spectroscopy studies have so far been limited [98,99], although they are nonetheless extremely important when conditions relevant to natural gas and carbon sequestration reservoirs are analyzed. Bowers et al. [100] studied the interaction between wet supercritical methane ($scCH_4$) and hectorite under conditions relevant to fracking and carbon sequestration (323 K and 90 bar) using ^{13}C MAS-NMR spectroscopy. Their results provided novel insight into the molecular-scale behavior of CH_4/smectite binding and showed that CH_4 can be adsorbed in both the interlayer galleries (resonance between −6 and −7.8 ppm depending on the interlayer cation) and in larger external pores between clay particles (resonance at −10.3 ppm) (Fig. 6). The main resonance observable in Fig. 6a is due to CH_4 present as bulk $scCH_4$ fluid that does not interact with the hectorite particles on the NMR time scale. When increasing relative humidity (RH), the chemical shift of the peak associated to CH_4 in the interlayer space of smectite (ca. −6 ppm) becomes more negative and its relative intensity decreases (Fig. 6b), consistent with a decreasing preference of the interlayer space for CH_4 relative to H_2O. That means that CH_4 can be adsorbed in smectite interlayers only when the H_2O content is small, as may occur during a dry $scCO_2$ flood in a fracking exploitation.

In a very recent publication, Bowers et al. [101] analyzed the adsorption and dynamics of CH_4 for three smectites: synthetic laponite, natural SHCa-1 hectorite and a synthetic 100% fluorinated hectorite, using ^{13}C Bloch decay MAS-NMR and 2D MAS exchange spectroscopy NMR (EXSY) at 323 K and P_{fluid} = 90 bar, conditions equivalent to 1 km depth in the earth. They observed three distinct sites for CH_4 in smectites: in the interlayer nanopores (between −7.84 and −3.2 ppm), in pores between the clay particles (ca. −10 ppm) and in bulk fluid likely in the headspace of the NMR rotors (at −10.3 ppm). They observed that the ^{13}C chemical shift of CH_4 is sensitive to the size of the interlayer pore, the size of the exchangeable cation and the humidity. Moreover, the smectite layer charge is the most influent factor in CH_4 uptake. They also proved that 2D EXSY NMR is an effective method to investigate site or conformation exchange in clay minerals, and for the first time, this technique had been used to directly probe CH_4 exchange between adsorption sites in smectites. Bowers et al. examined Cs-laponite (vacuum dried) at variable mixing times, from 0.1 ms to 400 ms, and observed that when mixing times were > 5 ms, the EXSY spectra (Fig. 7) contained cross peaks between the peak for interlayer CH_4 at −7.4 ppm and that for interparticle CH_4 at −9.4 ppm, meaning an exchange frequency between 10^2 and 10^4 Hz. Cross peaks, indicating exchange between the interlayer and the bulk-like CH_4, first appeared at a mixing time of 50 ms (20 Hz exchange rate). These exchange dynamics contribute to the chemical shift distribution and the presence of the different CH_4 adsorption sites in smectites making these results especially useful in the fluid transport during oil or gas production from shales.

2.1.3. Nuclear waste disposal

Deep geological repositories (DGR) are considered the most promising sites for disposing of nuclear waste containing long-lived radionuclides. This confinement is based on a multibarrier concept [102] that typically comprises the natural geological barrier provided by the repository host rock and an engineered barrier system (EBS). The isolation of wastes is achieved first through the inclusion of wastes in a chemically inert vitreous matrix inside corrosion-resistant metallic containers, second, through the geological barrier and the host rock. The vitreous matrix and the metal containers are protected by structural components such as concrete and clay minerals, which constitute the EBS. Clay-based materials are used to surround and protect the containers, to fill the void spaces in the repository and to limit the movement of groundwater and dissolved material.

The main challenge of DGR is to demonstrate that nuclear wastes will be effectively encapsulated for so long that any release that might take place in the future will have no impact on human health or on the environment. SS-NMR methods have been extensively applied in this context, especially in the first nuclear waste isolation step, vitrification, due to the amorphous character of

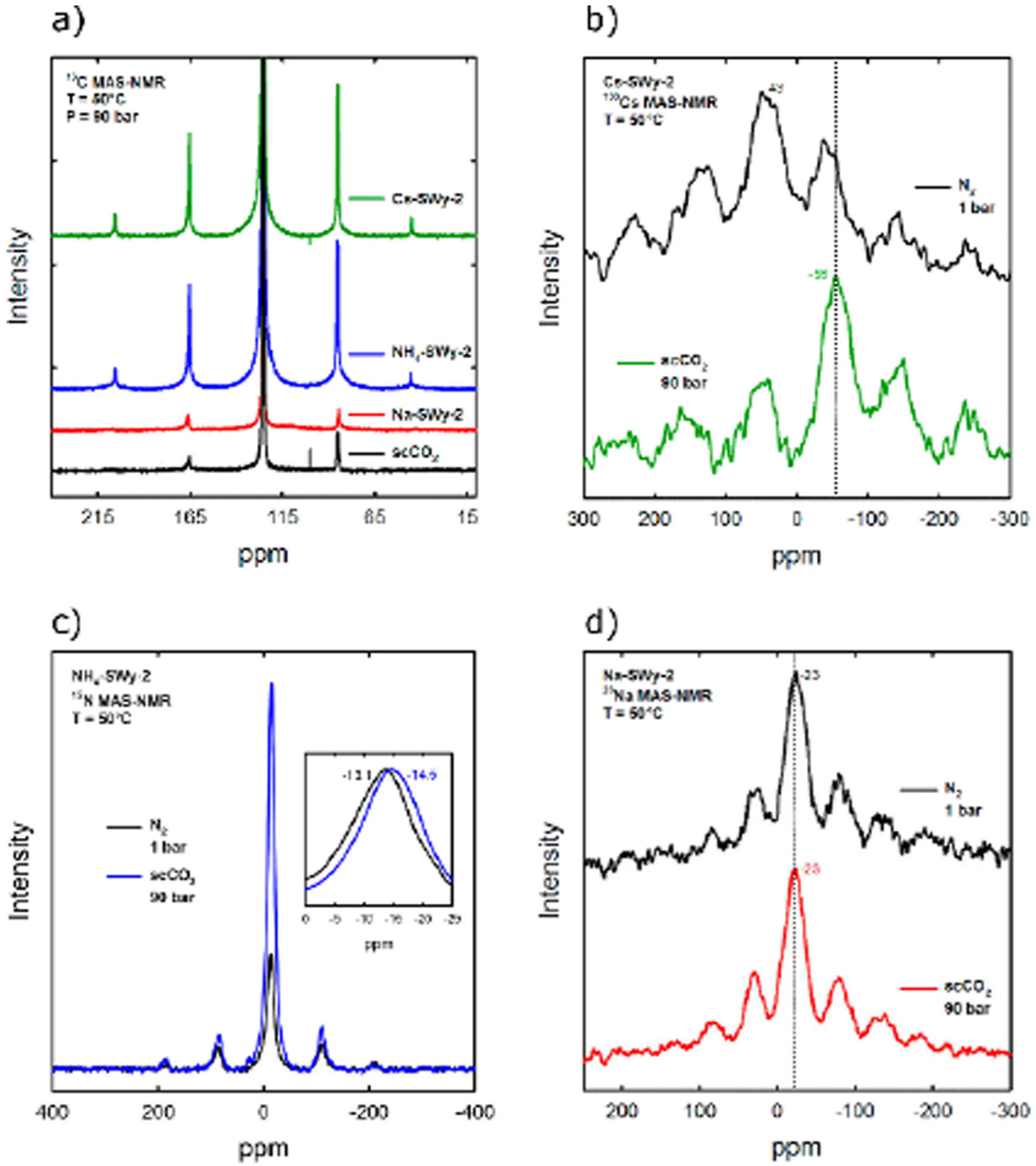

Fig. 5. a) ^{13}C MAS NMR spectra of neat $scCO_2$, Na-Wy-2-$scCO_2$, NH_4-SWy-2-$scCO_2$, and Cs-SWy-2-$scCO_2$; b) ^{133}Cs MAS NMR spectra of Cs-SWy-2 (top) and Cs-SWy-2-$scCO_2$ (bottom); c) ^{15}N MAS NMR spectra of NH_4-SWy-2 before (bottom) and during (top) exposure to $scCO_2$; and d) ^{23}Na MAS NMR of Na-SWy-2 (top) and Na-SWy-2-$scCO_2$ (bottom). Reproduced with permission from ref [96].

the proper vitreous matrix [103]. This technique has proved to be useful for obtaining information about the stability, chemical durability, reactivity and loading capacity of the different glasses investigated as vitreous immobilizers [104-108]. However, fewer studies can be found in the literature about the application of SS-NMR in studying the safety of the EBS. Clay minerals play a key role in this area, and SS-NMR can be a very useful technique due to its intrinsic short-range analyzing capacity and isotope-selectivity.

One of the main drawbacks of the EBS is that the surrounding geosphere is saturated with water. This groundwater will gradually flow back and eventually will cause a filtration of radionuclides (RN), from the canister barrier to the EBS and may provoke the clay mineral alteration, compromising their effectiveness as an engineering barrier [109-112].

Alba et al. [113-120] have extensively analyzed the interactions between RN and clay minerals, using rare earth elements (REE), especially lanthanides as RN simulators. During their work, they discovered a new retention mechanism, beyond the cation exchange, that allows the formation of new and stable silicate phases [113] containing REE cations, namely $REE_2Si_2O_7$. The use of ^{29}Si MAS NMR in determining of the extent of conversion into this new long-term retention mechanism has been crucial [114-119]. They established that the structure that favors the formation of this new disilicate phase, $REE_2Si_2O_7$, was: 2:1 clay mineral with trioctahedral character, no isomorphic substitution in the octahedral sheet and a small Si/Al ratio on the tetrahedral sheet. Moreover, having Na^+ as the interlayer cation was better than having Ca^{+2} [114]. The swelling effect did not affect to the formation of

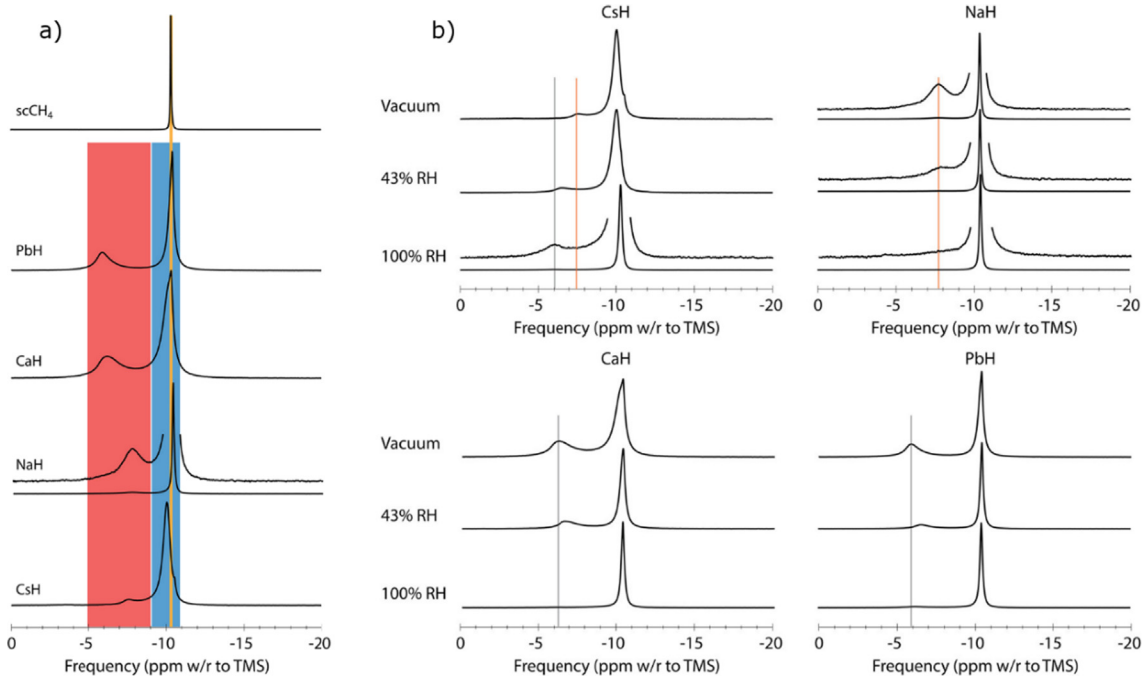

Fig. 6. ^{1}H-decoupled ^{13}C MAS NMR spectra of bulk $scCH_4$ in the various hectorite samples a) under vacuum and b) under different %RH values. See Ref. [100] for further details related to acquisition. Reprinted with permission from Ref. [100].

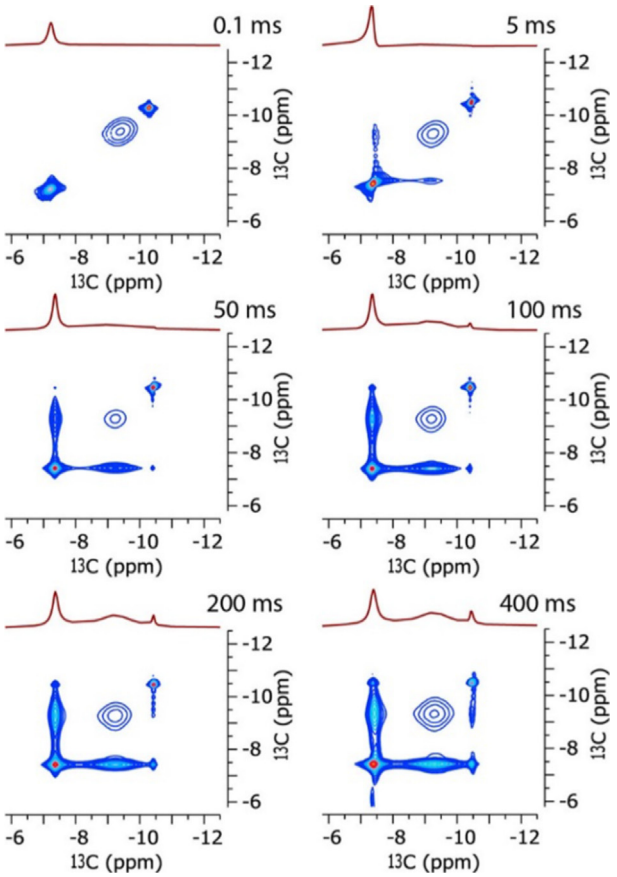

Fig. 7. 2D ^{13}C EXSY NMR spectra of vaccum dried Cs-hectorite. 1D trace at the top of each spectrum is the slice at −7.4 ppm showing interlayer CH_4. See Ref. [101] for further details and discussion. Reprinted with permission from Ref. [101].

these new phases [120], but the stability of the clay mineral did [118,119].

For economic and logistic reasons, the use of purified smectites is not considered in the high level radioactive waste (HLRW) international storage programs where FEBEX and MX80 bentonites have been selected as reference materials for the sealing of repositories [121]. Osuna et al. [122] analyzed their capacity for immobilizing actinides by chemical reaction, showing, thanks to ^{29}Si MAS-NMR, that both bentonites were able to form $REE_2Si_2O_7$ phases, and the MX80 sample is the most efficient barrier material as a higher amount of insoluble disilicate phase was generated [122].

MAS-NMR was also applied to study the hydrothermal stability of these two bentonites in water, basic and acid media. When bentonite is in contact with either acidic pore water or basic media, its structure can be modified, which is crucial for the safety of radioactive waste disposal. Using ^{29}Si MAS-NMR Osuna et al. [122] showed that after hydrothermal treatment in acidic medium the Q^4 component in the FEBEX spectrum was less intense (Fig. 8) and they inferred that there was a diminution in the amount of impurities in MX80 bentonite. In the FEBEX sample, after the hydrothermal treatment, the Q^3(1Al) signal was lost, indicating the leaching of tetrahedral Al. With ^{27}Al MAS-NMR they corroborated the dissolution of the impurities after hydrothermal treatment, as, in both cases, the q^4 environments are absent in the spectra (Fig. 8)

Nuclear accidents, like the one at Fukushima Daiichi nuclear plant in 2011 [123,124] and Chernobyl in 1986 [125,126] have resulted in the release of numerous radionuclides into nearby soil [127-130]. Among them, radioactive Cesium is one of the most hazardous radionuclides due to the emission of gamma radiation, long half-life ($t_{½}$ =30.2 years), high solubility in water and chemical similarity to potassium ion that facilitates its mobility in soils and clay minerals [131-135]. Hence, fundamental understanding of the interactions between Cs and clay minerals, as soils' main component, is of great importance in nuclear waste disposal and remediation. The migration of radioactive cesium in bentonites has been

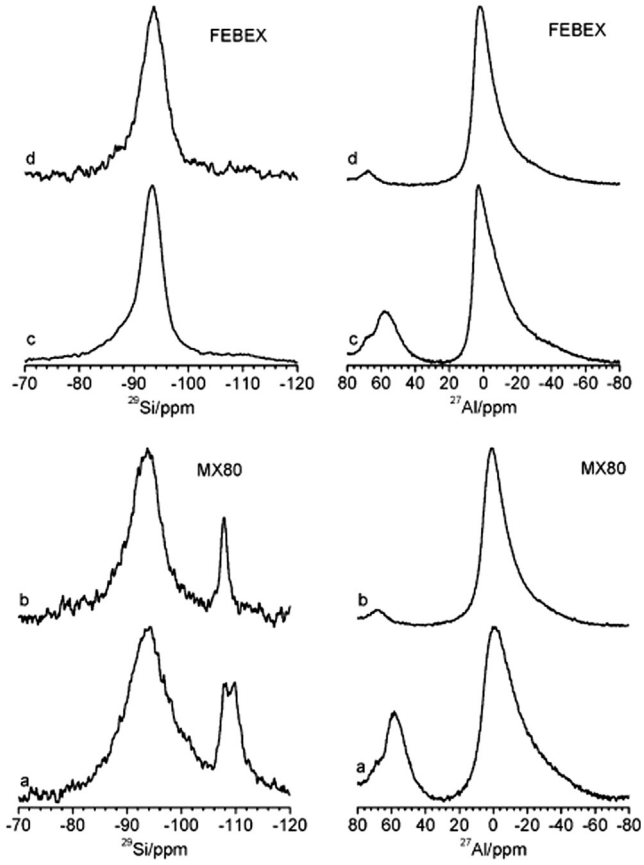

Fig. 8. ^{29}Si and ^{27}Al MAS NMR spectra of bentonite FEBEX (upper) and MX80 (down): (a, c) starting materials, and, (b, d) after hydrothermal treatment at 300 °C for 48 h in 0.01 M HNO_3. . Reproduced with permission from [122]

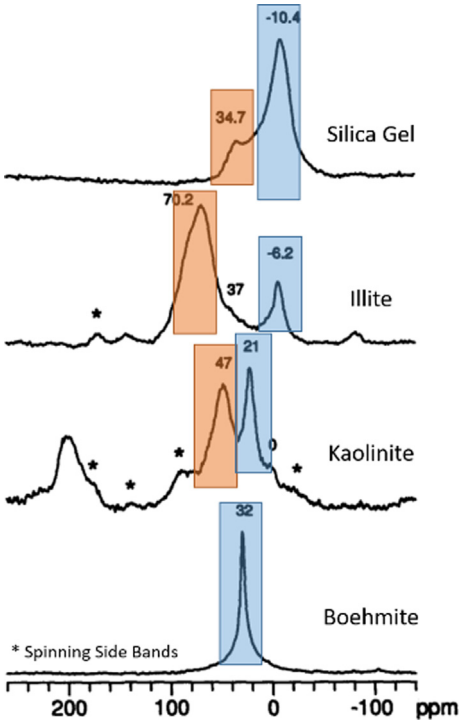

Fig. 9. ^{133}Cs MAS NMR spectra of the different clay minerals analyzed by Kim et. al. [141] See original paper for further details about acquisition. Adapted with permission from Ref. [141].

extensively studied, and it is generally accepted that Cs^+ adsorbs on montmorillonite through a cation exchange reaction, having minor contributions from a small number of frayed edge sites [127,136]. ^{133}Cs SS-NMR is found to be a useful technique to examine the adsorption of Cs in clay minerals [137-145].

In fact, Kim et al. [141] studied the adsorption of Cs on illite, kaolinite, bohemite and silica gel using ^{133}Cs, showing that there were two Cs adsorption sites, namely Cs1 (blue region in Fig. 9) and Cs2 (red region in Fig. 9). The first of these corresponds to a tightly bonded site forming inner sphere complexes, whereas the second, Cs2, comprised loosely bonded or outer sphere complexes [140]. Moreover, they discovered that humidity, and clay structure greatly affect the chemical shift of these two Cs sites.

Later, Ejeckam et al. [138] studied the influence of temperature and pressure on the adsorption of Cs^+ by a set of clay minerals to simulate conditions similar to those present in the DGR. They examined clay minerals with different chemical compositions and swelling capacity: montmorillonite (STx-1), kaolinite (KGa-1) and vermiculite (VTx-1), and applied ^{27}Al, ^{29}Si and ^{133}Cs MAS NMR. ^{133}C MAS NMR allowed quantification of the amount of cesium incorporated into the clay minerals in the two distinct sites, Cs1 and Cs2. The authors showed that montmorillonite can absorb Cs^+ and effectively remove it from aqueous solutions. The majority of the Cs^+ adsorbed is strongly bonded to the basal oxygen atoms of the tetrahedral sheet. This sorption site ensures that Cs^+ will be strongly held in case that a linkage from the DGR occurred. Moreover, they observed that the incorporation of cesium into the interlayer space of the clay caused adjacent Si and Al to become more shielded, causing negative shifts in the ^{27}Al and ^{29}Si MAS NMR spectra.

However, recently Ohkubo et al. [146] used DFT calculations, ^{133}Cs MAS-NMR and high magnetic fields (18.8 T) to conduct a methodical study of the adsorption of Cs^+ in montmorillonite clays and investigated the correlations between ^{133}Cs chemical shift and local structure on these clay minerals. Synthetic and natural montmorillonites with different amounts of adsorbed Cs^+ and different hydration states were analyzed. Despite previous publications where two distinct sites for Cs were identified in clay minerals [137,138,141,144,145], these authors found three distinct peaks in ^{133}Cs spectra of dehydrated clays. This results were obtained thanks to the enhanced resolution obtained at high magnetic field (Fig. 10). DFT calculations were carried out to allow correct assignment of these peaks (Fig. 11):

- Peak A (100 to −10 ppm): adsorbed Cs^+ around the center of hexagonal cavity containing Al^{+3}.
- Peak B (-30 to −70 ppm): adsorbed Cs^+ around the center of an empty hexagonal cavity.
- Peak C (-100 to −140 ppm): adsorbed Cs^+ on the open nanopore surface.

When the amount of incorporated Cs^+ is small, the preferred adsorption site is site A; however, when more Cs^+ is incorporated the other two sites can be occupied. When hydration increased, only one narrow peak was observable in the ^{133}Cs MAS NMR, resulting from Cs^+ hydration, meaning that Cs^+ hydration structure was identical for the resolved three sites due to motional averaging.

Subcritical pressures and temperatures occurring in the deep geological repositories (DGR), may provoke a chemical interaction between RN, as seen before, and the clay minerals present in the DGR in case that a linkage of the radionuclide occurs. Osuna et al. [142] analyzed what would happens if Cs^+ is in contact with high charge swelling micas, a proposed new material to be used in

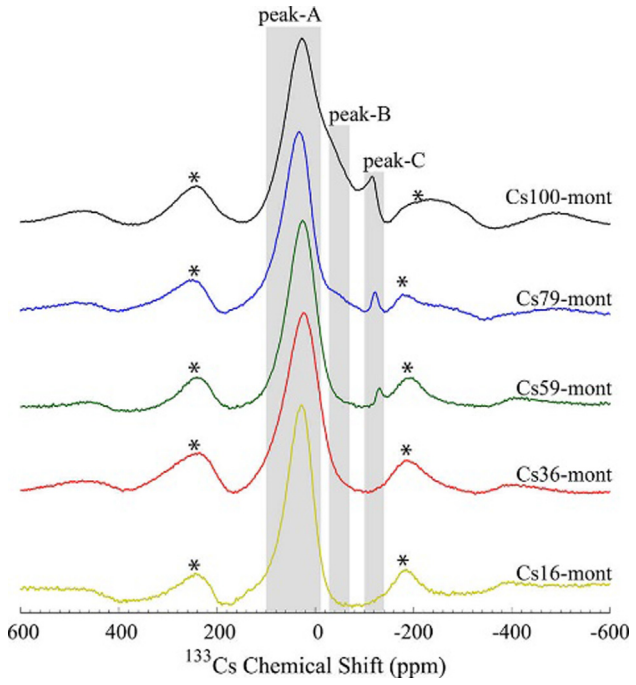

Fig. 10. ^{133}Cs MAS NMR spectra of dehydrated montmorillonite with 16, 36, 59, 79 and 100% Cs exchange recorded at 18.8 T. The symbol * denotes the spinning side bands. Reproduced with permission from Ref. [146].

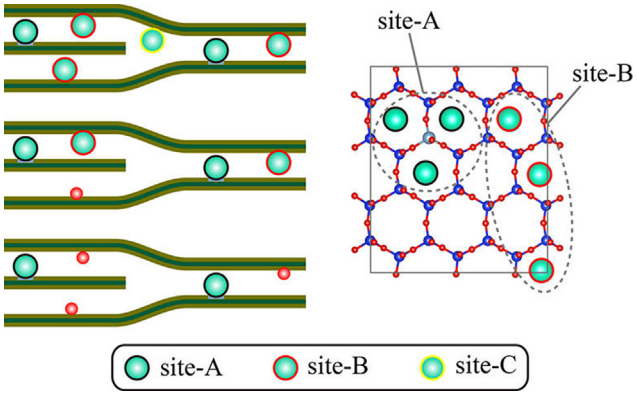

Fig. 11. Schematic illustration of Cs^+ adsorption with increasing Cs substitution. Cyan bars correspond to Al positions in tetrahedral sheets. Red balls on the sheet represent Na. Cs at site-A, B and C are outlined in black, red and yellow respectively. See Ref. [146] for further discussion. Reproduced with permission from [146].

the DGR that offers better reactivity and cation exchange capacity than natural clays [117]. Using a multinuclear NMR approach combining ^{133}Cs, ^{29}Si, ^{23}Na and ^{27}Al data, they concluded that high charge swelling micas were able to immobilize Cs^+ under subcritical conditions, combining cation exchange reactions with adsorption at their surface and chemical reaction [142].

2.1.4. Heavy metal removal

Environmental remediation has increased the need for obtaining fundamental knowledge about the interactions between heavy metal cations and clay minerals. Indeed, questions such as how heavy metals are bound to layer silicates, their mobility in these materials or the chemical environment of the adsorbed ions are of fundamental importance in order to have a proper understanding of the remediation mechanisms.

Heavy metals persistence in the environment provokes ecotoxicological effects due to their accumulation. Clay minerals have been extensively studied as inexpensive adsorbents materials for these pollutants. There are several reviews about the main advances on heavy metal adsorption by clay minerals [147-151]. However, few of them use SS-NMR to understand the reactions involved in the adsorption of these important pollutants, although this technique has previously shown its potential to investigate the environment of exchangeable cations. Hence, it can be very useful in determining and elucidating the adsorption mechanism of heavy metals by clay minerals [152,153].

Among heavy metal cations, Pb^{+2}, Hg^{+2}, Cu^{+2}, Cd^{+2}, Cr^{+2} and Zn^{+2} constitute a major threat to human health, due to their abundance and toxicity [148]. The determination by SS-NMR of their chemical environment once adsorbed into clay mineral is challenging, which might be one reason why there are only a few relevant studies. Table 2 shows a summary of the main heavy metal nuclei active visible by NMR. Heavy NMR-active nuclei such as ^{195}Pt, ^{199}Hg, and ^{207}Pb commonly exhibit chemical shifts over ranges of well over 1000 ppm. Thus, acquiring NMR spectra of polycrystalline samples is often an experimental challenge because of the resulting very broad powder patterns.

For example, ^{207}Pb spectra often cover 11.500 ppm or more due to the large chemical shift anisotropies (CSAs), and in addition it has relatively long spin–lattice relaxation times that necessitate long spectral accumulation times [154]. Furthermore, its chemical shifts are very sensitive to temperature [155] and consequently high spinning speed is not recommended due to sample heating and temperature gradients across the sample, making the acquisition of this nucleus a very difficult task in SS-NMR [156,157].

The same issues occur for ^{199}Hg, one of the main heavy metal pollutants due to its toxicity. It also has relatively long spin–lattice relaxation times and large CSAs, hence its study was for a long time restricted to the solution state. At the end of the 20th century, however, SS-NMR measurements of ^{199}Hg started to be reported in proteins [158-160] and inorganic mercury compounds [161] using slow MAS experiments. However, the number of SS-NMR experiments of ^{199}Hg is still limited and their acquisition remains challenging.

In recent times, a new perspective is opening in relation to these nuclei, as novel methodologies developed in SS-NMR have made possible the acquisition of high-resolution spectra from these heavy metal nuclei [162,163]. Other heavy metal nuclei, except cadmium, as we will see later, are quadrupolar, and hence they are intrinsically difficult to measure by SS-NMR (Table 2).

Cadmium represents a good option to study the interactions between clay minerals and heavy metals. The two NMR-active Cd nuclei have a ½ spin and similar natural abundance (Table 2). However, ^{113}Cd has a relative receptivity slightly better than ^{111}Cd, making it the preferred NMR nucleus in many Cd NMR studies. ^{113}Cd has a chemical shift range larger than 900 ppm, and as we will see later, chemical shifts depend on the nature, number and geometric arrangement of the coordinated atoms. Despite the considerable literature concerning ^{113}Cd SS-NMR in proteins and coordination compounds [164,165], only a few articles address the interaction between Cd^{+2} and swelling phyllosilicates.

The first study of ^{113}Cd SSNMR in clay minerals was carried out in 1989, by Bank et al. [166]. They studied cadmium exchanged montmorillonite and found two components (around 10 ppm) with the same chemical shift but different FWHM values. They interpreted them as arising from the Cd^{+2} sites heterogeneity in the montmorillonite structure. Later, Tinet et al. [167] using static NMR analysis, observed ^{113}Cd NMR peaks in Cd-exchanged hectorite and montmorillonite with two components that were attributed to signal anisotropy rather than to different adsorption sites. The anisotropy was supposed to be due to Cd^{+2} interaction with OH^- groups from the different smectites.

Table 2
Active NMR Heavy metal nuclei properties compared with ^{1}H nuclei.

Cation	Spin	Quadrupolar moment (10^{-30} m^2)	Natural abundance	Sensitivity		NMR frequency (MHz) at a field (T)	
				rel*	abs**	14.0926	18.7900
^{1}H	½	–	99.98	1.00	1.00	600.00	800.00
^{207}Pb	½	–	22.6	$9.16{\cdot}10^{-3}$	$2.07{\cdot}10^{-3}$	125.530	167.374
^{199}Hg	½	–	16.84	$5.67{\cdot}10^{-3}$	$9.54{\cdot}10^{-4}$	106.962	142.618
^{201}Hg	3/2	38.6	13.22	$1.44{\cdot}10^{-3}$	$1.9{\cdot}10^{-4}$	39.598	52.798
^{63}Cu	3/2	–22	69.09	$9.31{\cdot}10^{-2}$	$6.43{\cdot}10^{-2}$	159.030	212.040
^{65}Cu	3/2	−20.4	30.91	0.11	$3.52{\cdot}10^{-2}$	170.366	227.154
^{111}Cd	½	–	12.75	$9.54{\cdot}10^{-3}$	$1.21{\cdot}10^{-3}$	127.232	169.642
^{113}Cd	½	–	12.26	$1.09{\cdot}10^{-2}$	$1.33{\cdot}10^{-3}$	133.096	177.462
^{53}Cr	3/2	−15	9.55	$9.03{\cdot}10^{-4}$	$8.62{\cdot}10^{-3}$	33.912	45.216
^{67}Zn	5/2	15	4.11	$2.85{\cdot}10^{-3}$	$1.17{\cdot}10^{-2}$	37.524	50.320

Di Leo and O'Brien[168] analyzed the influence of the cadmium solution concentration when exchanged with montmorillonite. They found that when the amount of cadmium involved in the exchange was small, only one peak was observable in the ^{113}Cd MAS spectrum, meaning a single adsorption site for this cation. However, when the Cd^{+2} concentration was high, three components were detected. The authors interpreted these peaks as a combination of two species on two adsorption sites: fully hydrated Cd^{+2} in the interlayer (−11 ppm), partially hydrated Cd^{+2} on the external surface of the smectite (−40 ppm) and $CdCl^{+}$ in the interlayer (116 ppm).

The mobility of cadmium in clay minerals has also been studied. Using ^{1}H-^{113}Cd and ^{27}Al-^{133}Cd double-resonance NMR experiments (VACP and SEDOR, respectively), Sullivan et al.[169,170] observed that the mobility of Cd^{+2} in dehydrated Cd-smectite was very low [169]. They concluded that the Cd^{+2} cation was held in the pseudotrigonal cavities of the interlayer. Later, Di Leo and Cuadros [171] analyzed the influence of the smectite structure in the cadmiun adsorption. They used two different smectites (montmorillonite and hectorite) and a low concentration solution of Cd^{+2}, as the cadmium concentration in surface waters is very low. In these conditions, only one main peak was observable at around 10 ppm, as in the previous studies by Di Leo and Brien [168]. They found that in the absence of tetrahedral substitutions (hectorite), all Cd^{+2} ions occupy the center of the interlayer, surrounded by water molecules. The particular montmorillonite exhibited small number of tetrahedral substitutions. In this clay, some Cd^{+2} ions seemed to be attracted toward the nearest oxygen atoms with excess of negative charge, interacting more strongly with them. This interaction results in a second ^{113}Cd NMR peak at a more negative value (around −25 ppm) than the main peak (around 10 ppm).

Heavy metal adsorption by clay minerals can be enhanced through a chemical modification of their interlayer space [172], as their cation exchange capacity is not sufficient for large-scale applications [173]. To increase the selectivity and adsorption capacity for heavy metals cations, the immobilization of chelating agents on clay minerals has been proposed as an effective alternative. Among all the possible surface modifications, thiol groups, -SH, exhibit a high binding selectivity toward the heavy metal cation and their intercalation in clay minerals through several organic compounds has been shown to increase the affinity and adsorption capacity of the silicates [172,174].

SS-NMR can help to analyze and understand the interactions that occur in the interlayer space of clay minerals when a chelating agent is present. Many such studies are focused on the characterization of the modified clay minerals but little information is provided about the changes in the structure after heavy metal adsorption.[175-178] There are a few articles dealing with the changes resulting from adsorption of heavy metal by these modified clay minerals. As an example, ElAdraa et al. [173] have studied, at the molecular level, the capacity of a cysteine-montmorillonite composite to adsorb several heavy metal cations, namely Hg^{2+}, Zn^{2+}, Co^{2+}, Cd^{2+}, Pb^{2+}, and Cu^{2+}, employing ^{13}C MAS-NMR experiments. In cysteine (Fig. 12), three signals attributed to C1 (thiol function, 30.3 ppm), C2 at 58 ppm and C3 (carboxylate) at 176.1 ppm can be easily identified in the ^{13}C MAS-NMR spectrum. The same signals can be identified in the montmorillionite sample with cysteine and after the adsorption of the different heavy metal cations. However, a shift in the C1 and C2 position is observed for Cd-, Hg-, Pb- and maybe Zn-cysteine-montmorillonite samples. This suggests the coexistence of two different cysteines with different bonding states. The shift is higher for C1 than C2, which indicates that this difference is related to the thiol group. Hence, NMR spectra highlighted the presence of complexes via the shifts observed for the different functional groups (C-SH and COO^{-}). These complexes may be responsible for the better adsorption behavior of the modified montmorillonite compared with the raw one.

2.1.5. Organic effluents cleaner /organic pollutant adsorption

Adsorption mechanisms of organic molecules in general, and organic pollutants in particular, in clay minerals have been previ-

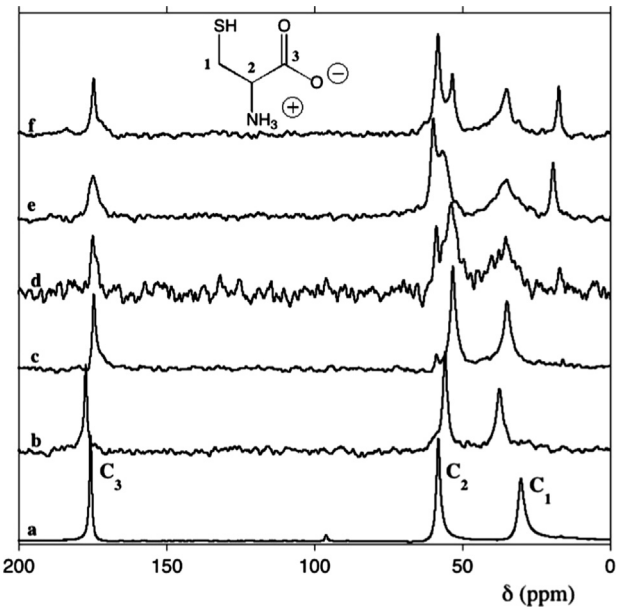

Fig. 12. ^{13}C MAS-NMR spectra of a. bulk cysteine, b. Cys-Montmorillonite, c. Zn-Cys-Montmorillonite, d. Cd- Cys-Montmorillonite, e. Hg-Cys-Montmorillonite, f. Pb-Cys-Montmorillonite. Reprinted with permission from Ref. [173].

ously discussed in reviews [179-189]. Interactions between layer silicates and organic molecules play an important role in pollutant migration, bioavailability and biodegradation. Among several available characterization techniques, SS-NMR has a huge potential to characterize the interactions of organic molecules with inorganic matrices such as clay minerals, as was recently reviewed by Bonhomme et al. [190]. However, its use is more focused on clay mineral based nanocomposites [191] than on organic pollutants adsorption, with some exceptions that will be discussed in the following section.

Maciel's group has extensively analyzed the adsorption of organic pollutants by clay mineral systems. Pesticide adsorption has already been described in Section 2.1.1; in the following, the main results concerning other organic pollutants are discussed.

Clay behavior when in contact with carbon tetrachloride, CCl_4 (known to cause ozone depletion and to affect the human central nervous system) and aromatic compounds (benzene) was examined by a SS-NMR approach (Fig. 13 and Table 3) [192]. Tao and Maciel used ^{13}C DP-MAS and CP-MAS experiments to shed a light on the interactions and catalytic behavior of three clay minerals (Ca-montmorillonite, K-10 montmorillonite and kaolinite) with these harmful organic pollutants. Fig. 13 shows that in DP-MAS experiments with the raw clay minerals (Fig. 13 A a-c) only the signals for benzene and $^{13}CCl_4$ can be observed (values shown in Table 3) and there is no evidence of chemical transformation of these pollutants. Differences are observed in the ^{13}C CP-MAS spectra, where the signal for benzene is only observed in the montmorillonite samples, whereas kaolinite spectra exhibited no signal from either benzene or $^{13}CCl_4$. It is reasonable that the carbon tetrachloride signal did not appear in the CP-MAS experiments because there was no intramolecular proton source that could contribute to the polarization. In kaolinite, the absence of the benzene signal suggested a liquid like motion of this molecule in this clay or a weak benzene-kaolinite interaction. However, in montmorillonite samples, a benzene signal is clearly observable in the ^{13}C CP-MAS experiment, indicating that this molecule is less mobile in these systems, implying a much stronger interaction with the clay mineral.

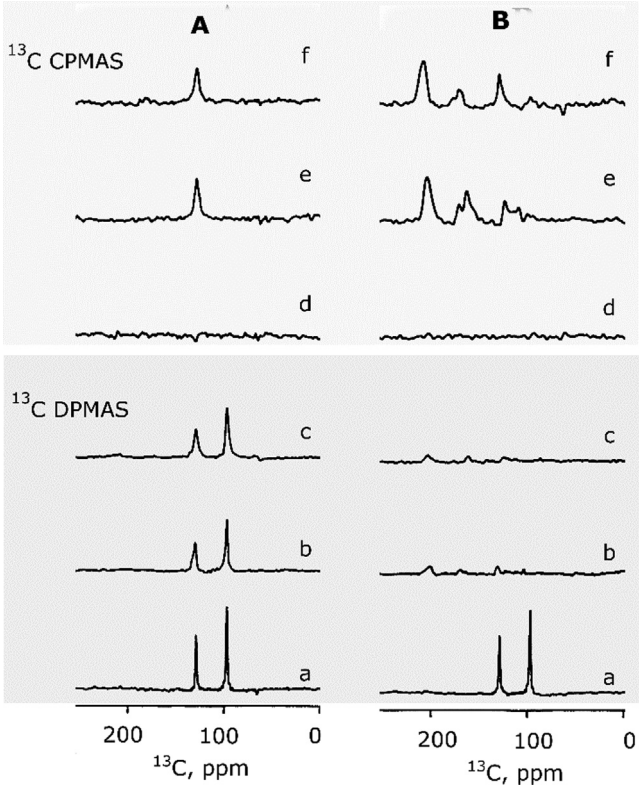

Fig. 13. ^{13}C DP-MAS (a-c) and CP-MAS (d-f) NMR spectra of samples of benzene and ^{13}C-labeled carbon tetrachloride on (A-a, A-d) kaolinite, (A-b, A-e) Ca-montmorillonite, (A-c, A-f) K-10 montmorillonite, (B-a, B-d) Zn^{2+}-exchanged kaolinite, (B-b, B-e) Zn^{2+}-exchanged Ca-montmorillonite, and (B-c, B-f) Zn^{2+}-exchanged K-10 montmorillonite. See Ref. [192] for further information about acquisition. Adapted with permission from Ref. [192].

A different behavior is observed when Zn^{+2} is intercalated in the interlayer space of the three clays that were analyzed (Fig. 13B). Whereas there is no difference between the CP-MAS and DP-MAS spectra of the Zn^{+2}-kaolinite sample compared with the raw one, both Zn^{+2}-montmorillonites spectra showed that these clays can catalyze the reaction of carbon tetrachloride and benzene, converting these volatile pollutants into less volatile compounds: triphenylmethyl carbon cation (~209 ppm) and benzophenone (~197 ppm).

The adsorption of benzene into Cu^{+2}-montmorillonite was previously analyzed by Hinedi et al. [193]. However, only poor-quality spectra were obtained due to paramagnetic interactions with Cu^{2+} centers. Nevertheless, they were able to observe signals in the aliphatic region, showing that benzene was chemically unstable in this environment. Later, Xiong and Maciel [194] using ^{2}H NMR experiments on ^{2}H-labeled benzene adsorbed on Ca-montmorillonite clay provided new insight into the molecular motion of benzene in these clays. They observed that benzene loading into the clay affects the bonding formed between them, and that the fraction of benzene molecules that underwent isotropic reorientation increased with temperature. With higher benzene loading, above 2.7% w/w, the excess benzene molecules were weakly adsorbed in the clay. They showed that that ^{2}H NMR experiments were an extremely powerful tool for elucidating details of local motions of organic pollutants adsorbed on a soil component.

Another organic pollutant adsorbed onto clay minerals that was analyzed by Maciel's group was trichloroethylene (TCE). Tao et al. [195] used ^{13}C DP-MAS to analyze the capability of Ca^{+2}-montmorillonite, Cu^{+2}-montmorillonite, Zn^{+2}-montmorillonite and kaolinite to degrade TCE induced by irradiation by long-wavelength UV light. TCE is an environmentally significant pollutant, widely used in dry cleaning among other industrial processes [196]. ^{13}C DP-MAS experiments showed that dichloroacetic acid, a known animal carcinogen more potent than TCE, was the major organic product/intermediate (δ (TCE) = 116 and 123 ppm, vs δ (dichloroacetic acid = 65 and 169 ppm). Substantial amounts of pentachloroethane (δ = 80 and 100 ppm) and trichloroacetic acid (δ = 90 and 166 ppm) were also identified in the ^{13}C DP-MAS spectra of Ca-montmorillonite samples. The authors observed that, qualitatively, the conversion of trichloroethylene to dichloroacetic acid in a 48-h period occurred with the following order of efficiencies: Zn^{2+}-montmorillonite > kaolinite > Ca^{2+}-montmorillonite > C u^{2+}-montmorillonite.

2.1.6. CO_2 capture

Carbon sequestration has been proposed as an effective method to reduce atmospheric CO_2, especially from stationary sources [198]. Among the several materials investigated, amine-modified nanoporous materials, in particular clay minerals, have been proposed. [199-204] However, the characterization of the interaction between CO_2 gas, grafted amine groups and the surface of clay minerals at the molecular level is a challenging task. SS-NMR can allow comprehensive study of the interaction of CO_2 molecules with the grafted amine groups and the correlation of this information with the CO_2 adsorbed amounts, adsorption heats, and amine loadings.

In fact, Pinto et al. [197] analyzed the interaction between CO_2 and porous clay heteroestructures (PCH), derived from natural

Table 3
^{13}C Chemical Shifts and Line Widths of ^{13}C DP-MAS Spectra of ^{13}C-Labeled Carbon Tetrachloride and Benzene adsorbed onto Kaolinite, Ca-Montmorillonite, and K-10 Montmorillonite.

	Carbon tetrachloride		Benzene	
	$\Delta\nu_{1/2}$ (Hz)[a]	δ (ppm)[b]	$\Delta\nu_{1/2}$ (Hz)[a]	δ (ppm)[b]
Ca-montmorillonite	41.3	95.4	61.1	128.2
K-10 montmorillonite	75.6	96.1	92.8	128.6
kaolinite	34.1	95.3	39.3	127.5

[a] ± 3.4 Hz; [b] ± 0.2 ppm.

clays and modified with 3-aminopropyltriethoxysilane (APTES) using ^{13}C high power decoupling (HPDEC), ^{13}C CP-MAS and ^{15}N CP-MAS (Fig. 14 and Fig. 15, respetively).

In the ^{13}C HPDEC NMR spectrum of PCH a single peak was observed at ca. 125 ppm, attributed to CO_2 physically adsorbed with high mobility. However, for the sample with APTES, four more resonances were seen, three peaks assigned to APTES propyl chain carbons (43, 22 and 9 ppm) [205] and one strong peak at 164 ppm. This last peak was identified as corresponding to carbamate species, formed during the reaction of CO_2 with the amine groups on the surface of the solid [206-211].

^{15}N CP-MAS NMR spectra, recorded in natural abundance, revealed that when CO_2 is adsorbed in a PCH-APTES sample, two peaks associated to the carbamate species and to amine can be observed at −297 and −350 ppm, respectively. Those peaks are not observable in the samples without CO_2. These results confirmed that the nitrogen nuclei of the amine group undergo changes when CO_2 is adsorbed due the interactions between the CO_2 molecule and NH_2-R groups. They also showed that the amount of CO_2 adsorption was related to the amine loading of the PCH material.

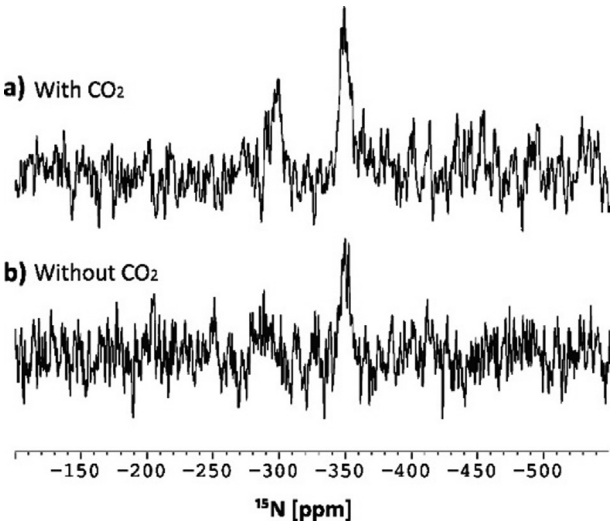

Fig. 15. ^{15}N CP-MAS NMR spectra of PCH + APTES a) with and b) without adsorbed CO_2. Reprinted with permision from Ref. [197].

2.2. Pharmaceutical applications-Drug delivery

Clay minerals are widely employed in the pharmaceutical industry as both excipients and active substances that allows a target antibiotic or targeted therapy to treat cancer [212]. Moreover, in recent years, clays and their modified forms have been proposed as drug delivery systems, DDS, due to their high retention capacity as well as swelling and colloidal properties. In this sense, several review articles discuss drug-clay interactions [212-221], but unfortunately, less work is dedicated to fully understanding the mechanisms that produce the slow drug delivery using SS-NMR. Table 4 gathers the most recent research where solid-state NMR (mostly $^{13}C/^{1}H$ CP-MAS) is applied to study interactions between clay minerals and drugs.

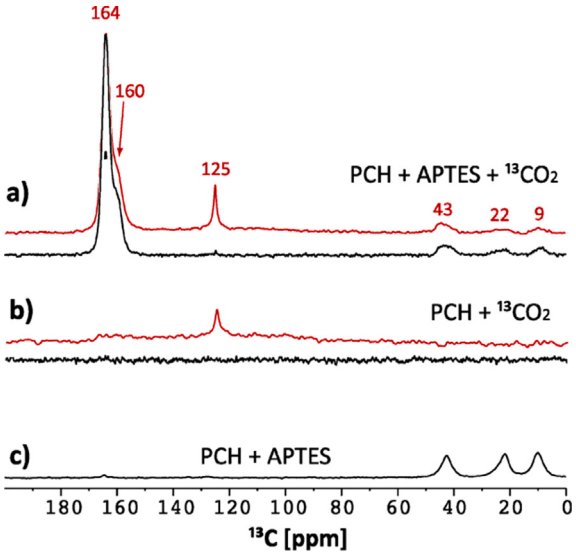

Fig. 14. ^{13}C CP-MAS NMR spectra (black) and HPDEC NMR specta (red) of a) PCH + APTES with adsorbed $^{13}CO_2$ b) PCH, with adsorbed $^{13}CO_2$ and c) PCH + APTES. Adapted with permision from Ref. [197].

SS-NMR has also been applied in the development of new nanocomposites based on clay minerals and polymers and biopolymers, especially designed to improve drug delivery systems. For example, Wang et al. [222] analyzed a novel chitosan derivate, QCMC (Quaternized carboxymethyl chitosan) intercalated into rectorite (2:1 phyllosilicate from mica family) and an organic modified rectorite to improve the former drug delivery capacity. By interpreting ^{27}Al MAS NMR and ^{29}Si MAS NMR, they concluded that the strong interaction between QCMC and the clay minerals is responsible for the improved thermal stability and drug-controlled release properties. ^{1}H NMR relaxometry analysis in a low-field NMR spectrometer was used by Correia Villaça et al. [223] to characterize a layered silicate nanocomposite, composed of montmorillonite and different polymers (PVP, polyvinylpyrolidine and PQH, polyquaternium-H), with broad applications in the pharmaceutical industry. The low relaxation parameter value obtained for the nanocomposite PQH-Montmorillonite confirmed that strong interactions occurred between the polymer and montmorillonite which include dispersion of the hydrophilic silicate in the polymer chains. Moreover, in the PVP-montmorillonite nanocomposite, the analysis of the T_1H value suggested the formation of a new system with a high degree of exfoliation without clay intercalation products and an increased molecular mobility of the polymer chains.

Table 4
Controlled release systems studied by SS-NMR.

Drug	Drug properties	Clay mineral	NMR technique	Ref.	Date
Sertraline	antidepressant	Montmorillonite-K10 MCM-41	^{29}Si MAS ^{13}C MAS ^{29}Si/^{1}H CP-MAS ^{13}C/^{1}H CP-MAS DFT calculations	[224]	2007
Nicotine	smoking cessation therapy	Magnesium aluminum silicate [226,226]	^{29}Si CP-MAS	[227]	2009
Propranolol hydrochloride (PPN)	angina and hypertension	Magnesium aluminum silicate [226,226]	^{29}Si CP-MAS	[228]	2010
Pravastatin	Hypercholestor-olaemia	Layered double hydroxide, LDH	^{13}C MAS ^{13}C/^{1}H CP-MAS	[229]	2012
EUS[230]	UV-B adsorber; sunscreen agent	Mg/Al LDH Zn/Al LDH	^{13}C/^{1}H CP-MAS	[231]	2013
PABA[232]	UV-B adsorber; sunscreen agent	Mg/Al LDH Zn/Al LDH	^{13}C/^{1}H CP-MAS	[231]	2013
GLI[233]	diabetes mellitus type II	Mg/Al LDH Zn/Al LDH	^{13}C/^{1}H CP-MAS	[231]	2013
FURO[230]	diuretic drug	Mg/Al LDH Zn/Al LDH	^{13}C/^{1}H CP-MAS	[231]	2013
DIK[235,235]	anti-inflammatory	Mg/Al LDH Zn/Al LDH	^{13}C/^{1}H CP-MAS	[231]	2013
KET[236]	anti-inflammatory	Mg/Al LDH Zn/Al LDH	^{13}C/^{1}H CP-MAS	[231]	2013
RET	metabolite of vitamin A_1	Mg/Al LDH Zn/Al LDH	^{13}C/^{1}H CP-MAS	[231]	2013
Clipidogrel bisulfate	antiplatelet, reduces the risk of heart disease	Montmorillonite-APTES- β-Cyclodextrin	^{29}Si MAS ^{1}H MAS	[237]	2014
Ibuprofen (Ibu)	anti-inflammatory	LDH-D Layer Hydroxide salts, LHS-D	^{13}C/^{1}H CP-MAS	[238]	2015
Naproxen (Nap)	anti-inflammatory	LDH-D LHS-D	^{13}C/^{1}H CP-MAS	[238]	2015
Ketoprofen (Ket)	anti-inflammatory	LDH-D LHS-D	^{13}C/^{1}H CP-MAS	[238]	2015
Dexamethasone, DEX	corticosteroid	Laponite	^{13}C/^{1}H CP-MAS ^{13}C DD	[239]	2016
Pilocarpine (Pilo)	controls intraocular pressure associated with glaucoma	Laponite	^{13}C/^{1}H CP-MAS	[240]	2017
Metformin (MF) hydrochloride	type 2-diabetes	Montmorillonite	^{13}C/^{1}H CP-MAS	[241]	2018

2.3. Heterogeneous catalysis

The diverse catalytic activity of clay minerals is derived mainly from four sources: Brønsted acidity, Lewis acidity, presence of redox active species and introduction of catalytically active (mainly) transition metals or cations. Such activity can be either a natural property of the clay or induced by cation exchange, acid activation or deposition of the co-catalyst into the clay surface.

There is an extensive literature describing the use of SS-NMR spectroscopy for catalyst processes involving clay minerals. In this review, petrochemical processes, hydrogenation, oxidation and polymerization have been selected as examples of the most common catalytic applications where clay minerals are involved and SS-NMR can provide a significant insight.

In general, SS-NMR was used for studying the catalyst active center, its structure and to follow the 'in situ' transformations of the adsorbed species at the catalyst clay surface.

2.3.1. Petrochemical processes

In this section, we will discuss the contribution that SS-NMR brings to elucidating the influence of clay minerals on basic catalytic reactions such as cracking, isomerization and reforming involved in the petrochemical processes.

Most of the NMR studies have been applied to pillaring clays, PILCs, with Keggin cations, a polyoxycation of aluminum with formulae $[Al^{IV}(Al_{12})^{VI}O_4(OH)_{24}]^{7+}$, as they have been employed as cracking catalysts [242-244] due to their high thermal stability and surface area with a two-dimensional porous structure [245]. These studies have been applied to analyze the improvement of their catalytic properties due to a variety of pillaring agents, preparative conditions, active centers or structure. In the following, the main SS-NMR results in this area during the last years are exposed classified in two sections. In the first one, the influence of the heavy metal ions incorporated in the Keggin cation on the catalytic behavior of PILCs will be discussed. In the second, modifications on the PILCs synthesis route will be analyzed:

2.3.1.1. Catalytic properties modification by the incorporation of metallic ions in the Keggin cation. Although the most common pillared clays (PILCs - clay minerals with hydroxypolymers in the interlayer space) are prepared with aluminum polymers and (generally) montmorillonite, several reports investigated the effect of coexistence of some other metallic ions or complexes with Al-PILC [246-248].

In particular, Zhao et al. [249] investigated new routes of synthesis and characterization of LaAl-PILC, and its catalytic properties in cumene cracking and disproportionation and alkylation of 1,2,4-trimethylbenzene (1,2,4-TrMB). ^{27}Al MAS NMR spectra suggested that when La^{3+} was added after aging of hydroxy-Al oligocations, La^{3+} replaces Al^{3+} in the Al_{13} complex to produce a species $[Al^{IV}(Al_{12-x}La_x)^{VI}O_4(OH)_{24}]^{7+}$, in PILCs [249]. However, when hydroxy-LaAl oligocations were prepared before aging, La^{3+} copolymerized with Al^{3+}. When La^{3+} was incorporated into the alumina pillar the thermal stability was enhanced and, moreover, the cracking activity of cumene and selectivity for disproportionation of 1,2,4-TrMB increased.

Based on a ^{27}Al MAS NMR study, Kurian and Sugunan [250] reported the activities of iron and iron aluminum mixed pillared montmorillonites (Fe-PILC and FeAl-PILC, respectively) for the decomposition of cyclohexanol. Fe-PILC showed two ^{27}Al resonances: one at 1.38 ppm that was ascribed to octahedral Al atoms and the other at 66.0 ppm attributed to tetrahedral coordinated Al atoms; the positions and intensities of these peaks were closely similar to those of the parent montmorillonite. Thus, although the peaks were somewhat broader due to the paramagnetic centers, it was concluded that there were no Al atoms in the extra framework region. The ^{27}Al MAS NMR spectrum for FeAl-PILC showed an Al resonance at 65.8 ppm that is a signature of the so-called Keggin cation structure [250] while the octahedral Al signal shifted to 1.97 ppm. Thus, the pillaring solution could be made from Keggin cations in which Al^{3+} is partially replaced by Fe^{3+}. Moreover, ^{27}Al MAS NMR supported the incorporation of metal oxides into the porous network rather than attached to the PILC pillars.

The ^{29}Si MAS NMR spectrum of the parent montmorillonite showed a main peak at −93.98 ppm (Q^3(1Al)) and two shoulder peaks: a large one at −104.5 ppm (Q^3(0Al)) and a small one at −90.3 ppm (Q^3(2Al)). This silicon distribution amongst various environments was not affected by pillaring. A slight shift in ppm values, lower than 1–2 ppm, was observed and confirmed that there were no chemical bonds between exchanged polymeric species and clay layers; if Al-O-Si linkage between the pillars and silicate layers had been formed, the spectra would have contained a Q^3(3Al) resonance. The presence of basic sites was important in acid-base catalyzed reactions.

From this it was deduced that transition metals were incorporated on PILC did not alter the local environment of Si atoms, and thus that metal oxides were not in the immediate environment of Si sheet; they may be present in the porous network of the pillared system.

Some authors [251] observed that silicon incorporation in the pillaring component provides moderate catalytic activity for hydroisomerization. Thus, the synthesis of well-defined hydroxyl-SiAl (HSA) oligocations is interesting for the formation of products having stable SiO_2-Al_2O_3 pillars [252,253]. Moreover, the surface silanol groups could react with various catalytically active compounds and introduce new active functional groups in pillared smectite catalysts [254]. Zhao et al. [255] reported the synthesis and characterization of PILC materials with HSA oligocations prepared by two different methods. Evidence for the structure of a hydroxy-SiAl oligocation was provided by ^{27}Al MAS NMR, which showed two peaks at 62.76 and 0.45 ppm similar to that of the hydroxy-Al oligocation. J. Akitt et al. [253] showed that the former band may arise from tetrahedral alumina in hydroxy-Al oligocation, $[Al_{13}O_4(OH)_{24}(H_2O)_{12}]^{7+}$, and the latter band arose from free Al^{3+} cation. This suggested that the structures of HSA with various Si/Al ratios prepared by two different synthetic routes were similar to that of the hydroxy-Al oligocation, with Keggin structures. However, compared to hydroxyl-Al pillared clay, those HSA had higher concentrations of both Brønsted and Lewis acid sites and higher cracking activity of cumene and conversion and selectivity for disproportionation of 1,2,4-trimethylbenzene.

2.3.1.2. New ecofriendly routes of metallic ions incorporation in the Keggin cation. The insertion of zirconium or aluminum species into porous clay heterostructures was traditionally performed in two steps. A one-step pillaring process was possible with the use of an organic Si-source, followed by the post-synthesis grafting of aluminum onto the mesostructured interlayer space silica framework of a silica-pillared clay (Si-PILC), leading to an aluminosilicate intercalate (Al-PILC) [256]. The ^{27}Al MAS NMR spectrum for PILC showed a main resonance at 6 ppm and small wide resonance at about 58 ppm that was assigned to octahedral and tetrahedral coordinated aluminum, respectively. Each aluminum derivative exhibited a peak at 50 ppm, assigned to tetrahedral aluminum grafted onto the silica in the interlayer space. The absence of increased signal near 12 ppm for octahedral aluminum indicated that nearly all the aluminum was incorporated into the siliceous interlayer framework. The strongly basic $NaAlO_2$ solution facilitated the insertion of aluminum onto the silica in the interlayer space and all of the Al-PILC intercalates exhibited high catalytic activity for cumene cracking reaction.

Kooli et al. [257] described a novel method that reduced the use of organic surfactants and inserted zirconium directly into the silica framework of the porous clay heterostructures in one step. They used ^{29}Si MAS NMR to stablish the changes that were produced during PILC formation from montmorillonite (Mt) and the presence of Zr^{4+}. The ^{29}Si MAS NMR spectrum of raw clay (Mt), Fig. 16a, exhibited an intense resonance peak at −94 ppm typical of Q^3 Si atoms in dioctahedral smectites [258] and a second peak at −110 ppm corresponded to silica impurities. Fig. 16b indicated that precursor montmorillonite intercalated with zirconium, Zr-Mt, exhibited features similar to the starting clay. However, a different spectrum was obtained for the PCH from Zr-Mt, PZr-MtCH precursor, (Fig. 16c), exhibiting two additional peaks at −100 and −111.2 ppm that were attributed unambiguously to the $Si(OSi)_x(-OH)_{4-x}$ framework units, where x = 3 (Q^3) and x = 4 (Q^4), respectively. After calcinations at 550 °C, the Q^4 species represented the dominant compound due to the dehydration/polycondensation of the silica species between the clay layers [259], and a small shift was observed for the Q^3 and Q^4 sites. The peak related to the clay layers at −95 ppm vanished and became embedded in the intense peaks of the silica species. These data indicated that the PZr-MtCH structure was maintained with some transformation of the silica

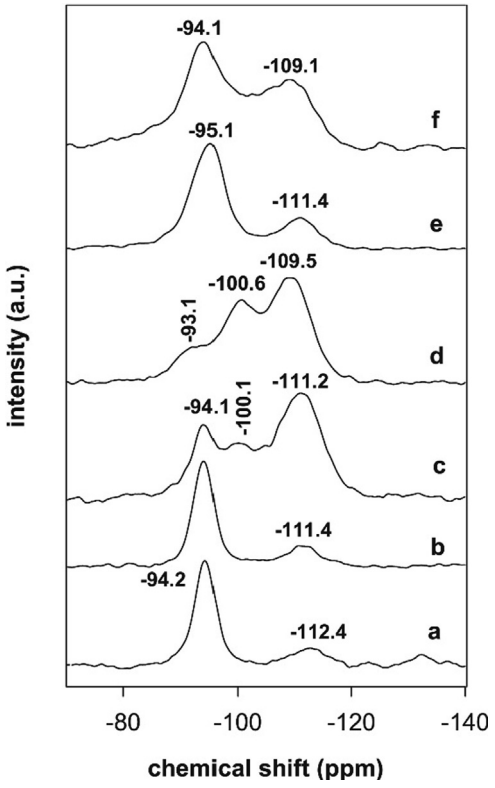

Fig. 16. ^{29}Si MAS NMR spectra of (a) raw clay, (b) Zr-Mt, (c) PZr-MtCH precursor and (d) after calcination at 550 °C; (e) corresponds to pillared Zr-Mt-PILC and (f) its PZr-MtCH-PILC precursor calcined at 550 °C. Reprinted with permission from Ref. [257].

intercalated species (Fig. 16d). ^{29}Si MAS NMR spectra were comparable to those of PCHs prepared in the conventional way [260] and to mesoporous silica materials [261]. The Zr-PILC exhibited features similar to the Zr-Mt, with broadened bandwidths at −95.1 and −111.4 ppm. The presence of a Si-O-Zr_{pillar} site may be responsible for the broadened resonance observed in the spectrum of Zr-Mt-PILC (Fig. 16e) [262]. The derived PZr-MtCH-PILC exhibited a similar spectrum than Zr-Mt-PILC, with an additional resonance peak at −109.1 ppm due to the amorphous silica phase formed on the external surface of the pillared clays (Fig. 16f), as reported for PCH prepared from alumina pillared clays [263]. The insertion of Zr species in hexagonal silica mesoporous materials was confirmed by the presence of Q^3 and Q^4 bands at −94.6 ppm and −107.2 ppm, respectively [264]. Stronger Brønsted acid sites were developed into the PCHs materials, in addition to Lewis sites, and n-heptane was converted to isomers and cracking products.

2.4. Hydrogenation

Hydrogenation plays a key role in chemical synthesis. Homogeneous hydrogenation has become increasingly important in recent decades, mainly due to its application in the industrial production of specific chemicals, mainly in fats and oils industry. Enhanced hydrogenation reaction rates are obtained when metal complex homogeneous catalysts are attached to suitable supports such as clay minerals. In this section, we will show how SS-NMR techniques have made a difference to the understanding of hydrogenation reactions of several important compounds.

As one example, functional groups such as diphenylphosphine, triphenylphosphine, and 4-picoline have been intercalated in montmorillonite, and subsequent complexation with palladium has led to the synthesis of various interlamellar montmorillonite-anchored palladium(II) complexes [265].

^{31}P MAS-NMR was already used for the studies of homogeneous transition metal complexes [266], and was also applied for the study of surface-anchored polymer-silica transition metal phosphine complexes (Rh, Pt, Pd, and Ni) [267,268] and phosphinated silica-anchored carbonyl osmium clusters [266]. The ^{31}P signal shifted downfield when anchored phosphorous is complexed with Pd(II), Fig. 17. CP-MAS spectra at different ratios of Pd/P showed a central band with three different finely resolved isotropic chemical shifts, that were attributed to unreacted anchored phosphorus (10.5 and 16.9 ppm) and phosphorus complexed with Pd(II) (23.7 ppm). Increasing the Pd/P ratio caused progressive intensification of the last peak whereas the former two disappeared [265]. These results suggested rigidity of the montmorillonite interlayer channels, disallowing complexation with a second phosphine group anchored at different sites.

Using ^{1}H NMR spectroscopy, Swamy et al. [269] reported kinetics and mechanism of the hydrogenation of stilbene, cinnamaldehyde and cinnamic acid by anchored montmorillonite-bipyridinepalladium (II) acetate. ^{1}H MAS NMR confirmed that peaks corresponding to olefinic protons of substrate were absent in the hydrogenated products and that the total hydrogen consumed corresponded to complete saturation of the C = C which was present in the substrate.

^{1}H MAS NMR was also used for the study of the cobalt–molybdenum catalysts supported on saponite for upgrading squalene ($C_{30}H_{50}$), a hydrocarbon related to *B. braunii oil* [270]. The data showed that saponites supporting catalysts with different Al:Si ratios have different reactivity in the micro-reactor at a temperature around 400 °C. The amount of vinylic protons (≡CH–) attributable to squalene attained a lower value when the Al:Si ratio was 1:20, 1:10 and 1:2. ^{1}H MAS-NMR spectra of the collected volatiles also indicated the presence of squalene and an unusual ester as major products. Based on the results obtained from ^{1}H MAS NMR analysis, the yield of cyclic product was 77.9%, 71.8%, 80.4%, 52.5% and 22.9% for reactions involving 1:2, 1:10, 1:20, 1:30 and 1:50 saponite supported catalysts, respectively. The trend shown by the vinylic protons of squalene in the liquid products appeared to be correlated with the amount of octahedral aluminum in the catalyst. These results suggested that increasing octahedral aluminum in the saponite samples increases the reactivity towards cyclic products until an equilibrium condition is reached at 1:20.

^{19}F, ^{31}P and ^{11}B MAS-NMR experiments have been used for the study of rhodium complexes immobilized in clay montmorillonite K-10 [272] that form highly active, selective and reusable catalysts for the hydroboration reaction of styrene [273]. The spectra recorded during the impregnation process provided evidence that montmorillonite K-10 may immobilize ionic metal complexes throughout the cationic and anionic However, when bentonite was used as the solid, only the cationic metal complex was immobilized through cationic exchange while the counter anion remained in solution.

Finally, ^{27}Al MAS-NMR was employed for the characterization of a series of Me/Al-PILC catalysts (Me = Ni, Rh, Pd, Ce) for the catalyst of methane reforming with CO_2 [271]. The ^{27}Al MAS NMR spectra showed at least two overlapping resonances with two maxima located in the range characteristic of four- and six-fold coordinated aluminium, Al^{IV} and Al^{VI}, indicating that several Al species were present in raw and impregnated Al-PILC. The two kinds of resonances, as well as a broad band at ca. 20 ppm, were observed in the spectrum of Al-PILC and all Me/Al-PILC catalysts. The impregnation step by 3% Me^{n+} followed by calcination did not seem to alter the environment of aluminum significantly.

For quantification, it was necessary to analyze more closely the shape of the resonance, and a MQ-MAS experiment was performed on 3% Ni/Al-PILC, enabling the identification of two different sites. The resonance of Al^{IV} located at an isotropic chemical shift δ_{iso} = 58.8 ppm was well defined without distribution, and it was simulated with a symmetrical shape close to a Gaussian line (Fig. 18). The second resonance located in the Al^{VI} isotropic chemical shift range with a distribution of quadrupolar constant (i.e., the resonance was along the δ_{QIS} line) was simulated using the Czjzek

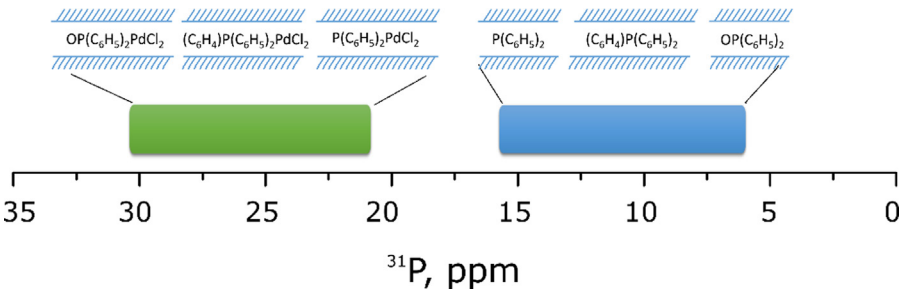

Fig. 17. ^{31}P chemical shifts range of polymer-silica transition metal phosphine complexes. Adapted from Ref. [265].

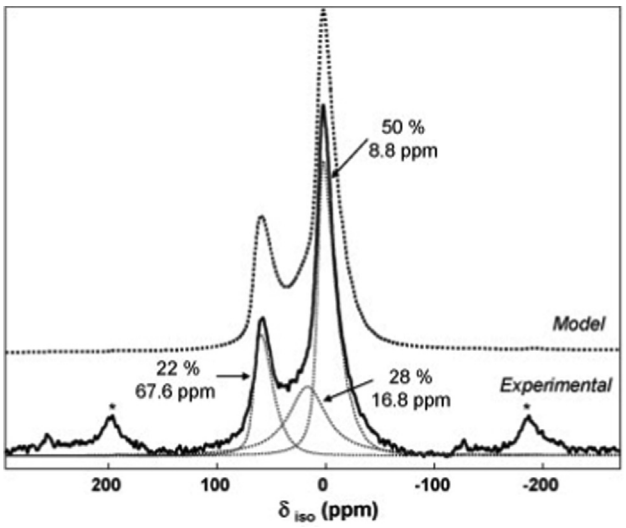

Fig. 18. ^{27}Al MAS spectrum of 10% Ni/Al-PILC (full line: observed spectrum; dotted lines: deconvoluted pattern). Reproduced from Ref. [271].

model [274] in the DMFIT program [275]. Using the shape determined with the MQ-MAS experiment, the ^{27}Al MAS spectra of the Al-PILC series were fitted. Fig. 18 represents a typical fit in the case of 10% Ni/Al-PILC representative of the full series. Data obtained for the other catalysts using the same resonances is gathered in Table 5.

The two resonances revealed by the MQ-MAS experiment did not fully account for the pattern seen in the spectrum and a third line was introduced at ca. 16.8 ppm. This resonance did not appear in the MQ-MAS experiment due to its fast decrease relaxation in the 3Q. This phenomenon could be due to line-broadening resulting from an asymmetric environment of this type of Al and, thus, the geometry around the aluminum atoms may be distorted octahedral or pentahedral.

The impregnation and calcination steps did not modify the environment of Al but they did modify the amount of Al^{VI} in the samples as shown by the value of the ratio between Al species (Table 5). The Al^{VI}/Al^{IV} ratio was lower than expected (Al^{VI}/Al^{IV} = 11.4 in Na-montmorillonite and 12 in Al_{13}), as well as when pseudo-octahedral species were taken into account ($Al^{VI} + A^{V}/Al^{IV}$ ratio). This was particularly the case for 10% Ni/Al-PILC, where the amount of octahedral Al present in Al-PILC strongly decreased, as Al^{VI}/Al^{IV} and Al^{VI}/A^{V} were 35 and 43% lower, respectively, compared to 3% Ni (Table 5). The values of δ_{iso} for Al^{IV} and Al^{VI} were at ca. 59 and 8.8 ppm, respectively. Typical values of δ_{iso} for tetrahedral Al in Al_{13} pillared clays were at ca. 56 and 67 ppm, respectively in synthetic pillared hectorite after calcination at 400 °C, and 63–67 ppm for pure dried Al_{13} salts. The first value (56 ppm vs. 59 ppm) confirmed the presence of Al_{13} pillars in those materials. The formation of γ-alumina particles was discarded because the ^{27}Al δ_{iso} in crystallized γ-alumina (spinel) were 76 and 14.5 ppm for Al^{IV} and Al^{VI}, respectively, and the ratio Al^{VI}/Al^{IV} ranged from 1.33 to 1.5.

2.4.1. Oxidation

Redox reactions are associated with catalyst doped with transition metals. Zeolites and clay minerals have been extensively used as host materials for those catalysts. In the case of clay minerals, the transition metals can be found as heteroatoms in the octahedral or tetrahedral sheets of the clay mineral or as exchangeable cations between the clay mineral layers. Among them, pillared clays doped with metals such as Cr, Ti, V, Ce, Sn, La or Th, used as redox catalyst, were studied by SS-NMR spectroscopy.

Kiricsi et al. [276] followed the co-hydrolysis of $CrCl_3$ and $AlCl_3$ in the presence of montmorillonite by ^{27}Al MAS-NMR spectroscopy. They observed that the ratio of octahedral to tetrahedral aluminum was close to 12, even in presence of chromium, meaning that isomorphous substitution of chromium for aluminum did not occur; rather co-hydrolysis and co-pillaring took place. Upon heat treatment, loss of outer-sphere water and dehydroxylation at higher temperatures resulted in the formation of bulky alumina pillars decorated with chromic species. These species became more and more accessible to the reactant because in the oxidation reaction the specific activity increased with chromium content.

Solids doped with titanium exhibited excellent catalytic properties in redox reactions that encompassed the oxidation of a variety of organic substrates [277,278]. Khedher et al. [279] described how the use of the commercial montmorillonite K10 allowed the preparation of a titanium supported K10 catalyst (Ti-K10), using ^{27}Al and ^{29}Si MAS-NMR for their characterization. They showed that the chemical shifts corresponding to the different Al species were not affected by the presence of titanium species in the lattice, and thus, it seems there is not interaction between titanium and aluminum.

Moreover, ^{29}Si MAS NMR data suggested that the lattice silicon interacted with the titanium species. K10 structure modification was probably due to the distribution of the titanium species in the lattice as consequence of the interaction between the Ti and the Si presented in the broken clay layers.

V_2O_5 is an excellent catalyst for the selective oxidation of H_2S [281,282], especially when supported on delaminated zirconia-pillared clay. In this case, ^{51}V MAS-NMR could play an important role in determining the local environment of vanadium that is related to the catalyst selectivity. The ^{51}V wide-line NMR spectra for series of V/Zr-PILC catalysts, based on montmorillonites, Fig. 19, showed at least three types of signals with varying intensities depending on the vanadium content [280]. At low vanadium loading, a peak around − 620 to − 650 ppm was observed, which was mainly due to tetrahedral vanadium species on the catalyst surface. As the vanadium loading increased, the peak shifted to the range − 340 to − 360 ppm, which was generally assigned to distorted octahedral vanadium species [283,284]. The tetrahedral and octahedral vanadium species detected by ^{51}V MAS NMR were mainly monomeric and polymeric vanadium, respectively [285]. For the higher vanadium loading, 11 wt% and 14 wt%, a low intensity peak around − 1250 ppm was observed due to the formation

Table 5
Quantification of ^{13}Al MAS NMR resonances for the Al-PILC support and impregnated Me/Al-PILC catalysts. (Reprinted with permission from Ref. [271]. Copyright 2009 Elsevier).

Catalyst	Al^{VI}	Al^{IV}	Al^{V}	Al^{VI}/Al^{IV}	$Al^{VI} + Al^{V}/Al^{IV}$
Al-PILC	60.4	14.5	25.1	4.2	5.9
3% Ni/Al-PILC	62.4	17.1	20.5	3.7	4.9
10% Ni/Al-PILC	50.1	21.1	28.8	2.4	3.7
3% Rh/Al-PILC	53.5	14.9	31.6	3.6	5.7
3% Pd/Al-PILC	52.3	15.9	31.8	3.3	5.3

δ_{iso} Al^{IV} = 58.8 ppm; δ_{iso} Al^{VI} = 8.8 ppm; δ_{iso} Al^{V} = 16.8 ppm.

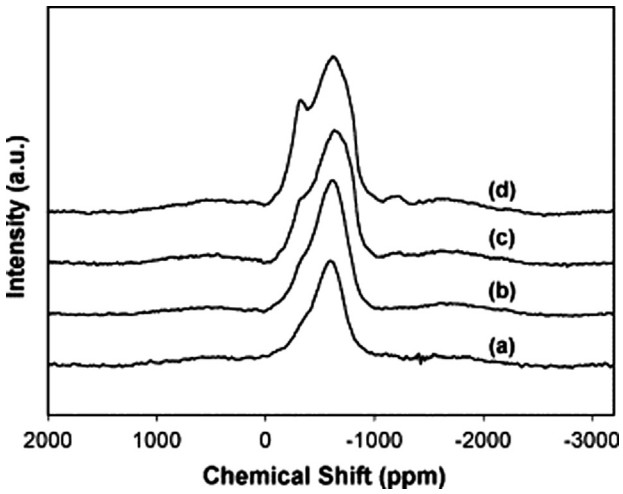

Fig. 19. ^{51}V NMR spectra of V/Zr-PILC catalysts: (a) 2 wt% V/Zr-PILC, (b) 6 wt% V/Zr-PILC, (c) 11 wt% V/Zr-PILC, (d) 14 wt% V/Zr-PILC. Reproduced with permission from Ref. [280].

of crystalline vanadium with a square pyramidal coordination [283,284].

Sanabria et al. [286] proposed a new methodology for the modification of clays with mixed Al–Fe and Al–Ce–Fe systems that was applied to the wet peroxide oxidation of phenol in dilute aqueous medium. They demonstrated a catalytic activity comparable to that of solids modified by conventional methods. The pillaring agents Al_{13}-X, Al_{13}-X + Fe and Al_{13}-X + Ce + Fe (X = SO_4^{2-} or NO_3^-) were characterized by ^{27}Al MAS-NMR spectroscopy. ^{27}Al MAS-NMR spectra of sulphates showed the Al13 polycation characteristic peak (62 ppm) [287], whereas no signal attributed to basic aluminum sulphate was observable (3.42 and 5.72 ppm or 9.98 in case monocline crystalline system) [288,289]. In the nitrates case, however, ^{27}Al MAS-NMR showed two contributions, one coming from the aluminum in tetrahedral coordination in the Keggin cation (61.5 ppm) and the other centered at ca. 3 ppm attributed to Al_{13}–NO_3, Al_{13}–NO_3 + Fe and Al_{13}–NO_3 + Ce + Fe [288]. The difference in the signal position for each polymer was associated with differences in the chemical environment of Al^{VI}, caused by the effect of the added Fe and Ce. Taking into account changes in the NMR signal of Al^{VI} in sulphates and nitrates, an effective isomorphous substitution of octahedral Al^{3+} for Fe^{3+} in Keggin ion salts was proposed.

Sn catalysts based on lithium taeniolite (TN) have also been investigated with SS-NMR. Hara et al. [290] synthesized three classes of lithium taeniolite (TN)-intercalated Sn by varying the Sn loading amount, Sn(X)/TN (X = loading amount of the Sn species, mmol/g), by a conventional cation-exchange method. These catalysts were used for the Baeyer–Villiger oxidation of various ketones with hydrogen peroxide as an oxidant [290]. Based on the results of ^{7}Li and ^{119}Sn MAS-NMR, the authors proposed that an isolated Sn species, such as $[Sn^{IV}(OH)_x(H_2O)_{5-x}]^{(4-x)+}$ (x = 0–3), was formed in the clay interlayers. Those clay-intercalated Sn catalysts showed extremely high performance in Bayer–Villiger oxidation and were also reusable without any significant loss of activity or selectivity.

Iron pillared montmorillonite exchanged with La, Ce and Th metal salts are excellent catalysts for hydroxylation of phenol underlining the use of environmentally friendly clay catalysts for effective removal of pollutants. The local environment of the clay after pillaring and exchanging with rare earth cations was analyzed by ^{27}Al and ^{29}Si SS-NMR spectroscopy [291]. After the exchange, ^{27}Al MAS-NMR spectra showed no variation in peak width or position. It was thus concluded that the incorporation of the rare earth metals did not affect the structural stability of the layers and pillars. A slight shift of the ^{29}Si MAS-NMR signal was observable for pillared samples, indicating that the strain in the local environment of the Si atoms could be due to the bulky intercalated species. ^{29}Si MAS-NMR spectra of rare earth exchanged systems showed that the chemical shifts values did not alter substantially with rare earth metal exchange. Hence, it was inferred that the metal oxides were not in the immediate environment of the Si sheet, implying they may be present in the porous network of the pillared system (as also evidenced by surface area data and ^{27}Al MAS-NMR spectra). All those systems were excellent oxidation catalysts for organic pollutants, specifically La/Fe PILC showed the maximum activity.

2.4.2. Polymerization

Polymerization is the process by which relatively small molecules or monomers, chemically combine to produce a very large chainlike or network molecule or polymer. Catalysts based on clays allow control to be exerted over structural details that have important effects on the properties of the polymer.

Tabernero et al. [292] reported the polymerization behavior of commercial acid treated montmorillonites (*K*10 and K30) as activating supports. These materials were modified by treatment with different aluminum compounds in order to obtain enriched aluminum clays and to modify the global Brønsted/Lewis acidity. They were used for ethylene polymerization using a zirconocene complex as catalyst. SS-NMR was used to characterize them.

The short-range order analysis of the montmorillonites treated with AlR_3 complexes [R = trimethylaluminum (TMA), triethylaluminum (TEA)] demonstrated a decrease in the silicon content associated to the clay fraction (more significant after treatment with TEA than with TMA) and an increase of the quartz Si amount (more significant in the treatment with TMA than with TEA complex). ^{27}Al MAS-NMR spectra of those samples revealed the presence of a new signal at ca. 30 ppm due to pentacoordinate aluminum, which resulted from the AlR_3 interaction with the hydroxyl group of the silicate surface through Lewis acid sites.

The behavior of these Al-enriched acid montmorillonites was compared to one natural montmorillonite (SAz-2) and one hectorite (SHCa-1). They were tested with: i) their natural interlayer cation, ii) after the exchange with NH_4^+ or Al^{3+} cations to obtain smectite/M^{n+} (M^{n+}= NH_4^+ or Al^{3+}), and, iii) after acid treatment with H_2SO_4 (smectite/H) [293]. ^{27}Al MAS NMR spectroscopy revealed that aluminum reacted with acidic protons and after TMA treatment the most remarkable observation in all samples was the detection of new signals from pentahedral aluminum species generated in situ (Al^{v}) (for montmorillonite/TMA and hectorite/TMA) [294,295]. According to literature data [296,297], the reaction of TMA took place with both isolated silanol groups and with strained siloxane bridges, so this environment for the aluminum atom could be the result of a reaction with an acidic hydrogen together with an interaction with neighboring silanol groups [298,299].

For the starting smectites, ^{1}H signals in the MAS NMR spectra corresponded to: i) structural hydroxyl groups, at 1.4 ppm for montmorillonite and 0.3 ppm for hectorite; ii) water in their structure, at 4.3 ppm; and iii) protons with Brønsted acidic character, at 6.4 ppm in montmorillonite [300]. The treatment with TMA caused: i) the appearance of new peaks corresponding to aliphatic protons in the range from 0 to 4 ppm, indicating a successful incorporation reaction of the aluminum compound [296]; and; ii) the disappearance of the protons assigned to water molecules, as is crucial to ensure use of these materials as cocatalysts. The most interesting feature was the presence of new signals corresponding to new acidic protons at 6.5–7.0 ppm, which was only observed after TMA treatment, but not after interlayer cation exchange.

All the results indicated that the performance of these materials as cocatalysts did not depend on the number of incorporated aluminum atoms, but rather on the nature of these species on the clay. Careful characterization of the support activators showed that pentahedral aluminum was responsible for cationic species formation. These aluminum species resulted from a synergistic effect between the aluminum centers produced after TMA reaction and the SiOH groups located in the clay, which generated more acidic protons than were present in the starting materials. This cooperative effect was responsible for active species generation.

2.5. Industrial applications

Clays are used as raw materials in many industrial fields such as optical, energy, textile or building fields, among others [301]. Their applications depend upon their structure, composition, and physical properties [302]. An in-depth understanding of these characteristics is key to maximizing their utility and, eventually, may open up new areas of applications. In this section we will review industrial applications where SS-NMR has proved to be a key characterization technique for short-range ordering in clays.

2.5.1. Optical application

In recent years, many functional materials have been obtained from the covalent grafting of organic fragments on inorganic surfaces, such as clay minerals, [303-305] that has created the possibility of obtaining materials where the host imposes a specific and organized orientation to the active molecules (guests) [304,305].

NMR has been mainly used for the characterization of materials based on clay minerals with luminescence properties, using mostly ^{29}Si, ^{27}Al and ^{13}C MAS-NMR. For example, Ma et al. [306] prepared an europium complex covalently attached to silylated attapulgite (Atta), using APTES (3-(Aminopropyl)triethoxysilane), with luminescence properties. ^{29}Si MAS-NMR was used to analyze the interaction between attapulgite and APTES. The Atta-APTES spectrum showed peaks related to the organosiloxane T^n (T^n = $RSi(OSi)_nOH_{3-n}$, n = 1–3) and siloxane Q^m (Q^m = $Si(OSi)_m(OH)_{4-m}$, m = 2–4) species. The dominance of T^3 NMR signals at −64 ppm for Atta-APTES suggested that the hydrolysis and condensation of APTES on the surfaces of the matrix was nearly complete, resulting in a strong linkage (three Si-O-Si covalent bonds) between APTES and the matrix. Q^2 (-87 ppm) and Q^3 (-93, −97 ppm) peaks in Atta-APTES were assigned to the Si-OH groups inside the channels, whereas APTES was covalently bonded onto the outer surfaces of Atta [306]. The Atta-APTES surface allowed covalent bonding of the Eu^{3+}complexes onto the outer surfaces of Atta and provided efficient emission, as well as higher thermal stability and exposure durability, since the matrix interacted strongly with europium complexes.

Inorganic luminescent materials usually consist of a host material containing luminescent activators such as rare earth ions. The host must allow the activators to be effectively incorporated and dispersed, and the chemical and thermal stability of the host is an important factor for real-world applications. In a recent publication, Rogers et al. [307] described the preparation of a geopolymer from a dehydroxylated kaolinite-type clay (dehydroxylated halloysite) that was used as a host for trivalent rare earth ions, Sm^{3+} and Eu^{3+}, to produce new photoluminescent materials. The ^{27}Al MAS-NMR spectrum of the unexchanged geopolymer host was typical of a well-formed geopolymer, containing predominantly the tetrahedral aluminum, at 60 ppm, [308] and a very small amount of octahedral aluminum at ~3 ppm [308]. The spectra of the Sm^{3+}- and Eu^{3+}- exchanged samples showed peak broadening and more intense spinning side bands due to the influence of the paramagnetic rare earth ions [308,309]. In addition, the peak corresponding to octahedral aluminum (2–3 ppm) was more intense and there was some limited evidence of 5-coordinate aluminum at 29 ppm [308], from the unreacted dehydroxylated halloysite due to inhomogeneous dehydroxylation of the clay.

Santos et al. [310] designed new clay minerals to act as host lattices for rare earth (REE) ions, Eu^{3+} and Tb^{3+}. Based on the hectorite structure, nano-chlorohectorites LS(Cl) and nano-fluorohectorites LS(F) were developed by replacing the OH^- present in the hectorite structure with Cl^- or F^-, thus avoiding the luminescence quenching that would be expected due to OH^- groups. ^{29}Si MAS-NMR spectra of the LS(X) (X = Cl^- or F^-) materials revealed Q^2 (-74 to −92 ppm) and Q^3 (−93 to −101 ppm) sites, but at lower chemical shifts than those expected for common hectorites. This confirmed the changes in the surroundings of the tetrahedral sheets due to the OH^-replacement by F^- or Cl^- ions in the octahedral units [311]. The Q^2/Q^3 ratio was used to evaluate the degree of branching relative to the extension of the orthosilicate chains [312] and indicated a higher degree of branching on the tetrahedral sheets for the LS(Cl) than for the LS(F).

Later, Moretti et al. [313] used ^{13}C and ^{29}Si MAS-NMR for describing the step-wise grafting of the fluorescent dye's dansyl group, (5-dimethylaminonaphthalene-sulfonyl chloride) in the interlayer space of kaolin, forming K-Dansyl. ^{13}C MAS-NMR spectrum showed a set of signals between 110 and 150 ppm due to the aromatic carbons typical of the dansyl moiety, indicating that the intercalations had occurred successfully. ^{29}Si MAS-NMR spectrum of K-Dansyl showed the two peaks previously observed in the kaolinite spectrum, at −90.5 and −91.5 ppm, maintaining the relative intensities, but with a small shoulder at −91.8 ppm, suggesting an increase in anisotropy around the silicon due to intercalation of the organic molecules.

SS-NMR has also been applied in the characterization of other optical materials as laser-dye or LEDs.

^{13}C CP MAS-NMR has been used for the structural characterization of hybridized alkyltrimethylammonium (C_nTMA^+) and rhodamine 6G (R6G) cations in the laponite (Lap) interlayer nanospace, R6G/C_nTMA^+/Lap, for designing typical laser-dye [314]. The spectra showed that the intensity of peaks from the alkyl chains of the trans (35 ppm) and gauche (33 ppm) forms was almost the same. In addition, the combined results of NMR and XRD showed that C_nTMA^+ cations were incorporated as the *trans*-gauche form into the Lap interlayer nanospace and R6G cations were intercalated parallel to the surface of Lap nanosheet (Fig. 20). The R6G/C*16*TMA$^+$/Lap solid material prepared under optimal conditions exhibited emission quantum yields of ca. 80%.

NMR has also been applied in clay mineral-based materials used as light emitting diodes. A great deal of attention is being paid to polymer-nanoparticle hybrid materials, used in the large-area light

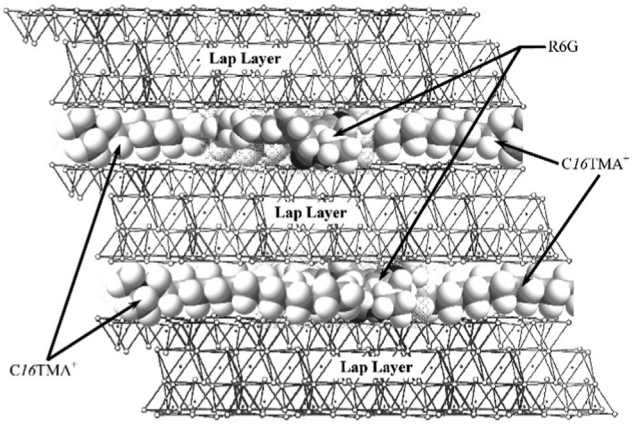

Fig. 20. Schematic nanostructural model of R6G/C16TMA+/Lap. Reprinted with permission from Ref. [314].

emitting diodes (LEDs), since the nanoscale multiphase materials can display some novel properties that are not present in the individual phases [315]. Jing et al. [316] demonstrated the in situ polymerization of poly(2-methoxy-5-(20-ethyl-hexyloxy)-1,4-phenylenevinylene), MEH-PPV, from the precursor 3,1,4-dibromo-2-methoxy-5-(20-ethyl-hexyloxy) xylene, in the presence of a natural montmorillonite modified with a ternary ammonium salt, OMMT, and the enhanced electroluminescent and thermal-tolerant properties of these polymer/clay nanocomposites. ^{1}H NMR and ^{13}C NMR spectroscopy are a useful tool to trace the reaction in situ.

A signal at 4.5–4.6 ppm in the ^{1}H NMR spectrum of monomer was assigned to the hydrogens of CH_2Br, which disappeared after polymerization. In the ^{1}H NMR spectrum of the final product there was a new peak at 7.5 ppm, assigned to the conjugated aromatic hydrogens of MEH-PPV.

The ^{13}C T1 values of both backbone (aromatic) and pendent groups (aliphatic) had smaller values in the nanocomposites than in the bulk, implying a shortened correlation time τ_C and an enlarged free volume in the nanocomposites compared with pure MEH-PPV. In the MEH-PPV/OMMT nanocomposites, the polymer matrix was separated at the nanophase level ~~le~~ by the exfoliated montmorillonite sheets. Furthermore, this nanophase-separated structure should reduce the interchain interactions at the excited states, thereby reducing the major cause of non-radiative decay and enhancing radiative recombination at the same time.

2.5.2. Clay minerals film

Functional materials are often found in film form. Particularly, two-dimensional clay minerals can be exfoliated into their elemental layers, and the layers can be reassembled together with other materials to form films at nanometer scale, which brings about not only improvement in functionality, but also brings novel properties [317].

A novel nuclear magnetic resonance technique for imaging materials exhibiting extremely short T_2 relaxation times (CWNMRI) has been applied to clay mineral films. Some examples of its application to materials of scientific and industrial interest were presented by Fagan and Lurien [318]. The temporal evolution of 1-D substance profiles by CWNMRI allowed determination of the diffusion coefficient of the substance of interest. In particular, the diffusion profile of water into bentonite from a reservoir and the diffusion profile of water between two bentonite clay layers shed a light on the porous connectivity of clay (Fig. 21). The profiles in Fig. 21a showed the concentration-driven diffusion waterfront moving into the bentonite sample. The right side of the sample was confined at the bottom of the sample container, and hence swelling of the sample as it progressively absorbed more water was evident at the interface between the bentonite and the laboratory tissue paper. In Fig. 21b, some residual H_2O content was evident on the left side of the sample despite heating the bentonite powder at 70 °C for 3 days in an attempt to remove all evaporable water. The absorption of atmospheric water by the highly hygroscopic bentonite powder and pick-up from ^{1}H in OH^- groups within the alumina layers of the bentonite accounted for this signal. Nevertheless, the gradual diffusion of the H_2O through the sample was clear.

In both cases, an analysis of the diffusion front as a function of time showed a t^2 dependence of the front line which indicated Fickian diffusion and allowed for the determination of a diffusion coefficient according to $x^2 = 2Dt$. The inter-diffusion coefficient was measured at $[1.15 \pm 0.05]\cdot10^{-9}$ m^2/s, while the self-diffusion coefficient was measured at $[8.4 \pm 0.5]\cdot10^{-10}$ m^2/s, which was the same order of magnitude as that recorded for non-swelling technical-grade kaolinite at similar water content.

Qin et al. [319] investigated the effects of organically modified montmorillonites (OMMTs) on the structures and properties of starch nanocomposite films prepared with hydroxypropyl distarch phosphate (HPDSP). As shown in the ^{13}C NMR spectra of the starch nanocomposite film, four main peaks were observed, which corresponded to various glucose carbons (Fig. 22A). The peaks C_1 (100–103 ppm), C_4 (81.4 ppm), $C_{2,3,5}$ (72.2 ppm), and C_6 (61.9 ppm) corresponded to the carbon atoms within the HPDSP molecules, as shown in Fig. 22B. The ordered spectrum at the C_1 peak (100–103 ppm) was resolved into the double-helix (series of peaks near 100 ppm) and single-helix (103 ppm) components of the starch molecule [320]. Then, the results of NMR analysis (Fig. 22) suggested that the starch-OMMT nanocomposite possessed comparatively large quantities of single-helix structures and micro-ordered amorphous regions.

2.5.3. Fuel cells

Ion-conducting polymeric membranes have been studied for their use in fuel cells. However, polymeric membranes available in the market show some disadvantages and the use of nanoclay is expected to improve their mechanical and thermal resistance [321]. SS-NMR has been applied for the characterization of these

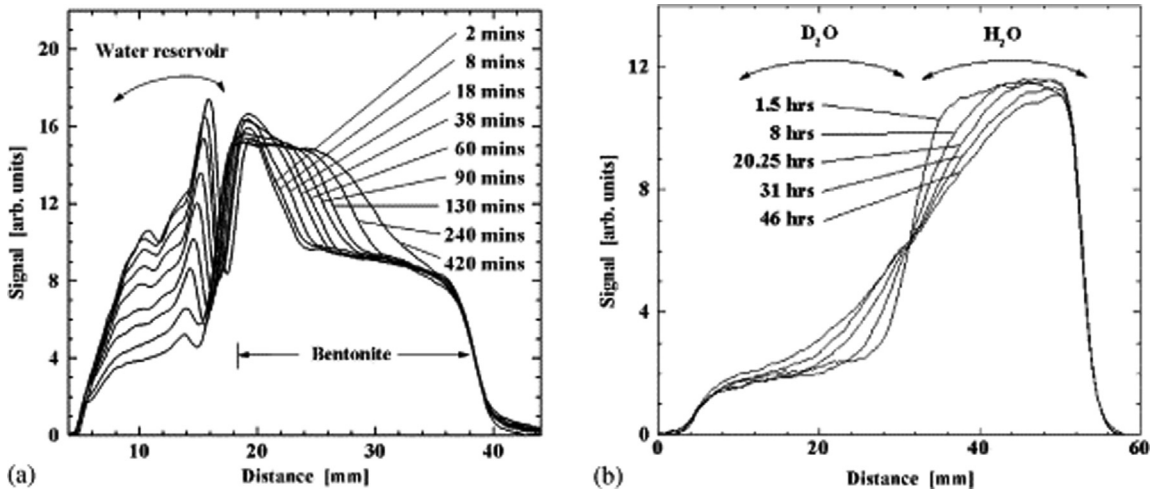

Fig. 21. Diffusion profiles of water into bentonite: (a) diffusion of water from a reservoir (left-hand side) into bentonite clay with initially 20% w/b water; (b) diffusion of water between two bentonite clay layers initially prepared D_2O and H_2O as indicated. Reprinted with permission from Ref. [318].

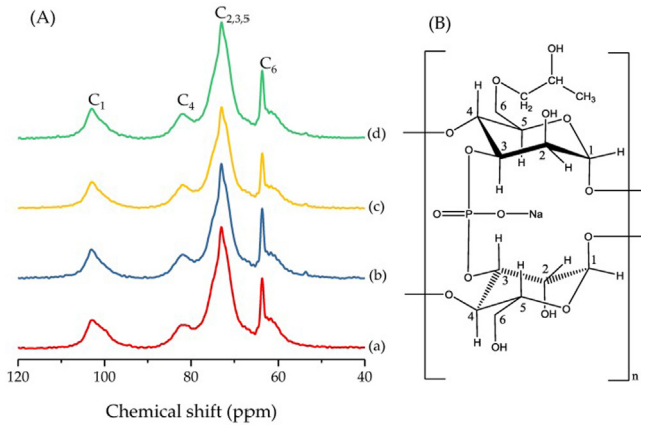

Fig. 22. A) ^{13}C nuclear magnetic resonance (NMR) spectra of (a) HPDSP-Na; (b) HPDSP-1231; (c) HPDSP-1631; (d) HPDSP-1831; and (B) the HPDSP structure. Reprinted with permission from Ref. [319].

new materials and has helped in the rationalization of their enhanced properties, as illustrated in the two examples below.

Nicotera et al. [322-324] used composite membranes based on Nafion with the inclusion of cationic and anionic nanoclays, Laponite (Naf-Lap), and layered double hydroxide (Naf-LDH), respectively, to increase the operating temperature of a direct methanol fuel cell (DMFC). Cell resistance measurements showed a significant improvement of the water retention capability at intermediate temperature for the composite membranes, in particular the LDH-based one. This feature was investigated and explained by NMR (diffusometry, relaxometry, and ^1H spectral analysis) of the different membranes. The pulsed field gradient stimulated-echo (PFG-STE) method [325] was used to measure self-diffusion coefficients of water and methanol. In both composite membranes, Naf-Lap and Naf-LDH, the water diffusion coefficient was always higher than that of methanol in the investigated temperature range, proving the beneficial blocking effect of the nanoparticles dispersed in the polymer. However, for the filler free Nafion, the diffusion coefficients of methanol were higher than those of water. This result was evidently responsible for the methanol crossover observed in the direct methanol fuel cell operation.

Singha and Jana [326] explored the influence of interface chemistry of nano-clay on the properties of a poly(4,40-diphenylether-5,50-bibenzimidazole)(OPBI)/organoclay nanocomposite proton exchange membrane for a fuel cell. ^{13}C CP-MAS NMR spectra of the OPBI/organoclay-7% nanocomposite membranes showed that the organo-clay gave no peak at 32 ppm, indicating that the surfactant molecules were completely displaced from the clay galleries by the OPBI chains during nanocomposite membrane formation. Furthermore, the chemical shifts and intensity of the line spectra of the nanocomposite membranes compared to neat OPBI membrane changed due to hydrogen bonding interactions between the -N- atom of imidazole ring of OPBI chains and the oxygen atoms of the silicate basal plane of the nano-clay. Those interactions could help in enhancing the mechanical stability required to keep the membrane from degrading at higher operation temperatures.

2.5.4. Building materials

There is a long tradition of SS-NMR studies of building materials, with special focus on porous materials. The main reason is that moisture and (dissolved) ions can give rise to damage. Knowledge of the transport properties of moisture and salt is therefore critical to understanding of durability. Many NMR methods have been developed to measure water diffusivity in porous materials, which is challenging due to the presence of large internal magnetic field gradients originating from magnetic impurities (Fe).

The water diffusivity in porous materials is quite related to the tortuosity of the pore structure and several efforts have been made to shield a light on this parameter. Petkovic et al. [327] proposed a new analytical equation for the long-time signal decay in the measurement of diffusion. It was experimentally confirmed by measurements on representative materials with large internal gradients (fired-clay brick and sintered crushed glass) and a material with very small internal gradients (glass filter). A spin echo pulse sequence [325] was applied and the ratio of the amplitudes of the simulated echo, M_{st}, and the primary echo, M_{pt}, was measured as a function of the echo time, by changing the time interval between the second and third RF pulse. The complete set of data was obtained by varying the interpulse time τ and the applied external gradient G. The diffusivity, D, was determined from the slope, R, of the fitted exponential decay, $\ln(M_{st}/M_{pt})$, as a function of $(\gamma G)^2\ \tau^2$:

$$R = 1/T_1 + (\gamma G)^2 D\tau^2$$

They observed that the tortuosity of different samples derived from the NMR data showed an excellent agreement with the macroscopic tortuosity measured by electrochemical impedance spectroscopy.

The introduction of montmorillonite into Portland cement-based material leads to many improvements which is of great interest in the construction industry. NMR spectroscopy has been used for the characterization of nano-clays added to cement, determining the effect of the cement hydration state and following the potential pozzolanic reaction between Portland cement paste and the high amount of silicon dioxide (SiO_2) in nano-clays [328].

^{29}Si MAS-NMR spectroscopy was used to determine the hydration state of Portland cement powder, hardened Portland cement paste and hardened Portland cement-clay composite [328]. The variation of Q^0 (signals at ca. −71 ppm) intensity was used to estimate the degree of hydration (α) for the cement based composite through the following equation [329].

$$\alpha = \left[1 - \frac{I\left(Q^0\right)}{I^0\left(Q^0\right)}\right] x100\%$$

where $I(Q^0)$ was the intensity of Q^0 in the hydrated cement based composite and $I^0(Q^0)$ was the value of Q^0 in the Portland cement powder. The addition of nano-montmorillonite increased the α values and the Q^2/Q^1 ratios, which correlated with the improved microstructures of hydrated cement composite.

^{29}Si MAS NMR spectroscopy was also used to quantify the potentially reactive phases of alkaline cements produced from dehydroxylated red, white and ball clays [330]. ^{29}Si MAS NMR spectra were deconvoluted and the Si/Al ratios were calculated using zeolite's equation [17] allowing the SiO_2/Al_2O_3 ratios to be determined. Comparison of the degree of reaction and the SiO_2/Al_2O_3 ratios of the reaction products with the compressive strengths of cements indicated that the gel composition had a greater impact than the amount of the added compound on satisfactory mechanical strength development in alkaline cements.

A lower impact alternative to cement stabilization for walling materials is the use of alkali activated un-calcined clays, such as montmorillonite or illite. From ^{27}Al and ^{29}Si MAS NMR, Alastair et al. [331] confirmed that alkali activation of uncalcined montmorillonite formed a N-A-S-H (sodium aluminum silicate hydrate) or (N,C)-A-S-H (sodium-calcium aluminum silicate hydrate) geopolymer as the major product phase, which increased at higher Na:Al molar ratio. However, alkali activated illite with similar Si:Al ratio

resulted in structural alteration that led to poor quality materials [331].

Lime is widely used as an additive to improve the mechanical properties of clay minerals to be used for building materials. Pomakhina et al. [332] investigated by ^{29}Si MAS-NMR spectroscopy the pozzolanic reaction occurring in lime-treated Ca-bentonite. They observed that montmorillonite was dissolved with rapid and total consumption of SiO_2-polymorph. Mechanism of C–S–H formation was a function of the Ca content in the system and matched the sorosilicate-tobermorite model described in cement systems.

Pozzolans produced from a mixture of clay and palm kernel shells were analyzed by ^{29}Si and ^{27}Al MAS-NMR to determine the aluminate and the silicate phases of the hydrated product [333]. The ^{27}Al MAS-NMR showed that the calcined clay/palm kernel shell pozzolan produced stable mono-sulphate compounds at the octahedral environment and ^{29}Si MAS-NMR results proved that additional calcium silicate hydrates were formed in the cement containing pozzolan. The formation of stable mono-sulphates coupled with formation of additional silicate hydrates enhanced the strength the calcined materials.

Specially designed NMR hardware [334] allowed simultaneous and quantitative measurement of moisture (^{1}H) and sodium (^{23}Na) profiles for analyzing the influence of NaCl on the drying behavior of porous building materials [335]. In the case of water saturated fired-clay brick, two drying stages were observed in good agreement with the standard drying behavior of water saturated porous media. However, at 0% RH, NaCl suppressed the formation of a drying front. In the case of salt saturated fired-clay brick, the evaporation rate was higher at high relative humidity and salt ions crystallized as efflorescence on the surface of the brick. Hence, drying with salt led to a paradoxical situation in which increasing the relative humidity in the external air or reducing the external evaporation demanded increased the evaporation rate.

Additionally, NMR has been used to measure moisture profiles during drying of mono-material plaster specimens and of specimens of the same plasters applied on fired-clay brick; transverse relaxation time was used to examine the pore water distribution [336]. The NMR moisture profiles showed that the drying behavior of the water-repellent mono-plasters differed slightly from the reference, but when applied on brick, it significantly hindered the drying of the substrate. The addition of linseed oil to the lime plaster negatively influenced the bonding process and created hydraulic resistivity for the moisture to flow from the brick to the plaster during drying.

2.5.5. Dyes-pigments

Although dyes and pigments are both sources of color, there are some differences between them. Dyes are water-soluble colorants and depend on physical and/or chemical reactions to impart their color, whereas pigments are particles of color that are insoluble in water, oils, and resins. Generally, soluble colorants are used for coloring textiles, paper, and other substances while pigments are used for coloring paints, inks, cosmetics and plastics.

Clay minerals are often used in the dyes and pigment industry. For example, cationic dyes are adsorbed on clay mineral surfaces because the spectroscopic properties of the dye molecules change. The adsorbed dyes often exhibit unique spectroscopic and photochemical properties. Orientation and aggregation of the intercalated dye molecules modify the absorption and luminescence spectra, in steady-state or time-resolved modes.

A common phenomenon observed for paintings is the photodegradation of the dyes that can be dealt with by the stabilization and immobilization of organic dyes on inorganic bases such as clay.

Many SS-NMR studies have been performed with the aim of: i) elucidating the interaction between dye-pigment and clay; and; ii) characterizing the orientation and aggregation of the intercalated dye molecules [337-341].

Maya Blue (MB) is a pigment with a peculiar palette, ranging from a bright turquoise to a dark greenish blue, and it has enormous resistance to the attack of acids, alkalis, organic reagents, and biodegradation. Those properties depend on the attachment of indigo to clay minerals, and SS-NMR spectroscopy has been used to study the structure and interaction between this dye and clay.

Doménech et al. [337] used SS-NMR to study the association of indigo to palygorskite to form Maya Blue-like systems (MB). ^{27}Al MAS-NMR signals of the MB-clay did not become broader as a consequence of the high electronic density of the dye molecule, showing that a direct Al-dye interaction did not occur. However, ^{29}Si MAS-NMR signals shifted to stronger fields and became broader because of dye incorporation to palygorskite. It seems that indigo could be adsorbed close to silicon atoms, maybe interacting through Si-OH groups of clay and polar groups or π bonds of the dye. In addition, indigo interaction with silicon could come from the indigo external attachment to the palygorskite surface via terminal silanols. The majority of ^{13}C peaks were attributed to indigo signals suffering peak splitting. However, signals at 174.3, 168.9, and 166.5 ppm could be attributed only to dehydroindigo signals (or indigo signals that underwent a considerably higher shift).

Therefore, Maya Blue must be viewed as a complex polyfunctional organic–inorganic hybrid material involving different topological isomers of indigo and dehydroindigo molecules, distributed in the surface of the palygorskite framework and in the clay channels. Such isomers could tentatively be assigned to different dye-clay interactions involving hydrogen bonds with Mg^{2+} and Al^{3+} ions mediated by structural water and interaction of dye molecules with silanol units of the clay.

Borsacchi et al. [338] used SS-NMR spectroscopy for the characterization of Laponite Blue, prepared by the intercalation of dimethyldioctadecylammonium chloride (Laponite-2C18) and the cationic dye methylene blue in Laponite. ^{29}Si CP-MAS NMR spectra of Laponite before and after methylene blue sorption were identical [338], indicating that methylene blue did not induce chemical modifications to the clay. Interesting information was obtained from ^{1}H MAS-NMR spectra. The Laponite Blue spectrum showed the same signals as observed for Laponite-2C18, confirming that the treatment with both 2C18 and methylene blue still determined the removal of most of the physisorbed water and of silanol hydrogen-bonds. Signals of MB protons were not observed, probably due to the low amount of the dye and the intrinsic broadness of its signals, not efficiently removed by MAS. It is worth noticing that the spectrum of Laponite Blue showed an appreciable narrowing with respect to that of Laponite-2C18, indicating a higher mobility of the organic components in Laponite Blue with respect to Laponite-2C18.

The relative strengths of ^{1}H-^{29}Si dipolar coupling in different samples could be estimated using ^{1}H-^{29}Si CP-MAS NMR. The T_{SiH} of Q^3 silicons was not modified by the presence of the dye, suggesting that methylene blue was not located in close proximity of the clay platelets surface, where 2C18 cations would remain dominant. Moreover, the $T_{1\rho}$ values, related to proton spin–lattice relaxation time in the rotating frame, measured in Laponite Blue were clearly smaller than those of Laponite-2C18, due either to a very small intrinsic $T_{1\rho}$ of methylene blue or an increase of mobility in the kHz regime of the most abundant alkyl chains. Useful information on Laponite Blue was also obtained from ^{13}C MAS-NMR spectra. All the observed signals in Laponite-2C18 corresponded to 2C18 alkyl chains. However, in Laponite Blue the relative intensity of the peak at 31 ppm was significantly larger, suggesting that a higher fraction of surfactant alkyl chains experienced significant mobility, in agreement with what had already been highlighted by ^{1}H MAS-NMR spectra and $T_{1\rho}$ results.

Fournier et al. [339] prepared hybrid materials based on one organic dye, carminic acid, and montmorillonite, Al-Mt, and investigated the fixation of the organic molecules into the phyllosilicate thorough ^{13}C MAS-NMR. ^{13}C NMR spectra of carminic acid showed distinct regions for the resonances of the anthraquinone partial structure and the carbohydrate moieties. The spectrum of the composite carminic acid Al–Mt exhibited globally the same peaks as carminic acid, but some signals shifted to higher frequency. This was directly correlated to the chelation of aluminum with the oxygen in the anthraquinone part. The examination of NMR data recorded in acidic media showed a shift for the carbon bearing the ketone and catechol functions, and it indicated the formation of a complex between these functions and the aluminum cations [342]. Thus, NMR helped to shed light on the role that the ketone and catechol functions of the dye play for its fixation, and emphasized the decrease of its mobility when the lake pigment was formed.

Trigueiro et al. [340] also investigated, thorough ^{13}C and ^{27}Al MAS-NMR spectroscopy, the stabilization of carminic acid (CA) and Alizarin (Aliz) on Ti- and Al-pillared montmorillonite (PILC-Ti and PILC-Al) at different pH conditions. A PILC-Al sample gave a ^{27}Al MAS-NMR spectrum with the characteristic chemical shifts of montmorillonite and Keggin cation [343]. A shift of the signals in dyed samples at different pH values was observed. This may suggest the interactions between Aliz or CA and Si-OH-Al-OH in the montmorillonite edges as well as with pillar formation.

Although the ^{13}C MAS NMR spectra of the CA in pillared clay composites exhibited almost the same signals as the raw dye some changes in the chemical shifts were observed [339], suggesting chelation between the metallic cations and anthraquinone groups in the dyes. The chromophore groups in anthraquinone dyes could also behave as binding functions between the dye molecule and the mineral support through an intermediate metal atom [344]. For Alizarin, the resonances of the anthraquinone partial structure and hydroxyl groups occur in distinct regions. In both pillared clays, the peaks corresponding to hydroxyl groups shifted to higher frequency and the signals assigned to ketone functions shifted to an ill-defined shoulder. These results suggested that the ketone and hydroxyl groups of the dyes were the main attachment sites for the modified inorganic matrix. Electrostatic forces drove the interactions between chromophore groups and clay surface and/or complexation between metallic cations in the interlayer space and ketone and hydroxyl functions in the dye molecule.

Montmorillonites (Mt) modified with cationic polymers (CPs) were also investigated by NMR for the photostabilization of carminic acid (CA) [341]. The ^{13}C MAS-NMR spectrum of the 1–1 CPs-Mt composite displayed all the peaks previously assigned to the cationic polymer [341]. Spectra of CA-CPs-Mt composites displayed two series of peaks: those corresponding to the dye molecule and those corresponding to the cationic polymer. The latter signals were not affected by the presence of the CA, which confirmed that polymer intercalation in montmorillonite was not modified in the presence of CA. In contrast, several changes were observed in the region assigned to the organic dye: a splitting of the peak assigned to the ketone functions was observed resulting in peaks at 186 and 181 ppm, while in the range corresponding to carboxylic acids additional peaks appeared at 168.8 and 166 ppm. The signals assigned to the carbons bearing the –OH (C1, C3, C4 and C6) were strongly affected in the region 147–158 ppm. Finally, the peak at 72.6 ppm assigned to the OH bearing carbon shifted to 71.3 ppm, where it overlaps the signal assigned to the nitrogen bearing carbon in the cationic polymer.

The main adsorption mechanism appeared to be hydrogen bonding from OH^- groups of the carminic acid to surface groups present on the edge faces of the clay mineral and adsorbed cationic polymers molecules present on basal faces.

3. Conclusions and perspectives

The application of multinuclear SS-NMR methodologies to clay minerals provides useful information on their structures and, as demonstrated in this review, on their applications. Evidence obtained with SS-NMR has been useful in bringing better understanding of some of the most important applications of clay minerals, ranging from environmental to heterogeneous catalysis, through applications in pharmaceuticals and industry. However, there is still a long way to go and a closer collaboration between clay mineral researchers and SS-NMR experts will lead to a better exploitation of SS-NMR.

For example, the application of correlation experiments, both heteronuclear and homonuclear, could be very advantageous in many of the above applications. Moreover, the use of SS-NMR in application to clay minerals is often limited by the presence of paramagnetic impurities in clays minerals, and new developments on SS-NMR of paramagnetic nuclei could be very useful in alleviating such difficulties. Another highly promising field is *in-situ* SS-NMR experiments, which can be crucial in studying the controlled release of nutrient or drugs by clay minerals, and in heterogeneous catalysis, among other areas. Last, but not least, SS-NMR experiments with radioactive isotopes could break new and interesting ground in the safe use of clay minerals in the management of radioactive waste.

Funding

Dr. Pavón thanks University of Seville for the financial support of her current contract from VI PPIT-US program. This research did not receive any specific grant from funding agencies in the public, commercial, or not-for-profit sectors

Declaration of Competing Interest

The authors declare that they have no known competing financial interests or personal relationships that could have appeared to influence the work reported in this paper.

Appendix A. List of Abbreviations

Aliz	Alizarin
APTES:	3-aminopropyltriethoxysilane
CA	Carminic Acid
CBC:	Charge balancing cation
CP-MAS:	Cross polarization Magic Angle Spinning
CPs	Cationic polymers
CSA	Chemical shift Anisotropy
CWNMRI	Continuous wave nuclear magnetic resonance imaging
D	Diffusivity
DD:	Dipolar Dephasing
DDS	Drug delivery systems
DFT	Density Functional Theory
DGR:	Deep Geological Repository
DMFC	Direct methanol fuel cell
DP-MAS:	Direct Polarization Magic Angle Spinining
EBS:	Engineered barrier system
EXSY	Exchange spectroscopy experiment
FWHM	Full width at half maximum
G	External gradient

(*continued on next page*)

GCMD:	Grand canonical Molecular dynamics
HLRW:	High level radioactive waste
HPDEC:	High power decoupling
HPDSP	Hydroxypropyl di-starch phosphate
HR MAS	High resolution Magic Angle Spinning
HSA	Hydroxyl-SiAl oligocations
K_{oc}	Organic carbon normalized sorption coefficients
Lap	Laponite
LDH	Layered double hydroxide
LED	Light emitting diodes
LS(Cl)	Nano-chlorohectorites
LS(F)	Nano-fluorohectorites
MAS-NMR:	Magic Angle Spinning Nuclear Magnetic Resonance
MB	Maya Blue
MD:	Molecular dynamics
MEH-PPV	Poly(2-methoxy-5-(20-ethyl-hexyloxy)-1,4-phenylenevinylene),
M_{pt}	Amplitud primary echo
MQ	Multiple quantum
MQ-MAS	Multiple quantum magic angle spinning
M_{st}	Amplitud of simulated echo
Mt	Montmorillonite
N-A-S-H	Sodium aluminum silicate hydrate
(N,C)-A-S-H	Sodium calcium aluminum silicate
OM	Organic Matter
OMMT	Montmorillonite modified with a ternary ammonium salt
OPBI	Poly(4,40-diphenylether-5,50-bibenzimidazole)
PCH	Porous Clay heteroestructures
PFG-STE	Pulsed field gradient stimulated-echo
PILC	Pillaring clay
QCMC	Quaternized carboxymethyl chitosan
R6G	Rhodamine 6G
REE:	Rare earth elements
RH	Humidity
RN:	Radionuclides
$scCH_4$	Supercritical CH_4
$scCO_2$:	Supercritical CO_2 (>304.25 K and > 7.39 MPa).
SEDOR	Spin Echo Double Resonance
SS-NMR	Solid State nuclear magnetic resonance
T_1	Spin-lattice relaxation time
$T_{1\rho}$	Proton spin–lattice relaxation time
T_2	Transverse relaxation time
TCE:	Trichloroethylene
TEA	Triethylaluminum
TMA	Trimethylaluminum
TN	Taeniolite
T_{SiH}	Cross spin constant time
UV	Ultraviolete
VACP	Variable amplitude cross polarization
α	Degree of cement hydration
τ_C	Correlation time

References

[1] B. Velde, Origin and Mineralogy of Clays, Springer-Verlag, New York, 1995.
[2] H.H. Murray, Applied Clay Mineralogy: Occurrences, Processing and Application of Kaolins, Bentonites, Palygorskite-Sepiolite, and Common Clays, in: Applied Clay Mineralogy: Occurrences, Processing and Application of Kaolins, Bentonites, Palygorskite-Sepiolite, and Common Clays, Elsevier Science Bv, Amsterdam, 2007, pp. 1–180.
[3] M. Rieder, G. Cavazzini, Y.S. D'Yakonov, V.A. Frank-Kamenetskii, G. Gottardi, S. Guggenheim, P.V. Koval, G. Muller, A.M.R. Neiva, E.W. Radoslovich, et al., Nomenclature of the micas, Clays Clay Miner. 46 (1998) 586–595.
[4] M.D. Foster, The Relation Between Composition and Swelling in Clays, Clays Clay Miner. 3 (1954) 205–220.
[5] E. Pavon, M.A. Castro, M. Naranjo, M. Mar Orta, M. Carolina Pazos, M.D. Alba, Hydration properties of synthetic high-charge micas saturated with different cations: An experimental approach, Am. Mineral. 98 (2013) 394–400.
[6] A.C. Perdigon, C. Pesquera, A. Cota, F.J. Osuna, E. Pavon, M.D. Alba, Heteroatom framework distribution and layer charge of sodium Taeniolite, Appl. Clay Sci. 158 (2018) 246–251.
[7] R.C. Mackenzie, The Classification and Nomenclature of Clay Minerals, Clay Minerals Bulletin 4 (1959) 52–66.
[8] F. Bergaya, G. Lagaly, M. Vayer, Chapter 2.11 - Cation and Anion Exchange, in: F. Bergaya, G. Lagaly (Eds.), Developments in Clay Science, Elsevier, 2013, pp. 333–359.
[9] R. Dohrmann, Cation exchange capacity methodology I: An efficient model for the detection of incorrect cation exchange capacity and exchangeable cation results, Appl. Clay Sci. 34 (2006) 31–37.
[10] R.A. Schoonheydt, C.T. Johnston, F. Bergaya, 1 - Clay minerals and their surfaces, in: R. Schoonheydt, C.T. Johnston, F. Bergaya (Eds.), Developments in Clay Science, Elsevier, 2018, pp. 1–21.
[11] R.A. Schoonheydt, C.T. Johnston, Chapter 3 Surface and Interface Chemistry of Clay Minerals, in: F. Bergaya, B.K.G. Theng, G. Lagaly (Eds.), Developments in Clay Science, Elsevier, 2006, pp. 87–113.
[12] I.E. Odom, Smectite clay Minerals: Properties and Uses, Philosophical Transactions of the Royal Society of London, Series A, Mathematical and Physical Sciences 311 (1984) 391–409.
[13] A. Meunier, Clays, Springer, New York, NY, 2004.
[14] J. Środoń, Chapter 2.2 - Identification and Quantitative Analysis of Clay Minerals, in: F. Bergaya, G. Lagaly (Eds.), Developments in Clay Science, Elsevier, 2013, pp. 25–49.
[15] J. Sanz, Chapter 12.7 Nuclear Magnetic Resonance Spectroscopy, in: F. Bergaya, B.K.G. Theng, G. Lagaly (Eds.), Developments in Clay Science, Elsevier, 2006, pp. 919–938.
[16] J. Sanz, D. Massiot, Chapter 2.8 - Nuclear Magnetic Resonance Spectroscopy, in: F. Bergaya, G. Lagaly (Eds.), Developments in Clay Science, Elsevier, 2013, pp. 233–274.
[17] G. Engelhardt, D. Michel, High-Resolution Solid-State NMR of Silicates and Zeolites, London (1987).
[18] S.E. Ashbrook, D.M. Dawson, NMR spectroscopy of minerals and allied materials, in: Nuclear Magnetic Resonance, vol. 45, The Royal Society of Chemistry, 2016, pp. 1–52.
[19] J. Sanz, J.M. Serratosa, Silicon-29 and aluminum-27 high-resolution MAS-NMR spectra of phyllosilicates, J. Am. Chem. Soc. 106 (1984) 4790–4793.
[20] H.J. Jakobsen, N.C. Nielsen, H. Lindgreen, Sequences of charged sheets in rectorite, Am. Mineral. 80 (1995) 247–252.
[21] S.P. Altaner, C.A. Weiss, R.J. Kirkpatrick, Evidence from ^{29}Si NMR for the structure of mixed-layer illite/smectite clay minerals, Nature 331 (1988) 699–702.
[22] J. Sanz, J.L. Robert, Influence of structural factors on ^{29}Si and ^{27}Al NMR chemical shifts of phyllosilicates 2:1, Phys. Chem. Miner. 19 (1992) 39–45.
[23] E. Pavón, M.A. Castro, A. Cota, F.J. Osuna, M.C. Pazos, M.D. Alba, Interaction of hydrated cations with mica-n (n = 2, 3 and 4) surface, J. Phys. Chem. C 118 (2014) 2115–2121.
[24] A.S. Cattaneo, S. Bracco, A. Comotti, M. Galimberti, P. Sozzani, H. Eckert, Structural Characterization of Pristine and Modified Fluoromica Using Multinuclear Solid-State NMR, J. Phys. Chem. C 115 (2011) 12517–12529.
[25] J. Grandjean, Solid-state NMR study of modified clays and polymer/clay nanocomposites, Clay Miner. 41 (2006) 567–586.
[26] J. Rocha, C.M. Morais, C. Fernandez, Novel nuclear magnetic resonance techniques for the study of quadrupolar nuclei in clays and other layered materials, Clay Miner. 38 (2018) 259–278.
[27] M.R. Seger, G.E. Maciel, NMR investigation of the behavior of an organothiophosphate pesticide, methyl parathion, sorbed on clays, Environ. Sci. Technol. 40 (2006) 552–558.
[28] M.R. Seger, G.E. Maciel, NMR investigation of the behavior of an organothiophosphate pesticide, chlorpyrifos, sorbed on montmorillonite clays, Environ. Sci. Technol. 40 (2006) 797–802.
[29] M.R. Seger, G.E. Maciel, NMR investigation of the behavior of an organothiophosphate pesticide, chlorpyrifos, sorted on soil components, Environ. Sci. Technol. 40 (2006) 791–796.
[30] C. Chamignon, N. Haroune, C. Forano, A.M. Delort, P. Besse-Hoggan, B. Combourieu, Mobility of organic pollutants in soil components. What role can magic angle spinning NMR play?, Eur J. Soil Sci. 59 (2008) 572–583.
[31] B. Combourieu, J. Inacio, C. Taviot-Guého, C. Forano, A.M. Delort, Pesticide Mobility Studied by Nuclear Magnetic Resonance, in: E. Lichtfouse, J. Schwarzbauer, D. Robert (Eds.), Environmental Chemistry: Green Chemistry and Pollutants in Ecosystems, Springer, Berlin Heidelberg, Berlin, Heidelberg, 2005, pp. 463–472.
[32] B. Combourieu, J. Inacio, A.M. Delort, C. Forano, Differentiation of mobile and immobile pesticides on anionic clays by ^{1}H HR MAS NMR spectroscopy, Chem. Commun. (2001) 2214–2215.
[33] M.A. Nanny, R.A. Minear, J.A. Leenheer, Nuclear Magnetic Resonance Spectroscopy in Environmental Chemistry, Oxford University Press, 1997.

[34] C.J. Golding, R.J. Smernik, G.F. Birch, Investigation of the role of structural domains identified in sedimentary organic matter in the sorption of hydrophobic organic compounds, Environ. Sci. Technol. 39 (2005) 3925–3932.
[35] A. Oren, B. Chefetz, Sorption-desorption behavior of polycyclic aromatic hydrocarbons in upstream and downstream river sediments, Chemosphere 61 (2005) 19–29.
[36] R. Ahmad, P.N. Nelson, R.S. Kookana, The molecular composition of soil organic matter as determined by ^{13}C NMR and elemental analyses and correlation with pesticide sorption, Eur. J. Soil Sci. 57 (2006) 883–893.
[37] R.J. Smernik, R.S. Kookana, J.O. Skjemstad, NMR characterization of ^{13}C-benzene sorbed to natural and prepared charcoals, Environ. Sci. Technol. 40 (2006) 1764–1769.
[38] J.L. Bonin, M.J. Simpson, Variation in phenanthrene sorption coefficients with soil organic matter fractionation: The result of structure or conformation?, Environ Sci. Technol. 41 (2007) 153–159.
[39] E.F. Emery, T. Junk, R.E. Ferrell Jr, R. De Hon, L.G. Butler, Solid-state ^{2}H MAS NMR studies of TNT absorption in soil and clays, Environ. Sci. Technol. 35 (2001) 2973–2978.
[40] M.A. Nanny, J.P. Maza, Noncovalent interactions between monoaromatic compounds and dissolved humic acids: A deuterium NMR T1 relaxation study, Environ. Sci. Technol. 35 (2001) 379–384.
[41] S.D. Kohl, P.J. Toscano, W. Hou, J.A. Rice, Solid-state ^{19}F NMR investigation of hexafluorobenzene sorption to soil organic matter, Environ. Sci. Technol. 34 (2000) 204–210.
[42] A.J. Simpson, M.J. Simpson, W.L. Kingery, B.A. Lefebvre, A. Moser, A.J. Williams, M. Kvasha, B.P. Kelleher, The application of ^{1}H high-resolution magic-angle spinning NMR for the study of clay-organic associations in natural and synthetic complexes, Langmuir 22 (2006) 4498–4503.
[43] Q. Solihin, W. Zhang, F. Tongamp, Saito, Mechanochemical route for synthesizing KM_gPO_4 and NH_4MgPO_4 for application as slow-release fertilizers, Ind. Eng. Chem. Res. 49 (2010) 2213–2216.
[44] Q. Solihin, W. Zhang, F. Tongamp, Saito, Mechanochemical synthesis of kaolin-KH_2PO_4 and kaolin-$NH_4H_2PO_4$ complexes for application as slow release fertilizer, Powder Technol. 212 (2011) 354–358.
[45] Q. Zhang, Solihin, F, Saito, Mechanochemical synthesis of slow-release fertilizers through incorporation of alumina composition into potassium/ammonium phosphates, Journal of the American Ceramic Society 92 (2009) 3070–3073.
[46] R. Borges, S.F. Brunatto, A.A. Leitaõ, G.S.G. De Carvalho, F. Wypych, Solid-state mechanochemical activation of clay minerals and soluble phosphate mixtures to obtain slow-release fertilizers, Clay Miner. 50 (2015) 153–162.
[47] Y. Li, J. Zhang, Agricultural diffuse pollution from fertilisers and pesticides in China, in: Water Science and Technology, 1999, pp. 25–32.
[48] A. Shaviv, Advances in controlled-release fertilizers, in: Advances in Agronomy, 2001, pp. 1–49.
[49] V. Balek, L.A. Pérez-Maqueda, J. Poyato, Z. Černý, V. Ramírez-Valle, I.M. Buntseva, J.L. Pérez-Rodríguez, Effect of grinding on thermal reactivity of ceramic clay minerals, J. Therm. Anal. Calorim. 88 (2007) 87–91.
[50] V. Balek, J. Šubrt, L.A. Pérez-Maqueda, M. Beneš, I.M. Bountseva, I.N. Beckman, J.L. Pérez-Rodríguez, Thermal behavior of ground talc mineral, J. Min. Metall. Sect. B. 44 (2008) 7–17.
[51] G.E. Christidis, F. Dellisanti, G. Valdre, P. Makri, Structural modifications of smectites mechanically deformed under controlled conditions, Clay Miner. 40 (2005) 511–522.
[52] G.E. Christidis, P. Makri, V. Perdikatsis, Influence of grinding on the structure and colour properties of talc, bentonite and calcite white fillers, Clay Miner. 39 (2004) 163–175.
[53] F. Dellisanti, G. Valdré, Study of structural properties of ion treated and mechanically deformed commercial bentonite, Appl. Clay Sci. 28 (2005) 233–244.
[54] A. Djukić, U. Jovanović, T. Tuvić, V. Andrić, J. Grbović Novaković, N. Ivanović, L. Matović, The potential of ball-milled Serbian natural clay for removal of heavy metal contaminants from wastewaters: Simultaneous sorption of Ni, Cr, Cd and Pb ions, Ceram. Int. 39 (2013) 7173–7178.
[55] A. Dumas, F. Martin, C. Le Roux, P. Micoud, S. Petit, E. Ferrage, J. Brendlé, O. Grauby, M. Greenhill-Hooper, Phyllosilicates synthesis: A way of accessing edges contributions in NMR and FTIR spectroscopies. Example of synthetic talc, Phys. Chem. Miner. 40 (2013) 361–373.
[56] M. Galimberti, M. Coombs, V. Cipolletti, A. Spatola, G. Guerra, A. Lostritto, L. Giannini, S. Pandini, T. Riccò, Delaminated and intercalated organically modified montmorillonite in poly(1,4-cis-isoprene) matrix. Indications of counterintuitive dynamic-mechanical behavior, Appl. Clay Sci. 97–98 (2014) 8–16.
[57] E. Mendelovici, Selective mechanochemical reactions on dry grinding structurally different silicates, J. Mater. Sci. Lett. 20 (2001) 81–83.
[58] U. Mingelgrin, L. Kliger, M. Gal, S. Saltzman, Effect of grinding on the structure and behavior of bentonites, Clays Clay Miner. 26 (1978) 299–307.
[59] L. Petra, P. Billik, P. Komadel, Preparation and characterization of hybrid materials consisting of high-energy ground montmorillonite and α-amino acids, Appl. Clay Sci. 115 (2015) 174–178.
[60] A.R. Ramadan, A.M.K. Esawi, A.A. Gawad, Effect of ball milling on the structure of Na^{+}-montmorillonite and organo-montmorillonite, Cloisite 30B, Appl. Clay Sci. 47 (2010) 196–202.
[61] P.J. Sánchez-Soto, A. Wiewióra, M.A. Avilés, A. Justo, L.A. Pérez-Maqueda, J.L. Pérez-Rodríguez, P. Bylina, Talc from Puebla de Lillo, Spain. II. Effect of dry grinding on particle size and shape, Appl. Clay Sci. 12 (1997) 297–312.
[62] C. Vizcayno, R.M. de Gutiérrez, R. Castello, E. Rodriguez, C.E. Guerrero, Pozzolan obtained by mechanochemical and thermal treatments of kaolin, Appl. Clay Sci. 49 (2010) 405–413.
[63] R. Borges, L. MacEdo Dutra, A. Barison, F. Wypych, MAS NMR and EPR study of structural changes in talc and montmorillonite induced by grinding, Clay Miner. 51 (2016) 69–80.
[64] R. Borges, V. Prevot, C. Forano, F. Wypych, Design and Kinetic Study of Sustainable Potential Slow-Release Fertilizer Obtained by Mechanochemical Activation of Clay Minerals and Potassium Monohydrogen Phosphate, Ind. Eng. Chem. Res. 56 (2017) 708–716.
[65] R. Borges, F. Wypych, E. Petit, C. Forano, V. Prevot, Potential sustainable slow-release fertilizers obtained by mechanochemical activation of MgAl and MgFe layered double hydroxides and K_2HPO_4, Nanomaterials 9 (2019).
[66] R.B. Jackson, A. Vengosh, J.W. Carey, R.J. Davies, T.H. Darrah, F. O'Sullivan, G. Pétron, The Environmental Costs and Benefits of Fracking, Annu. Rev. Environ. Resour. 39 (2014) 327–362.
[67] S. Bachu, D. Bonijoly, J. Bradshaw, R. Burruss, S. Holloway, N.P. Christensen, O. M. Mathiassen, CO_2 storage capacity estimation: Methodology and gaps, Int. J. Greenhouse Gas Control 1 (2007) 430–443.
[68] S.M. Benson, D.R. Cole, CO_2 sequestration in deep sedimentary formations, Elements 4 (2008) 325–331.
[69] E. Berrezueta, L. González-Menéndez, D. Breitner, L. Luquot, Pore system changes during experimental CO_2 injection into detritic rocks: Studies of potential storage rocks from some sedimentary basins of Spain, Int. J. Greenhouse Gas Control 17 (2013) 411–422.
[70] M.J. Bickle, Geological carbon storage, Nat. Geosci. 2 (2009) 815–818.
[71] I.C. Bourg, L.E. Beckingham, D.J. DePaolo, The Nanoscale Basis of CO_2 Trapping for Geologic Storage, Environ. Sci. Technol. 49 (2015) 10265–10284.
[72] A. Busch, P. Bertier, Y. Gensterblum, G. Rother, C.J. Spiers, M. Zhang, H.M. Wentinck, On sorption and swelling of CO_2 in clays, Geomech. Geophys. Geo-Energy Geo-Resour. 2 (2016) 111–130.
[73] D.R. Cole, A.A. Chialvo, G. Rother, L. Vlcek, P.T. Cummings, Supercritical fluid behavior at nanoscale interfaces: Implications for CO_2 sequestration in geologic formations, Phil. Mag. 90 (2010) 2339–2363.
[74] K. Edlmann, S. Haszeldine, C.I. McDermott, Experimental investigation into the sealing capability of naturally fractured shale caprocks to supercritical carbon dioxide flow, Environ. Earth Sci. 70 (2013) 3393–3409.
[75] I. Gaus, Role and impact of CO_2-rock interactions during CO_2 storage in sedimentary rocks, Int. J. Greenhouse Gas Control 4 (2010) 73–89.
[76] L.M. Hamm, I.C. Bourg, A.F. Wallace, B. Rotenberg, Molecular simulation of CO2- and CO3 -brine-mineral systems, in: Reviews in Mineralogy and Geochemistry, 2013, pp. 189–228.
[77] R. Heller, M. Zoback, Adsorption of methane and carbon dioxide on gas shale and pure mineral samples, J. Unconven. Oil Gas Resour. 8 (2014) 14–24.
[78] K.S. Lackner, A guide to CO_2 sequestration, Science 300 (2003) 1677–1678.
[79] R.S. Middleton, J.W. Carey, R.P. Currier, J.D. Hyman, Q. Kang, S. Karra, J. Jiménez-Martínez, M.L. Porter, H.S. Viswanathan, Shale gas and non-aqueous fracturing fluids: Opportunities and challenges for supercritical CO_2, Appl. Energy 147 (2015) 500–509.
[80] S.I. Plasynski, J.T. Litynski, H.G. McIlvried, D.M. Vikara, R.D. Srivastava, The critical role of monitoring, verification, and accounting for geologic carbon dioxide storage projects, Environ. Geosci. 18 (2011) 19–34.
[81] D.J.K. Ross, R. Marc Bustin, The importance of shale composition and pore structure upon gas storage potential of shale gas reservoirs, Mar. Pet. Geol. 26 (2009) 916–927.
[82] J. Rutqvist, The geomechanics of CO_2 storage in deep sedimentary formations, Geotech. Geol. Eng. 30 (2012) 525–551.
[83] D.W. Hoyt, R.V.F. Turcu, J.A. Sears, K.M. Rosso, S.D. Burton, A.R. Felmy, J.Z. Hu, High-pressure magic angle spinning nuclear magnetic resonance, J. Magn. Reson. 212 (2011) 378–385.
[84] R.V.F. Turcu, D.W. Hoyt, K.M. Rosso, J.A. Sears, J.S. Loring, A.R. Felmy, J.Z. Hu, Rotor design for high pressure magic angle spinning nuclear magnetic resonance, J. Magn. Reson. 226 (2013) 64–69.
[85] G.M. Bowers, D.W. Hoyt, S.D. Burton, B.O. Ferguson, T. Varga, R.J. Kirkpatrick, In situ ^{13}C and ^{23}Na magic angle spinning NMR investigation of supercritical CO_2 incorporation in smectite-natural organic matter composites, J. Phys. Chem. C 118 (2014) 3564–3573.
[86] R.T. Cygan, V.N. Romanov, E.M. Myshakin, Molecular simulation of carbon dioxide capture by montmorillonite using an accurate and flexible force field, J. Phys. Chem. C 116 (2012) 13079–13091.
[87] R.J. Kirkpatrick, A.G. Kalinichev, G.M. Bowers, A.O. Yazaydin, M. Krishnan, M. Saharay, C.P. Morrow, Review. NMR and computational molecular modeling studies of mineral surfaces and interlayer galleries: A review, Am. Mineral. 100 (2015) 1341–1354.
[88] G.M. Bowers, H. Todd Schaef, J.S. Loring, D.W. Hoyt, S.D. Burton, E.D. Walter, R. James Kirkpatrick, Role of cations in CO_2 adsorption, dynamics, and hydration in smectite clays under in situ supercritical CO_2 conditions, J. Phys. Chem. C 121 (2017) 577–592.
[89] N. Loganathan, G.M. Bowers, A.O. Yazaydin, H.T. Schaef, J.S. Loring, A.G. Kalinichev, R.J. Kirkpatrick, Clay Swelling in Dry Supercritical Carbon Dioxide: Effects of Interlayer Cations on the Structure, Dynamics, and Energetics of CO_2 Intercalation Probed by XRD, NMR, and GCMD Simulations, J. Phys. Chem. C 122 (2018) 4391–4402.

[90] A. Kadoura, A.K. Narayanan Nair, S. Sun, Molecular Simulation Study of Montmorillonite in Contact with Variably Wet Supercritical Carbon Dioxide, The J. Phys. Chem. C 121 (2017) 6199–6208.
[91] E.M. Myshakin, W.A. Saidi, V.N. Romanov, R.T. Cygan, K.D. Jordan, Molecular Dynamics Simulations of Carbon Dioxide Intercalation in Hydrated Na-Montmorillonite, The J. Phys. Chem. C 117 (2013) 11028–11039.
[92] M. Makaremi, K.D. Jordan, G.D. Guthrie, E.M. Myshakin, Multiphase Monte Carlo and Molecular Dynamics Simulations of Water and CO_2 Intercalation in Montmorillonite and Beidellite, The J. Phys. Chem. C 119 (2015) 15112–15124.
[93] Q. Rao, Y. Leng, Molecular Understanding of CO_2 and H_2O in a Montmorillonite Clay Interlayer under CO_2 Geological Sequestration Conditions, The J. Phys. Chem. C 120 (2016) 2642–2654.
[94] Q. Rao, Y. Leng, Effect of Layer Charge on CO_2 and H_2O Intercalations in Swelling Clays, Langmuir 32 (2016) 11366–11374.
[95] N. Loganathan, A.O. Yazaydin, G.M. Bowers, A.G. Kalinichev, R.J. Kirkpatrick, Molecular Dynamics Study of CO_2 and H_2O Intercalation in Smectite Clays: Effect of Temperature and Pressure on Interlayer Structure and Dynamics in Hectorite, The J. Phys. Chem. C 121 (2017) 24527–24540.
[96] H.T. Schaef, N. Loganathan, G.M. Bowers, R.J. Kirkpatrick, A.O. Yazaydin, S.D. Burton, D.W. Hoyt, K.S. Thanthiriwatte, D.A. Dixon, B.P. McGrail, et al., Tipping Point for Expansion of Layered Aluminosilicates in Weakly Polar Solvents: Supercritical CO_2, ACS Appl. Mater. Interfaces 9 (2017) 36783–36791.
[97] A.G. Ilgen, J.E. Heath, I.Y. Akkutlu, L.T. Bryndzia, D.R. Cole, Y.K. Kharaka, T.J. Kneafsey, K.L. Milliken, L.J. Pyrak-Nolte, R. Suarez-Rivera, Shales at all scales: Exploring coupled processes in mudrocks, Earth Sci. Rev. 166 (2017) 132–152.
[98] D.R. Cole, S. Ok, A. Striolo, A. Phan, Hydrocarbon behavior at nanoscale interfaces, in: Reviews in Mineralogy and Geochemistry, 2013, pp. 495–545.
[99] S. Ok, D.W. Hoyt, A. Andersen, J. Sheets, S.A. Welch, D.R. Cole, K.T. Mueller, N. M. Washton, Surface Interactions and Confinement of Methane: A High Pressure Magic Angle Spinning NMR and Computational Chemistry Study, Langmuir 33 (2017) 1359–1367.
[100] G.M. Bowers, J.S. Loring, H.T. Schaef, E.D. Walter, S.D. Burton, D.W. Hoyt, S.S. Cunniff, N. Loganathan, R.J. Kirkpatrick, Interaction of Hydrocarbons with Clays under Reservoir Conditions: In Situ Infrared and Nuclear Magnetic Resonance Spectroscopy and X-ray Diffraction for Expandable Clays with Variably Wet Supercritical Methane, ACS Earth Space Chem. 2 (2018) 640–652.
[101] G.M. Bowers, J.S. Loring, E.D. Walter, S.D. Burton, M.E. Bowden, D.W. Hoyt, B. Arey, R.K. Larsen, R.J. Kirkpatrick, Influence of Smectite Structure and Hydration on Supercritical Methane Binding and Dynamics in Smectite Pores, J. Phys. Chem. C 123 (2019) 29231–29244.
[102] B. Ma, L. Charlet, A. Fernandez-Martinez, M. Kang, B. Madé, A review of the retention mechanisms of redox-sensitive radionuclides in multi-barrier systems, Appl. Geochem. 100 (2019) 414–431.
[103] M.D. Alba, J.I. Corredor, E. Pavón, Structural studies of radionuclides immobilized matrix by solid state NMR, in: L. Sánchez-Muñoz, L. Garrido Fernández, J. Sanz (Eds.), Applications of NMR spectroscopy in the solid state Consejo Superior de Investigaciones Científicas, Madrid, 2019, pp. 171–195.
[104] T. Charpentier, L. Martel, A.H. Mir, J. Somers, C. Jégou, S. Peuget, Self-healing capacity of nuclear glass observed by NMR spectroscopy, Sci. Rep. 6 (2016).
[105] N. Forler, F. Vasconcelos, S. Cristol, J.F. Paul, L. Montagne, T. Charpentier, F. Mauri, L. Delevoye, New insights into oxygen environments generated during phosphate glass alteration: A combined ^{17}O MAS and MQMAS NMR and first principles calculations study, PCCP 12 (2010) 9053–9062.
[106] N. Ollier, T. Charpentier, B. Boizot, G. Petite, A structural approach by MAS NMR spectroscopy of mechanisms occurring under β-irradiation in mixed alkali aluminoborosilicate glasses, J. Phys.: Condens. Matter 16 (2004) 7625–7635.
[107] E. Nicoleau, F. Angeli, S. Schuller, T. Charpentier, P. Jollivet, M. Moskura, Rare-earth silicate crystallization in borosilicate glasses: Effect on structural and chemical durability properties, J. Non-Cryst. Solids 438 (2016) 37–48.
[108] F. Angeli, T. Charpentier, E. Molières, A. Soleilhavoup, P. Jollivet, S. Gin, Influence of lanthanum on borosilicate glass structure: A multinuclear MAS and MQMAS NMR investigation, J. Non-Cryst. Solids 376 (2013) 189–198.
[109] D. Savage, C. Watson, S. Benbow, J. Wilson, Modelling iron-bentonite interactions, Appl. Clay Sci. 47 (2010) 91–98.
[110] A. Gaudin, S. Gaboreau, E. Tinseau, D. Bartier, S. Petit, O. Grauby, F. Foct, D. Beaufort, Mineralogical reactions in the Tournemire argillite after in-situ interaction with steels, Appl. Clay Sci. 43 (2009) 196–207.
[111] L. Carlson, O. Karnland, V.M. Oversby, A.P. Rance, N.R. Smart, M. Snellman, M. Vähänen, L.O. Werme, Experimental studies of the interactions between anaerobically corroding iron and bentonite, Phys. Chem. Earth, Parts A/B/C 32 (2007) 334–345.
[112] O. Bildstein, L. Trotignon, M. Perronnet, M. Jullien, Modelling iron–clay interactions in deep geological disposal conditions, Physics and Chemistry of the Earth, Parts A/B/C 31 (2006) 618–625.
[113] E. Galunin, M.D. Alba, M. Vidal, Stability of rare-earth disilicates: Ionic radius effect, J. Am. Ceram. Soc. 94 (2011) 1568–1574.
[114] P. Chain, A. Cota, S. El Mrabet, E. Pavón, M.C. Pazos, M.D. Alba, Evaluation of rare earth on layered silicates under subcritical conditions: Effect of the framework and interlayer space composition, Chem. Geol. 347 (2013) 208–216.
[115] M.D. Alba, P. Chain, M.M. Orta, Chemical reactivity of argillaceous material in engineered barrierRare earth disilicate formation under subcritical conditions, Appl. Clay Sci. 43 (2009) 369–375.
[116] M.D. Alba, P. Chain, M.M. Orta, Rare-earth disilicate formation under Deep Geological Repository approach conditions, Appl. Clay Sci. 46 (2009) 63–68.
[117] M.D. Alba, M.A. Castro, M. Naranjo, E. Pavón, Hydrothermal reactivity of Na-n-micas (n = 2, 3, 4), Chem. Mater. 18 (2006) 2867–2872.
[118] M.D. Alba, A.I. Becerro, M.A. Castro, A.C. Perdigón, Hydrothermal reactivity of Lu-saturated smectites: Part II. A short-range order study, Am. Mineral. 86 (2001) 124–131.
[119] M.D. Alba, P. Chain, Interaction between Lu cations and 2:1 aluminosilicates under hydrothermal treatment, Clays Clay Miner. 53 (2005) 37–44.
[120] M. Mantovani, A. Escudero, M.D. Alba, A.I. Becerro, Stability of phyllosilicates in $Ca(OH)_2$ solution: Influence of layer nature, octahedral occupation, presence of tetrahedral Al and degree of crystallinity, Appl. Geochem. 24 (2009) 1251–1260.
[121] P. Sellin, O.X. Leupin, The Use of Clay as an Engineered Barrier in Radioactive-Waste Management- A Review, Clays Clay Miner. 61 (2013) 477–498.
[122] F.J. Osuna, P. Chain, A. Cota, E. Pavón, M.D. Alba, Impact of hydrothermal treatment of FEBEX and MX80 bentonites in water, HNO_3 and $Lu(NO_3)_3$ media: Implications for radioactive waste control, Appl. Clay Sci. 118 (2015) 48–55.
[123] K. Buesseler, M. Aoyama, M. Fukasawa, Impacts of the Fukushima Nuclear Power Plants on Marine Radioactivity, Environ. Sci. Technol. 45 (2011) 9931–9935.
[124] S. Endo, S. Kimura, T. Takatsuji, K. Nanasawa, T. Imanaka, K. Shizuma, Measurement of soil contamination by radionuclides due to the Fukushima Dai-ichi Nuclear Power Plant accident and associated estimated cumulative external dose estimation, J. Environ. Radioact. 111 (2012) 18–27.
[125] S.V. Fesenko, S.I. Spiridonov, N.I. Sanzharova, R.M. Alexakhin, Dynamics of ^{137}Cs bioavailability in a soil-plant system in areas of the Chernobyl Nuclear Power Plant accident zone with a different physico-chemical composition of radioactive fallout, J. Environ. Radioact. 34 (1997) 287–313.
[126] R.E. Linnemann, Soviet Medical Response to the Chernobyl Nuclear Accident, JAMA 258 (1987) 637–643.
[127] C.W. Park, B.H. Kim, H.-M. Yang, B.-K. Seo, K.-W. Lee, Enhanced desorption of Cs from clays by a polymeric cation-exchange agent, J. Hazard. Mater. 327 (2017) 127–134.
[128] D. Ding, Z. Zhang, Z. Lei, Y. Yang, T. Cai, Remediation of radiocesium-contaminated liquid waste, soil, and ash: a mini review since the Fukushima Daiichi Nuclear Power Plant accident, Environ. Sci. Pollut. Res. 23 (2016) 2249–2263.
[129] T. Yamamoto, Radioactivity of fission product and heavy nuclides deposited on soil in Fukushima Dai-Ichi Nuclear Power Plant accident, J. Nucl. Sci. Technol. 49 (2012) 1116–1133.
[130] Y. Muramatsu, W. Rühm, S. Yoshida, K. Tagami, S. Uchida, E. Wirth, Concentrations of ^{239}Pu and ^{240}Pu and their isotopic ratios determined by ICP-MS in soils collected from the Chernobyl 30-km zone, Environ. Sci. Technol. 34 (2000) 2913–2917.
[131] L.N. Lammers, I.C. Bourg, M. Okumura, K. Kolluri, G. Sposito, M. Machida, Molecular dynamics simulations of cesium adsorption on illite nanoparticles, J. Colloid Interface Sci. 490 (2017) 608–620.
[132] A.J. Fuller, S. Shaw, M.B. Ward, S.J. Haigh, J.F.W. Mosselmans, C.L. Peacock, S. Stackhouse, A.J. Dent, D. Trivedi, I.T. Burke, Caesium incorporation and retention in illite interlayers, Appl. Clay Sci. 108 (2015) 128–134.
[133] J.P. McKinley, J.M. Zachara, S.M. Heald, A. Dohnalkova, M.G. Newville, S.R. Sutton, Microscale Distribution of Cesium Sorbed to Biotite and Muscovite, Environ. Sci. Technol. 38 (2004) 1017–1023.
[134] T.C. Maiti, M.R. Smith, J.C. Laul, Colloid Formation Study of U, Th, Ra, Pb, Po, Sr, Rb, and Cs in Briny (High Ionic Strength) Groundwaters: Analog Study for Waste Disposal, Nucl. Technol. 84 (1989) 82–87.
[135] R.N.J. Comans, M. Haller, P. De Preter, Sorption of cesium on illite: Non-equilibrium behaviour and reversibility, Geochim. Cosmochim. Acta 55 (1991) 433–440.
[136] K. Fukushi, H. Sakai, T. Itono, A. Tamura, S. Arai, Desorption of Intrinsic Cesium from Smectite: Inhibitive Effects of Clay Particle Organization on Cesium Desorption, Environ. Sci. Technol. 48 (2014) 10743–10749.
[137] L. Bergaoui, J.F. Lambert, R. Prost, Cesium adsorption on soil clay: Macroscopic and spectroscopic measurements, Appl. Clay Sci. 29 (2005) 23–29.
[138] R.B. Ejeckam, B.L. Sherriff, A ^{133}Cs, ^{29}Si, and ^{27}Al MAS NMR spectroscopic study of Cs adsorption by clay minerals: Implications for the disposal of nuclear wastes, Can. Mineral. 43 (2005) 1131–1140.
[139] Y. Kim, R.T. Cygan, R.J. Kirkpatrick, ^{133}Cs NMR and XPS investigation of cesium adsorbed on clay minerals and related phases, Geochim. Cosmochim. Acta 60 (1996) 1041–1052.
[140] Y. Kim, R.J. Kirkpatrick, ^{23}Na and ^{133}Cs NMR study of cation adsorption on mineral surfaces: Local environments, dynamics, and effects of mixed cations, Geochim. Cosmochim. Acta 61 (1997) 5199–5208.
[141] Y. Kim, R.J. Kirkpatrick, R.T. Cygan, ^{133}Cs NMR study of cesium on the surfaces of kaolinite and illite, Geochim. Cosmochim. Acta 60 (1996) 4059–4074.
[142] F.J. Osuna, A. Cota, E. Pavón, M.C. Pazos, M.D. Alba, Cs^+ immobilization by designed micaceous adsorbent under subcritical conditions, Appl. Clay Sci. 143 (2017) 293–299.

[143] M. Tansho, K. Tamura, T. Shimizu, Identification of multiple Cs^+ adsorption sites in a hydroxy-interlayered vermiculite-like layered silicate through ^{133}Cs MAS NMR analysis, Chem. Lett. 45 (2016) 1385–1387.
[144] C.A. Weiss Jr., R.J. Kirkpatrick, S.P. Altaner, The structural environments of cations adsorbed onto clays: ^{133}Cs variable-temperature MAS NMR spectroscopic study of hectorite, Geochim. Cosmochim. Acta 54 (1990) 1655–1669.
[145] C.A. Weiss Jr, R.J. Kirkpatrick, S.P. Altaner, Variations in interlayer cation sites of clay minerals as studied by ^{133}Cs MAS nuclear magnetic resonance spectroscopy, Am. Mineral. 75 (1990) 970–982.
[146] T. Ohkubo, T. Okamoto, K. Kawamura, R. Guégan, K. Deguchi, S. Ohki, T. Shimizu, Y. Tachi, Y. Iwadate, New Insights into the Cs Adsorption on Montmorillonite Clay from ^{133}Cs Solid-State NMR and Density Functional Theory Calculations, J. Phys. Chem. A 122 (2018) 9326–9337.
[147] M.K. Uddin, A review on the adsorption of heavy metals by clay minerals, with special focus on the past decade, Chem. Eng. J. 308 (2017) 438–462.
[148] S. Gu, X. Kang, L. Wang, E. Lichtfouse, C. Wang, Clay mineral adsorbents for heavy metal removal from wastewater: a review, Environ. Chem. Lett. 17 (2019) 629–654.
[149] H. Han, M.K. Rafiq, T. Zhou, R. Xu, O. Mašek, X. Li, A critical review of clay-based composites with enhanced adsorption performance for metal and organic pollutants, J. Hazard. Mater. 369 (2019) 780–796.
[150] G.J. Churchman, W.P. Gates, B.K.G. Theng, G. Yuan, Chapter 11.1 Clays and Clay Minerals for Pollution Control, in: F. Bergaya, B.K.G. Theng, G. Lagaly (Eds.), Developments in Clay Science, Elsevier, 2006, pp. 625–675.
[151] B. Baeyens, M. Marques Fernandes, 5 - Adsorption of heavy metals including radionuclides, in: R. Schoonheydt, C.T. Johnston, F. Bergaya (Eds.), Developments in Clay Science, Elsevier, 2018, pp. 125–172.
[152] G. Sposito, Adsorption as a problem in coordination chemistry. The concept of the surface complex, Aquatic Chemistry: Interfacial and Interspecies Processes (1995) 33–57.
[153] C.T. Johnston, G. Sposito, W.L. Earl, Surface spectroscopy of environmental particles by Fourier transform infrared and nuclear magnetic resonance, Environmental Particles 2 (1993) 1–36.
[154] P. Zhao, S. Prasad, J. Huang, J.J. Fitzgerald, J.S. Shore, Lead-207 NMR spectroscopic study of lead-based electronic materials and related lead oxides, J. Phys. Chem. B 103 (1999) 10617–10626.
[155] G.E. Maciel, J.L. Dallas, ^{207}Pb Pulse Fourier Transform Nuclear Magnetic Resonance. A Promising New Tool for Studies in Lead Chemistry, J. Am. Chem. Society 95 (1973) 3039–3040.
[156] L.C.M. van Gorkom, J.M. Hook, M.B. Logan, J.V. Hanna, R.E. Wasylishen, Solid-state lead-207 NMR of lead(II) nitrate: Localized heating effects at high magic angle spinning speeds, Magn. Reson. Chem. 33 (1995) 791–795.
[157] C. Dybowski, G. Neue, Solid state ^{207}Pb NMR spectroscopy, Prog. Nucl. Magn. Reson. Spectrosc. 41 (2002) 153–170.
[158] R.A. Santos, E.S. Gruff, S.A. Koch, G.S. Harbison, Solid-state mercury-199 and cadmium-113 NMR studies of mercury- and cadmium-thiolate complexes. Spectroscopic models for [Hg(SCys)n] centers in the bacterial mercury resistance proteins, J. Am. Chem. Soc. 113 (1991) 469–475.
[159] L. Utschig, J. Bryson, T. O'Halloran, Mercury-199 NMR of the metal receptor site in MerR and its protein-DNA complex, Science 268 (1995) 380–385.
[160] L.M. Utschig, J.G. Wright, G. Dieckmann, V. Pecoraro, T.V. O'Halloran, The ^{199}Hg Chemical Shift as a Probe of Coordination Environments in Blue Copper Proteins, Inorg. Chem. 34 (1995) 2497–2498.
[161] R.K. Harris, A. Sebald, Experimental methodology for high-resolution solid-state NMR of heavy-metal spin-1½ nuclei, Magn. Reson. Chem. 25 (1987) 1058–1062.
[162] R. Siegel, T.T. Nakashima, R.E. Wasylishen, Application of multiple-pulse experiments to characterize broad NMR chemical-shift powder patterns from spin-1/2 nuclei in the solid state, J. Phys. Chem. B 108 (2004) 2218–2226.
[163] H. Nagashima, A.S. Lilly Thankamony, J. Trébosc, L. Montagne, G. Kerven, J.-P. Amoureux, O. Lafon, Observation of proximities between spin-1/2 and quadrupolar nuclei in solids: Improved robustness to chemical shielding using adiabatic symmetry-based recoupling, Solid State Nucl. Magn. Reson. 94 (2018) 7–19.
[164] I.M. Armitage, T. Drakenberg, B. Reilly, Use of 113Cd NMR to probe the native metal binding sites in metalloproteins: An overview, in: Metal Ions in Life Sciences, 2013, pp. 117–144.
[165] L. Hemmingsen, L. Olsen, J. Antony, S.P.A. Sauer, First principle calculations of ^{113}Cd chemical shifts for proteins and model systems, J. Biol. Inorg. Chem. 9 (2004) 591–599.
[166] S. Bank, J.F. Bank, P.D. Ellis, Solid-state ^{113}Cd nuclear magnetic resonance study of exchanged montmorillonites, J. Phys. Chem. 93 (1989) 4847–4855.
[167] D. Tinet, A.M. Faugere, R. Prost, ^{113}Cd NMR chemical shift tensor analysis of cadmium-exchanged clays and clay gels, J. Phys. Chem. 95 (1991) 8804–8807.
[168] P. Leo, P. O'Brien, Nuclear Magnetic Resonance (NMR) Study of Cd^{2+} Sorption on Montmorillonite, Clays Clay Miner. 47 (1999) 761–768.
[169] D.J. Sullivan, J.S. Shore, J.A. Rice, ^{113}Cd double-resonance NMR as a probe of clay mineral cation exchange sites, Am. Mineral. 85 (2000) 1022–1029.
[170] D.J. Sullivan, J.S. Shore, J.A. Rice, Assessment of cation binding to clay minerals using solid-state NMR, Clays Clay Miner. 46 (1998) 349–354.
[171] P. Di Leo, J. Cuadros, ^{113}Cd, ^{1}H MAS NMR and FTIR analysis of Cd^{2+} adsorption on dioctahedral and trioctahedral smectite, Clays Clay Miner. 51 (2003) 403–414.
[172] G.D. Yuan, B.K.G. Theng, G.J. Churchman, W.P. Gates, Chapter 5.1 - Clays and Clay Minerals for Pollution Control, in: F. Bergaya, G. Lagaly (Eds.), Developments in Clay Science, Elsevier, 2013, pp. 587–644.
[173] K. El Adraa, T. Georgelin, J.-F. Lambert, F. Jaber, F. Tielens, M. Jaber, Cysteine-montmorillonite composites for heavy metal cation complexation: A combined experimental and theoretical study, Chem. Eng. J. 314 (2017) 406–417.
[174] L. Mercier, C. Detellier, Preparation, Characterization, and Applications as Heavy Metals Sorbents of Covalently Grafted Thiol Functionalities on the Interlamellar Surface of Montmorillonite, Environ. Sci. Technol. 29 (1995) 1318–1323.
[175] M. Struijk, F. Rocha, C. Detellier, Novel thio-kaolinite nanohybrid materials and their application as heavy metal adsorbents in wastewater, Appl. Clay Sci. 150 (2017) 192–201.
[176] L.S. Kostenko, I.I. Tomashchuk, T.V. Kovalchuk, O.A. Zaporozhets, Bentonites with grafted aminogroups: Synthesis, protolytic properties and assessing Cu (II), Cd(II) and Pb(II) adsorption capacity, Appl. Clay Sci. 172 (2019) 49–56.
[177] I.L. Lagadic, M.K. Mitchell, B.D. Payne, Highly Effective Adsorption of Heavy Metal Ions by a Thiol-Functionalized Magnesium Phyllosilicate Clay, Environ. Sci. Technol. 35 (2001) 984–990.
[178] D.L. Guerra, R.R. Viana, C. Airoldi, Adsorption of mercury cation on chemically modified clay, Mater. Res. Bull. 44 (2009) 485–491.
[179] S.A. Boyd, C.T. Johnston, D.A. Laird, B.J. Teppen, H. Li, Comprehensive study of organic contaminant adsorption by clays: methodologies, mechanisms, and environmental implications, Biophysico-Chem. Process. Anthropog. Organ. Compoun. Environ. Syst. (2011) 51–71.
[180] J. Cornejo, R. Celis, I. Pavlovic, M.A. Ulibarri, Interactions of pesticides with clays and layered double hydroxides: A review, Clay Miner. 43 (2008) 155–175.
[181] C. Johnston, Sorption of organic compounds on clay minerals, in: Organic pollutants in the environment, The Clay Minerals Society, 1996.
[182] G. Lagaly, Pesticide-clay interactions and formulations, Appl. Clay Sci. 18 (2001) 205–209.
[183] M.M. Mortland, Clay-organic complexes and interactions, in: Advances in Agronomy, 1970, pp. 75–117.
[184] T. Thiebault, M. Boussafir, L. Le Forestier, C. Le Milbeau, L. Monnin, R. Guégan, Competitive adsorption of a pool of pharmaceuticals onto a raw clay mineral, RSC Adv. 6 (2016) 65257–65265.
[185] J.-F. Lambert, 7 - Organic pollutant adsorption on clay minerals, in: R. Schoonheydt, C.T. Johnston, F. Bergaya (Eds.), Developments in Clay Science, Elsevier, 2018, pp. 195–253.
[186] S. Nir, Y. El-Nahhal, T. Undabeytia, G. Rytwo, T. Polubesova, Y. Mishael, O. Rabinovitz, B. Rubin, Clays, clay minerals, and pesticides, in: Developments in Clay Science, Elsevier, 2013, pp. 645–662.
[187] G. Yuan, B. Theng, G. Churchman, W. Gates, Clays and clay minerals for pollution control, in: Developments in clay science, Elsevier, 2013, pp. 587–644.
[188] S. Thiele-Bruhn, Pharmaceutical antibiotic compounds in soils–a review, J. Plant Nutr. Soil Sci. 166 (2003) 145–167.
[189] Y. Park, G.A. Ayoko, R.L. Frost, Application of organoclays for the adsorption of recalcitrant organic molecules from aqueous media, J. Colloid Interface Sci. 354 (2011) 292–305.
[190] C. Bonhomme, C. Gervais, D. Laurencin, Recent NMR developments applied to organic–inorganic materials, Prog. Nucl. Magn. Reson. Spectrosc. 77 (2014) 1–48.
[191] J. Grandjean, Nuclear Magnetic Resonance Spectroscopy of Molecules and Ions at Clay Surfaces, in: F. Wypych, K.G. Satyanarayana (Eds.), Interface Science and Technology, Elsevier, 2004, pp. 216–246.
[192] T. Tao, G.E. Maciel, ^{13}C NMR Study of Co-Contamination of Clays with Carbon Tetrachloride and Benzene, Environ. Sci. Technol. 32 (1998) 350–357.
[193] Z.R. Hinedi, C.T. Johnston, C. Erickson, Chemisorption of benzene on Cu-montmorillonite as characterized by FTIR and ^{13}C MAS NMR, Clays Clay Miner. 41 (1993) 87–94.
[194] J. Xiong, G.E. Maciel, Deuterium NMR Studies of Local Motions of Benzene Adsorbed on Ca-Montmorillonite, J. Phys. Chem. B 103 (1999) 5543–5549.
[195] T. Tao, J.J. Yang, G.E. Maciel, Photoinduced Decomposition of Trichloroethylene on Soil Components, Environ. Sci. Technol. 33 (1999) 74–80.
[196] M.H. Forouzanfar, L. Alexander, V.F. Bachman, S. Biryukov, M. Brauer, D. Casey, M.M. Coates, K. Delwiche, K. Estep, J.J. Frostad, et al., Global, regional, and national comparative risk assessment of 79 behavioural, environmental and occupational, and metabolic risks or clusters of risks in 188 countries, 1990–2013: A systematic analysis for the Global Burden of Disease Study 2013, The Lancet 386 (2015) 2287–2323.
[197] M.L. Pinto, L. Mafra, J.M. Guil, J. Pires, J. Rocha, Adsorption and Activation of CO_2 by Amine-Modified Nanoporous Materials Studied by Solid-State NMR and $^{13}CO_2$ Adsorption, Chem. Mater. 23 (2011) 1387–1395.
[198] D.Y.C. Leung, G. Caramanna, M.M. Maroto-Valer, An overview of current status of carbon dioxide capture and storage technologies, Renew. Sustain. Energy Rev. 39 (2014) 426–443.
[199] U.H. Bhatti, H. Sultan, G.H. Min, S.C. Nam, I.H. Baek, Ion-exchanged montmorillonite as simple and effective catalysts for efficient CO2 capture, Chem. Eng. J. (2020).
[200] G. Gómez-Pozuelo, E.S. Sanz-Pérez, A. Arencibia, P. Pizarro, R. Sanz, D.P. Serrano, CO2 adsorption on amine-functionalized clays, Microporous Mesoporous Mater. 282 (2019) 38–47.

[201] W. Wang, J. Xiao, X. Wei, J. Ding, X. Wang, C. Song, Development of a new clay supported polyethylenimine composite for CO2 capture, Appl. Energy 113 (2014) 334–341.
[202] N. Horri, E.S. Sanz-Pérez, A. Arencibia, R. Sanz, N. Frini-Srasra, E. Srasra, Effect of acid activation on the CO2 adsorption capacity of montmorillonite, Adsorption 26 (2020) 793–811.
[203] H. Jedli, J. Brahmi, A. Chrouda, A. Jbara, S.G. Almalki, G. Osman, K. Slimi, CO2 adsorption performance of amine clay adsorbent, Appl. Phys. A Mater. Sci. Process. 127 (2021).
[204] L. Michels, J.O. Fossum, Z. Rozynek, H. Hemmen, K. Rustenberg, P.A. Sobas, G. N. Kalantzopoulos, K.D. Knudsen, M. Janek, T.S. Plivelic, et al., Intercalation and retention of carbon dioxide in a smectite clay promoted by interlayer cations, Sci. Rep. 5 (2015).
[205] M.L. Pinto, J. Pires, J. Rocha, Porous materials prepared from clays for the upgrade of landfill gas, The J. Phys. Chem. C 112 (2008) 14394–14402.
[206] A. Dibenedetto, M. Aresta, C. Fragale, M. Narracci, Reaction of silylalkylmono- and silylalkyldi-amines with carbon dioxide: evidence of formation of inter- and intra-molecular ammonium carbamates and their conversion into organic carbamates of industrial interest under carbon dioxide catalysis, Green Chem. 4 (2002) 439–443.
[207] F. Barzagli, F. Mani, M. Peruzzini, A ^{13}C NMR study of the carbon dioxide absorption and desorption equilibria by aqueous 2-aminoethanol and N-methyl-substituted 2-aminoethanol, Energy Environ. Sci. 2 (2009) 322–330.
[208] R.J. Hook, An investigation of some sterically hindered amines as potential carbon dioxide scrubbing compounds, Ind. Eng. Chem. Res. 36 (1997) 1779–1790.
[209] W. Böttinger, M. Maiwald, H. Hasse, Online NMR spectroscopic study of species distribution in MEA–H_2O–CO_2 and DEA–H_2O–CO_2, Fluid Phase Equilib. 263 (2008) 131–143.
[210] G.-J. Fan, A.G. Wee, R. Idem, P. Tontiwachwuthikul, NMR studies of amine species in MEA– CO_2– H_2O system: Modification of the model of vapor–liquid equilibrium, VLE, Ind. Eng. Chem. Res. 48 (2009) 2717–2720.
[211] T.C. Drage, A. Arenillas, K.M. Smith, C.E. Snape, Thermal stability of polyethylenimine based carbon dioxide adsorbents and its influence on selection of regeneration strategies, Microporous Mesoporous Mater. 116 (2008) 504–512.
[212] M. Massaro, C.G. Colletti, G. Lazzara, S. Riela, The Use of Some Clay Minerals as Natural Resources for Drug Carrier Applications, Journal of Functional Biomaterials 9 (2018) 58.
[213] M. Jafarbeglou, M. Abdouss, A.M. Shoushtari, M. Jafarbeglou, Clay nanocomposites as engineered drug delivery systems, RSC Adv. 6 (2016) 50002–50016.
[214] J.H. Park, H.J. Shin, M.H. Kim, J.S. Kim, N. Kang, J.Y. Lee, K.T. Kim, J.I. Lee, D.D. Kim, Application of montmorillonite in bentonite as a pharmaceutical excipient in drug delivery systems, Journal of Pharmaceutical Investigation 46 (2016) 363–375.
[215] W. Chrzanowski, S.Y. Kim, E.A. Abou Neel, Biomedical applications of clay, Aust. J. Chem. 66 (2013) 1315–1322.
[216] C. Viseras, P. Cerezo, R. Sanchez, I. Salcedo, C. Aguzzi, Current challenges in clay minerals for drug delivery, Appl. Clay Sci. 48 (2010) 291–295.
[217] L.A.D.S. Rodrigues, A. Figueiras, F. Veiga, R.M. de Freitas, L.C.C. Nunes, E.C. da Silva Filho, C.M. da Silva Leite, The systems containing clays and clay minerals from modified drug release: A review, Colloids Surf. B: Biointerfaces 103 (2013) 642–651.
[218] C. Aguzzi, P. Cerezo, C. Viseras, C. Caramella, Use of clays as drug delivery systems: Possibilities and limitations, Appl. Clay Sci. 36 (2007) 22–36.
[219] C. Viseras, C. Aguzzi, P. Cerezo, M.C. Bedmar, Biopolymer–clay nanocomposites for controlled drug delivery, Mater. Sci. Technol. 24 (2013) 1020–1026.
[220] S. ul Haque, A. Nasar, Inamuddin, 27 - Montmorillonite clay nanocomposites for drug delivery, in: Inamuddin, A.M. Asiri, A. Mohammad (Eds.), Applications of Nanocomposite Materials in Drug Delivery, Woodhead Publishing, 2018, pp. 633–648.
[221] H. Tomás, C.S. Alves, J. Rodrigues, Laponite®: A key nanoplatform for biomedical applications?, Nanomedicine: Nanotechnology, Biology and Medicine 14 (2018) 2407–2420.
[222] W. Xiaoying, L. Bo, W. Xiaohui, S. Runcang, Amphoteric Polymer-Clay Nanocomposites with Drug-Controlled Release Property, Curr. Nanosci. 7 (2011) 183–190.
[223] J.C. Villaça, L.C.R.P. da Silva, L.H.F. Barbosa, C.R. Rodrigues, L.M. Lira, F.A. do Carmo, V.P. de Sousa, M.I.B. Tavares, e.L.M. Cabral, Preparation and characterization of polymer/layered silicate pharmaceutical nanobiomaterials using high clay load exfoliation processes, J. Ind. Eng. Chem. 20 (2014) 4094–4101.
[224] C.D. Nunes, P.D. Vaz, A.C. Fernandes, P. Ferreira, C.C. Romão, M.J. Calhorda, Loading and delivery of sertraline using inorganic micro and mesoporous materials, Eur. J. Pharm. Biopharm. 66 (2007) 357–365.
[225] A.H. Kibbe, Pharmaceutical Excipients 2000, American Pharmaceutical Association (2000).
[226] C. Viseras, C. Aguzzi, P. Cerezo, A. Lopez-Galindo, Uses of clay minerals in semisolid health care and therapeutic products, Appl. Clay Sci. 36 (2007) 37–50.
[227] T. Pongjanyakul, W. Khunawattanakul, S. Puttipipatkhachorn, Physicochemical characterizations and release studies of nicotine–magnesium aluminum silicate complexes, Appl. Clay Sci. 44 (2009) 242–250.
[228] S. Rojtanatanya, T. Pongjanyakul, Propranolol–magnesium aluminum silicate complex dispersions and particles: Characterization and factors influencing drug release, Int. J. Pharm. 383 (2010) 106–115.
[229] V.R.R. Cunha, P.A.D. Petersen, M.B. Gonçalves, H.M. Petrilli, C. Taviot-Gueho, F. Leroux, M.L.A. Temperini, V.R.L. Constantino, Structural, Spectroscopic (NMR, IR, and Raman), and DFT Investigation of the Self-Assembled Nanostructure of Pravastatin-LDH (Layered Double Hydroxides) Systems, Chem. Mater. 24 (2012) 1415–1425.
[230] L. Perioli, V. Ambrogi, M. Nocchetti, M. Sisani, C. Pagano, Preformulation studies on host–guest composites for oral administration of BCS class IV drugs: HTlc and furosemide, Appl. Clay Sci. 53 (2011) 696–703.
[231] E. Conterosito, G. Croce, L. Palin, C. Pagano, L. Perioli, D. Viterbo, E. Boccaleri, G. Paul, M. Milanesio, Structural characterization and thermal and chemical stability of bioactive molecule–hydrotalcite (LDH) nanocomposites, PCCP 15 (2013) 13418–13433.
[232] L. Perioli, V. Ambrogi, B. Bertini, M. Ricci, M. Nocchetti, L. Latterini, C. Rossi, Anionic clays for sunscreen agent safe use: Photoprotection, photostability and prevention of their skin penetration, Eur. J. Pharm. Biopharm. 62 (2006) 185–193.
[233] V. Ambrogi, L. Perioli, V. Ciarnelli, M. Nocchetti, C. Rossi, Effect of gliclazide immobilization into layered double hydroxide on drug release, Eur. J. Pharm. Biopharm. 73 (2009) 285–291.
[234] V. Ambrogi, G. Fardella, G. Grandolini, L. Perioli, M.C. Tiralti, Intercalation compounds of hydrotalcite-like anionic clays with anti-inflammatory agents, II: Uptake of diclofenac for a controlled release formulation, AAPS PharmSciTech 3 (2002) 77–82.
[235] L. Perioli, T. Posati, M. Nocchetti, F. Bellezza, U. Costantino, A. Cipiciani, Intercalation and release of antiinflammatory drug diclofenac into nanosized ZnAl hydrotalcite-like compound, Appl. Clay Sci. 53 (2011) 374–378.
[236] U. Costantino, V. Ambrogi, M. Nocchetti, L. Perioli, Hydrotalcite-like compounds: Versatile layered hosts of molecular anions with biological activity, Microporous Mesoporous Mater. 107 (2008) 149–160.
[237] W. Li, L. Sun, L. Pan, Z. Lan, T. Jiang, X. Yang, J. Luo, R. Li, L. Tan, S. Zhang, et al., Dendrimer-like assemblies based on organoclays as multi-host system for sustained drug delivery, Eur. J. Pharm. Biopharm. 88 (2014) 706–717.
[238] R. Rojas, Y.G. Linck, S.L. Cuffini, G.A. Monti, C.E. Giacomelli, Structural and physicochemical aspects of drug release from layered double hydroxides and layered hydroxide salts, Appl. Clay Sci. 109–110 (2015) 119–126.
[239] J.M. Fraile, E. Garcia-Martin, C. Gil, J.A. Mayoral, L.E. Pablo, V. Polo, E. Prieto, E. Vispe, Laponite as carrier for controlled in vitro delivery of dexamethasone in vitreous humor models, Eur. J. Pharm. Biopharm. 108 (2016) 83–90.
[240] V.R.R. Cunha, F.C.D.A. Lima, V.Y. Sakai, L.M.C. Véras, J.R.S.A. Leite, H.M. Petrilli, V.R.L. Constantino, LAPONITE®-pilocarpine hybrid material: experimental and theoretical evaluation of pilocarpine conformation, RSC Adv. 7 (2017) 27290–27298.
[241] E.P. Rebitski, P. Aranda, M. Darder, R. Carraro, E. Ruiz-Hitzky, Intercalation of metformin into montmorillonite, Dalton Trans. 47 (2018) 3185–3192.
[242] J.M. Trillo, M.D. Alba, R. Alvero, M.A. Castro, A. Munoz, J. Poyato, M.M. Tobias, G. Lagaly, Montmorillonites intercalated with Al(III), La(III) and alumina pillars - structural aspects and reactivity, Solid State Ionics 63–5 (1993) 457–463.
[243] T.J. Pinnavaia, Intercalated clay catalysts, Science 220 (1983) 365–371.
[244] M.L. Occelli, in: L.G. Schultz, H. van Olphen, F.A. Mumpton (Eds.), Proceedings of the International Clay Conference, The Clay Minerals Society, Denver, 1985, pp. 319.
[245] D.E.W. Vaughan, R.J. Lussier, J.S. Magee, in, U.S. Patent, 1979.
[246] E.P. Giannelis, T.J. Pinnavaia, Intercalation of metal cluster complexes in smectite clay, Inorg. Chem. 24 (1985) 3602–3607.
[247] M. Tokarz, J. Shabtai, Cross-linked smectites.4. Preparation and properties of hydroxyaluminum-pillared Ce-montmorillonite and La-montmorillonite and fluorinated NH4+-montmorillonites, Clays Clay Miner. 33 (1985) 89–98.
[248] M.L. Occelli, J.T. Hsu, L.G. Galya, Propylene oligomerization with pillared clays, J. Mol. Catal. 33 (1985) 371–389.
[249] D. Zhao, Y. Yashu, G. Xiexian, Preparation and characterization of lanthanide-doped pillared clays, Matrial Research Bulletin 28 (1993) 939–949.
[250] M. Kurian, S. Sugunan, Characterisation of the acid-base properties of pillared montmorillonites, Microporous Mesoporous Mater. 83 (2005) 25–34.
[251] M.L. Occelli, New routes to the preparation of pillared montmorillonite catalysts, J. Mol. Catal. 35 (1986) 377–389.
[252] J.W. Akitt, A. Farthing, Al-27 Nuclear Magnetic Resonance studies of the hydrolysis of Aluminum (III). 2. Gel-permeation chromatography, J. Chem. Soc.-Dalton Trans. (1981) 1606–1608.
[253] S.I. Wada, K. Wada, Formation, composition and structure of hydroxy-aluminosilicate ions, J. Soil Sci. 31 (1980) 457–467.
[254] N.L. Holy, Homogeneous Catalysis with Phosphine Complexes, Plenum Press, New York, 1983.
[255] D.Y. Zhao, Y.S. Yang, X.X. Guo, Preparation and characterization of hydroxysilicoaluminum pillared clays, Inorg. Chem. 31 (1992) 4727–4732.
[256] H. Mao, B. Li, L. Yue, L. Wang, J. Yang, X. Gao, Aluminated mesoporous silica-pillared montmorillonite as acidic catalyst for catalytic cracking, Appl. Clay Sci. 53 (2011) 676–683.
[257] F. Kooli, Y. Liu, K. Hbaieb, R. Al-Faze, Characterization and catalytic properties of porous clay heterostructures from zirconium intercalated clay and its pillared derivatives, Microporous Mesoporous Mater. 226 (2016) 482–492.

[258] D.T.B. Tennakoon, W. Jones, J.M. Thomas, J.H. Ballantine, J.H. Purnell, Characterization of clay and pillared clay catalysts, Solid State Ionics 24 (1987) 205–212.
[259] J.T. Kloprogge, E. Booy, J.B.H. Jansen, J.W. Geus, The effect of thermal-treatment on the properties of hydroxy-Al and hydroxy-Ga pillared montmorillonite and beidellite, Clay Miner. 29 (1994) 153–167.
[260] S.A. Garea, A.I. Mihai, A. Ghebaur, C. Nistor, A. Sarbu, Porous clay heterostructures: A new inorganic host for 5-fluorouracil encapsulation, Int. J. Pharm. 491 (2015) 299–309.
[261] J. Villarroel Rocha, D. Barrera, K. Sapag, Improvement in the Pore Size Distribution for Ordered Mesoporous Materials with Cylindrical and Spherical Pores Using the Kelvin Equation, Top. Catal. 54 (2011) 121–134.
[262] F. Hussin, M.K. Aroua, W.M.A.W. Daud, Textural characteristics, surface chemistry and activation of bleaching earth: A review, Chem. Eng. J. 170 (2011) 90–106.
[263] F. Kooli, Porous clay heterostructures (PCHs) from Al-13-intercalated and Al-13-pillared montmorillonites: Properties and heptane hydro-isomerization catalytic activity, Microporous Mesoporous Mater. 184 (2014) 184–192.
[264] J.H. Choy, J.B. Yoon, H. Jung, J.H. Park, Zr K-edge XAS and Si-29 MAS NMR studies on hexagonal mesoporous zirconium silicate, J. Porous Mater. 11 (2004) 123–129.
[265] B.M. Choudary, K.R. Kumar, M.L. Kantam, Synthesis and catalytic activity in selective hydrogenation of palladium complexes anchored in montmorillonite, J. Catal. 130 (1991) 41–51.
[266] J.W. Diesveld, E.M. Menger, H.T. Edzes, W.S. Veeman, High-resolution solid-state P-31 nuclear magnetic-resonance of some triphenylphosphine transition-metal complexes, J. Am. Chem. Soc. 102 (1980) 7935–7936.
[267] A.J. Naaktgeboren, R.J.M. Nolte, W. Drenth, P-31 nuclear magnetic-resonance studies of polymer-anchored rhodium(i) complexes, J. Am. Chem. Soc. 102 (1980) 3350–3354.
[268] C.A. Fyfe, H.C. Clark, J.A. Davies, P.J. Hayes, R.E. Wasylishen, Polymer-immobilized complexes of Platinum(II) - their precursors and preparation studied by high-resolution solid-state P-31 NMR using magic-angle spinning techniques, J. Am. Chem. Soc. 105 (1983) 6577–6584.
[269] K.V. Swamy, D.T. Sadamand, B. Ramesh, P.K. Saiprakash, Hydrogenation kinetics and mechanism of stilbene, ciannamaldehyde and cinnamic acid by anchored montmorillonite bipyridinepalladium (II) acetate, Indian Journal of Chemistry 36A (1997) 98–101.
[270] L.O. Garciano II, N.H. Tran, G.S.K. Kannangara, A.S. Milev, M.A. Wilson, H. Volk, Developing saponite supported cobalt-molybdenum catalysts for upgrading squalene, a hydrocarbon from the microalgae Botryococcus braunii, Chem. Eng. Sci. 107 (2014) 302–310.
[271] S. Barama, C. Dupeyrat-Batiot, M. Capron, E. Bordes-Richard, O. Bakhti-Mohammedi, Catalytic properties of Rh, Ni, Pd and Ce supported on Al-pillared montmorillonites in dry reforming of methane, Catal. Today 141 (2009) 385–392.
[272] A.M. Segarra, R. Guerrero, C. Claver, E. Fernandez, How to turn the catalytic asymmetric hydroboration reaction of vinylarenes into a recyclable process, Chemistry-a European Journal 9 (2003) 191–200.
[273] A.M. Segarra, R. Guerrero, C. Claver, E. Fernandez, An unprecedented recyclable catalyst system for asymmetric hydroboration, Chem. Commun. (2001) 1808–1809.
[274] J.-B. d'Espinose de la Caillerie, C. Fretigny, D. Massiot, MAS NMR spectra of quadrupolar nuclei in disordered solids: The Czjzek model, J. Magn. Reson. 192 (2008) 244–251.
[275] D. Massiot, F. Fayon, M. Capron, I. King, S. Le Calve, B. Alonso, J.O. Durand, B. Bujoli, Z.H. Gan, G. Hoatson, Modelling one- and two-dimensional solid-state NMR spectra, Magn. Reson. Chem. 40 (2002) 70–76.
[276] I. Kiricsi, A. Molnar, I. Palinko, A. Fudala, J.B. Nagy, Nanoscale redox catalysts: Cr- and Cr, Al-pillared layer clays: Characterization and catalytic activity, Solid State Ionics 101 (1997) 793–797.
[277] B. Notari, Titanium silicalites, Catal. Today 18 (1993) 163–172.
[278] R.S. Reddy, J.S. Reddy, R. Kumar, P. Kumar, Sulfoxidation of thioethers using titanium silicate molecular-sieve catalysts, J. Chem. Soc.-Chem. Commun. (1992) 84–85.
[279] I. Khedher, A. Ghorbel, J.M. Fraile, J.A. Mayoral, Ti-IV exchanged K10-montmorillonite: characterisation and catalytic properties in liquid-phase sulfide oxidation, J. Chem. Res. (2008) 604–608.
[280] K.V. Bineesh, S.-Y. Kim, B.R. Jermy, D.-W. Park, Synthesis, characterization and catalytic performance of vanadia-doped delaminated zirconia-pillared montmorillonite clay for the selective catalytic oxidation of hydrogen sulfide, Journal of Molecular Catalysis a-Chemical 308 (2009) 150–158.
[281] D.W. Park, B.K. Park, D.K. Park, H.C. Woo, Vanadium-antimony mixed oxide catalysts for the selective oxidation of H_2S containing excess water and ammonia, Appl. Catal. A 223 (2002) 215–224.
[282] K.V. Bineesh, D.R. Cho, S.Y. Kim, B.R. Jermy, D.W. Park, Vanadia-doped titania-pillared montmorillonite clay for the selective catalytic oxidation of H_2S, Catal. Commun. 9 (2008) 2040–2043.
[283] H. Eckert, I.E. Wachs, Solid-state V-51 NMR structural studies on supported vanadium(v) oxide catalysts - vanadium-oxide surface-layers on alumina and titania supports, J. Phys. Chem. 93 (1989) 6796–6805.
[284] B.M. Reddy, E.P. Reddy, S.T. Srinivas, V.M. Mastikhin, A.V. Nosov, O.B. Lapina, Characterization of vanadium-oxide catalysts supported on TiO_2-ZrO_2 by solid-state V-51 and H-1-NMR spectroscopy, J. Phys. Chem. 96 (1992) 7076–7078.
[285] A.F. Popa, P.H. Mutin, A. Vioux, G. Delahay, B. Coq, Novel non-hydrolytic synthesis of a V_2O_5-TiO_2 xerogel for the selective catalytic reduction of NO_x by ammonia, Chem. Commun. (2004) 2214–2215.
[286] N.R. Sanabria, M.A. Centeno, R. Molina, S. Moreno, Pillared clays with Al-Fe and Al-Ce-Fe in concentrated medium: Synthesis and catalytic activity, Applied Catalysis a-General 356 (2009) 243–249.
[287] L. Allouche, C. Huguenard, F. Taulelle, 3QMAS of three aluminum polycations: space group consistency between NMR and XRD, J. Phys. Chem. Solids 62 (2001) 1525–1531.
[288] J.T. Kloprogge, J.W. Geus, J.B.H. Jansen, D. Seykens, Thermal-stability of basic aluminum sulfate, Thermochim. Acta 209 (1992) 265–276.
[289] A. Aouad, I. Mandalia, F. Bergyaya, A novel method of Al-pillared montmorillonite preparation for potential industrial up-scaling, Appl. Clay Sci. 28 (2005) 175–182.
[290] T. Hara, M. Hatakeyama, A. Kim, N. Ichikuni, S. Shimazu, Preparation of clay-supported Sn catalysts and application to Baeyer-Villiger oxidation, Green Chem. 14 (2012) 771–777.
[291] M. Kurian, M. Joy, D. Raj, Hydroxylation of phenol over rare earth exchanged iron pillared montmorillonites, J. Porous Mater. 19 (2012) 633–640.
[292] V. Tabernero, C. Camejo, P. Terreros, M. Dolores Alba, T. Cuenca, Silicoaluminates as "Support Activator" Systems in Olefin Polymerization Processes, Materials 3 (2010) 1015–1030.
[293] C. Camejo-Abreu, V. Tabernero, M. Dolores Alba, T. Cuenca, P. Terreros, Enhanced activity of clays and its crucial role for the activity in ethylene polymerization, Journal of Molecular Catalysis a-Chemical 393 (2014) 96–104.
[294] S. Milione, G. Milano, L. Cavallo, Pentacoordinated Organoaluminum Complexes: A Computational Insight, Organometallics 31 (2012) 8498–8504.
[295] D. Lee, H. Takahashi, A.S.L. Thankamony, J.-P. Dacquin, M. Bardet, O. Lafon, G. De Paepe, Enhanced Solid-State NMR Correlation Spectroscopy of Quadrupolar Nuclei Using Dynamic Nuclear Polarization, J. Am. Chem. Soc. 134 (2012) 18491–18494.
[296] J. Li, J.A. DiVerdi, G.E. Maciel, Chemistry of the silica surface: Liquid-solid reactions of silica gel with trimethylaluminum, J. Am. Chem. Soc. 128 (2006) 17093–17101.
[297] X. Cheng, Y. Liu, D. Chen, Mechanisms of Hydrolysis-Oligomerization of Aluminum Alkoxide $Al(OC_3H_7)_3$, J. Phys. Chem. A 115 (2011) 4719–4728.
[298] A.A. Gurinov, Y.A. Rozhkova, A. Zukal, J. Cejka, I.G. Shenderovich, Mutable Lewis and Bronsted Acidity of Aluminated SBA-15 as Revealed by NMR of Adsorbed Pyridine-N-15, Langmuir 27 (2011) 12115–12123.
[299] E.J.M. Hensen, D.G. Poduval, P.C.M.M. Magusin, A.E. Coumans, J.A.R. van Veen, Formation of acid sites in amorphous silica-alumina, J. Catal. 269 (2010) 201–218.
[300] M.D. Alba, A.I. Becerro, M.A. Castro, A.C. Perdigon, J.M. Trillo, Inherent acidity of aqua metal ions in solids: An assay in layered aluminosilicates, J. Phys. Chem. B 107 (2003) 3996–4001.
[301] L.L.Y. Chang, Industrial mineralogy Materials, processes, and uses. Upper Saddle River, Prentice Hall, New Jersey, 2002.
[302] R.E. Grim, Some applications of clay mineralogy, Am. Mineral. 45 (1960) 259–269.
[303] J.J. Pesek, Chemically Modified Oxide Surfaces, Gordon & Breach, New York, 1990.
[304] E. Ruiz-Hitzky, Functionalizing inorgnic solids: Towards organic-inorganic nanostructured materials for intelligent and bioinspired systems, Chem. Rec. 3 (2003) 88–100.
[305] P. Gómez-Romero, C. Sánchez, Functional Hybrid Materials, Wiley-VCH, Weinheim, 2004.
[306] Y. Ma, H. Wang, W. Liu, Q. Wang, J. Xu, Y. Tang, Microstructure, Luminescence, and Stability of a Europium Complex Covalently Bonded to an Attapulgite Clay, J. Phys. Chem. B 113 (2009) 14139–14145.
[307] J.J. Rogers, K.J.D. MacKenzie, W.J. Trompetter, New phosphors synthesised by ion exchange of a metakaolin-based geopolymer, Appl. Clay Sci. 157 (2018) 1–7.
[308] K.J.D. MacKenzie, M.E. ASmith, Multinuclear solid-state nuclear magnetic resonance of inorganic materials, Pergamon/elsevier, Oxford, 2002.
[309] R.H. Meinhold, K.J.D. Mackenzie, Effect of lanthanides on the relaxation rates of Y-89 and Si-29 in yttrium silicon oxynitride phases, Solid State Nucl. Magn. Reson. 5 (1995) 151–161.
[310] H.S. Santos, T. Laihinen, L.C.V. Rodrigues, J. Sinkkonen, E. Makila, P. Damlin, L. K.O. Nakamura, H.F. Brito, J. Holsa, M. Lastusaari, Red- and green-emitting nano-clay materials doped with Eu^{3+} and/or Tb^{3+}, Luminescence 34 (2019) 23–38.
[311] A. Gerstmans, L. Urbanczyk, R. Jerome, J.L. Robert, J. Grandjean, XRD and NMR characterization of synthetic hectorites and the corresponding surfactant-exchanged clays, Clay Miner. 43 (2008) 205–212.
[312] A. Peyvandi, I. Harsini, D. Holmes, A.M. Balachandra, P. Soroushian, Characterization of ASR in Concrete by Si-29 MAS NMR Spectroscopy, J. Mater. Civ. Eng. 28 (2016).
[313] E. Moretti, L. Storaro, G. Chessa, A. Talon, E. Callone, K.J. Mueller, F. Enrichi, M. Lenarda, Stepwise dansyl grafting on the kaolinite interlayer surface, J. Colloid Interface Sci. 375 (2012) 112–117.
[314] R. Sasai, T. Itoh, W. Ohmori, H. Itoh, M. Kusunoki, Preparation and Characterization of Rhodamine 6G/Alkyltrimethylammonium/Laponite Hybrid Solid Materials with Higher Emission Quantum Yield, J. Phys. Chem. C 113 (2009) 415–421.

[315] C.G. Wu, T. Bein, Conducting polyaniline filaments in a mesoporous channel host, Science 264 (1994) 1757–1759.
[316] C.J. Jing, L.S. Chen, Y. Shi, X.G. Jin, Synthesis and characterization of exfoliated MEH-PPV/clay nanocomposites by in situ polymerization, Eur. Polym. J. 41 (2005) 2388–2394.
[317] Y. Umemura, Preparation and application of clay mineral films, in: R. Schoonheydt, C.T. Johnston, F. Bergaya (Eds.), Surface and Interface Chemistry of Clay Minerals, vol. 9, 2018, pp. 377–396.
[318] A.J. Fagan, D.J. Lurie, Continuous-wave NMR imaging in the solid state, in: G. A. Webb (Ed.), Annual Reports on Nmr Spectroscopy, vol. 56, 2005, pp. 97–140.
[319] Y. Qin, W. Wang, H. Zhang, Y. Dai, H. Hou, H. Dong, Effects of Organic Modification of Montmorillonite on the Properties of Hydroxypropyl Di-Starch Phosphate Films Prepared by Extrusion Blowing, Materials 11 (2018).
[320] L. Shi, X. Fu, Q. Huang, B. Zhang, Single helix in V-type starch carrier determines the encapsulation capacity of ethylene, Carbohydr. Polym. 174 (2017) 798–803.
[321] A.C. de Oliveira Gomes, I.M. Muglia Machado, A.C. Ruvolo Filho, L.A. Pessan, C. M. Paranhos, Hybrid Membranes of Polymer/Clay for Fuel Cell Applications. Part 2. Sulphonated Poly(Carbonate) Nanocomposites, Polimeros-Ciencia E Tecnologia 24 (2014) 402–410.
[322] I. Nicotera, K. Angjeli, L. Coppola, A.S. Arico, V. Baglio, NMR and Electrochemical Investigation of the Transport Properties of Methanol and Water in Nafion and Clay-Nanocomposites Membranes for DMFCs, Membranes 2 (2015) 325–345.
[323] I. Nicotera, A. Enotiadis, K. Angjeli, L. Coppola, D. Gournis, Evaluation of smectite clays as nanofillers for the synthesis of nanocomposite polymer electrolytes for fuel cell applications, Int. J. Hydrogen Energy 37 (2012) 6236–6245.
[324] I. Nicotera, V. Kosma, C. Simari, C. D'Urso, A.S. Arico, V. Baglio, Methanol and proton transport in layered double hydroxide and smectite clay-based composites: influence on the electrochemical behavior of direct methanol fuel cells at intermediate temperatures, J. Solid State Electrochem. 19 (2015) 2053–2061.
[325] J.E. Tanner, Use of stimulated echo in NMR-diffusion studies, J. Chem. Phys. 52 (1970) 2523–3000.
[326] S. Singha, T. Jana, Influence of interfacial interactions on the properties of polybenzimidazole/clay nanocomposite electrolyte membrane, Polymer 98 (2016) 20–31.
[327] J. Petkovic, H.P. Huinink, L. Pel, K. Kopinga, Diffusion in porous building materials with high internal magnetic field gradients, J. Magn. Reson. 167 (2004) 97–106.
[328] T.-P. Chang, J.-Y. Shih, K.-M. Yang, T.-C. Hsiao, Material properties of portland cement paste with nano-montmorillonite, J. Mater. Sci. 42 (2007) 7478–7487.
[329] H. Justnes, I. Meland, B. J.O., J. Krane, S. T., SINTEF FCB Report, 1989, pp. 1.
[330] C. Ruiz-Santaquiteria, A. Fernandez-Jimenez, J. Skibsted, A. Palomo, Clay reactivity: Production of alkali activated cements, Appl. Clay Sci. 73 (2013) 11–16.
[331] M. Alastair, H. Andrew, P. Pascaline, E. Mark, W. Pete, Alkali activation behaviour of un-calcined montmorillonite and illite clay minerals, Appl. Clay Sci. 166 (2018) 250–261.
[332] E. Pomakhina, D. Deneele, A.-C. Gaillot, M. Paris, G. Ouvrard, Si-29 solid state NMR investigation of pozzolanic reaction occurring in lime-treated Ca-bentonite, Cem. Concr. Res. 42 (2012) 626–632.
[333] M. Bediako, J.T. Kevern, D. Dodoo-Arhin, Co-fired Ghanaian clay-palm kernel shells pozzolan: Thermogravimetric, Si-29 and Al-27 MA NMR characteristics, Constr. Build. Mater. 153 (2017) 430–435.
[334] K. Kopinga, L. Pel, One-dimensional scanning of moisture in porous materials with nmr, Rev. Sci. Instrum. 65 (1994) 3673–3681.
[335] S. Gupta, H.P. Huinink, M. Prat, L. Pel, K. Kopinga, Paradoxical drying of a fired-clay brick due to salt crystallization, Chem. Eng. Sci. 109 (2014) 204–211.
[336] C. Nunes, L. Pel, J. Kunecky, Z. Slizkova, The influence of the pore structure on the moisture transport in lime plaster-brick systems as studied by NMR, Constr. Build. Mater. 142 (2017) 395–409.
[337] A. Domenech, M. Teresa Domenech-Carbo, M. Sanchez del Rio, S. Goberna, E. Lima, Evidence of Topological Indigo/Dehydroindigo Isomers in Maya Blue-Like Complexes Prepared from Palygorskite and Sepiolite, J. Phys. Chem. C 113 (2009) 12118–12131.
[338] S. Borsacchi, M. Geppi, L. Ricci, A. Cardelli, G. Ruggeri, Preparation, characterization and solid state NMR investigation of a dye-containing smectite clay, Stud. Univ. Babes-Bolyai, Chem. 56 (2011) 15–26.
[339] F. Fournier, L. de Viguerie, S. Balme, J.-M. Janot, P. Walter, M. Jaber, Physico-chemical characterization of lake pigments based on montmorillonite and carminic acid, Appl. Clay Sci. 130 (2016) 12–17.
[340] P. Trigueiro, F.A.R. Pereira, D. Guillermin, B. Rigaud, S. Balme, J.-M. Janot, I.M. G. dos Santos, M.G. Fonseca, P. Walter, M. Jaber, When anthraquinone dyes meet pillared montmorillonite: Stability or fading upon exposure to light?, Dyes Pigm. 159 (2018) 384–394.
[341] D. Guillermin, T. Debroise, P. Trigueiro, L. de Viguerie, B. Rigaud, F. Morlet-Savary, S. Balme, J.-M. Janot, F. Tielens, L. Michot, et al., New pigments based on carminic acid and smectites: A molecular investigation, Dyes Pigm. 160 (2019) 971–982.
[342] P. Schmitt, H. Gunther, G. Hagele, R. Stilke, A H-1 and C-13 NMR-study of carminic acid, Organic Magnetic Resonance 22 (1984) 446–449.
[343] L. Bergaoui, J.F. Lambert, H. Suquet, M. Che, Cu-II on Al-13-pillared saponites - macroscopic adsorption measurements and EPR-spectra, J. Phys. Chem. 99 (1995) 2155–2161.
[344] A. Claro, M.J. Melo, S. Schafer, J.S.S. de Melo, F. Pina, K.J. van den Berg, A. Burnstock, The use of microspectrofluorimetry for the characterization of lake pigments, Talanta 74 (2008) 922–929.